Benedikt Brezina

Master Thesis 2016 supervised by
Univ.-Prof. Dipl.-Ing. Dr.mont. Gerhard Thonhauser
Dipl.-Ing. BSc Asad Elmgerbi

Analysis of Flow Behavior in Mud Return Lines of Open System Drilling Rigs

dpe DEPARTMENT PETROLEUM ENGINEERING

MONTAN UNIVERSITÄT

To my parents who supported me and enabled me to study in Leoben.

Affidavit

I declare in lieu of oath that I wrote this thesis and performed the associated research myself using only literature cited in this volume.

Eidesstattliche Erklärung

Ich erkläre an Eides statt, dass ich diese Arbeit selbständig verfasst, andere als die angegebenen Quellen und Hilfsmittel nicht benutzt und mich auch sonst keiner unerlaubten Hilfsmittel bedient habe.

_____

Benedikt Brezina, 21 September 2016

Abstract

Because easy oil is gone is gets ever more difficult to find new oil and gas reserves. New discoveries are usually smaller, deeper and much more difficult to get access to. Therefore new technologies, such as managed pressure drilling, real time data analysis and early kick/loss detection become more and more necessary to reach these reservoirs safely and economically. In order to be able to drill in very narrow pressure windows and to minimize non-productive time induced by kicks or lost circulation modern drilling systems incorporate a closed loop mud system to precisely control bottom hole pressure and to measure inflow and outflow of the well to identify kicks and losses early on. For measuring these mudflows in such closed loop systems it is common today to use Coriolis flowmeters, which have proven to be very accurate even under difficult mud properties.

This thesis' purpose is it to review all currently available measurement methods and flowmeters and evaluate their possible use on conventional drilling rigs. Due to the high complexity and cost of Coriolis type flowmeters a widespread use or upgrade of old rigs, especially onshore is not viable. Therefore the thesis tries to show alternative methods that are cost effective and equally capable of measuring flow or identify kicks and losses and distinguish them from ballooning effects. A computational fluid dynamics study is conducted to examine the outflow behavior of drilling fluid on conventional drilling rigs and how it may affect the accuracy and reliability of flow measurements in terms of early kick and loss detection.

Based on an initial case simulations have been conducted with varying flow rates, fluid return line angle, mud density and mud viscosity to determine the influencing factors for open channel flow rate measurement. It could be observed that drilling fluid properties in the range of conventional drilling fluids have little effect and that the ratio of the geometric factors such as pipe diameter and drop angle are the main factors for accurate flow rate measurement.

Zusammenfassung

Es wird immer schwieriger neue Öl- und Gasreserven zu finden. Neue Entdeckungen sind in der Regel kleiner, tiefer und viel schwieriger zugänglich. Daher sind neue Technologien, wie Managed Pressure Drilling, Echtzeit-Datenanalyse und frühe Kick / Verlusterkennung immer wichtiger, um diese Reservoirs sicher und wirtschaftlich zu erreichen. Um in der Lage zu sein, sehr schmale Druckfenster zu bohren und nicht-produktive Zeit aufgrund von Kicks oder Spülungsverlusten zu minimieren setzen moderne Bohrsysteme vorwiegend auf geschlossene Spülungskreisläufe um Bohrlochdrücke, Zu – und Abflüsse genau überwachen zu können und Kicks bzw. Spülungsverluste frühzeitig zu erkennen. Um Spülungsflüsse in solchen geschlossenen Kreislaufsystemen genau messen zu können, ist es heute üblich Coriolis-Durchflussmesser zu verwenden, die sich als sehr genau erwiesen haben auch unter schwierigen Bedingungen.

Der Zweck dieser Arbeit ist es, alle derzeit verfügbaren Messmethoden und Sensorsysteme zu untersuchen und ihre mögliche Verwendung auf herkömmlichen Bohranlagen zu bewerten. Aufgrund der hohen Komplexität und Kosten von Coriolis Durchflussmessern ist eine weitreichende Aufrüstung von alten Bohranlagen, speziell bei Landbohranlagen, nicht kosteneffizient. Daher versucht diese Arbeit, alternative Methoden zu zeigen, die kostengünstiger sind und gleichermaßen in der Lage sind genaue Durchflussmessungen durchzuführen und Kicks bzw. Spülungsverluste von Bohrlochaufblähungseffekten zu unterscheiden. Eine numerische Strömungsanalyse wurde durchgeführt, um das Abfluss - Verhalten von Bohrschlamm auf konventionellen Bohranlagen zu untersuchen und dessen Auswirkung auf Genauigkeit und Zuverlässigkeit dieser Messungen im Bezug auf die frühe Erkennung von Kicks und Spülungsverlusten zu ermitteln.

Nach einer ersten Fallstudiensimulation wurden Fälle mit unterschiedlichen Strömungsgeschwindigkeiten, Kanalneigungswinkeln, Schlammdichten und Viskositäten durchgeführt, um die Einflussfaktoren für Durchflussmessungen in offenen Kanälen zu ermitteln. Es konnte beobachtet werden, dass Spülungseigenschaften im Bereich konventioneller Bohrspülungen geringe Auswirkungen haben und dass das Verhältnis der geometrischen Faktoren wie Rohrdurchmesser und Neigungswinkel weit mehr Einfluss auf die Messungen nehmen können.

Acknowledgements

First and foremost I want to thank my thesis advisor Dipl.-Ing. Asad Elmgerbi from the University of Leoben for supporting and advising me over the duration of my work. He was always there for me and helped me when I didn't know further.

Furthermore I want to thank Dipl.-Ing. Dr.mont. Claudia Gruber giving me valuable technical advice for my thesis.

I also want to thank all employees and colleagues of the University of Leoben who provided an excellent learning environment.

Finally, I want to thank my friends and family who supported me during my time of study and were always there for me in times of desperation.

Contents

Chapter 1 Introduction

Safety during drilling operations becomes a more and more important factor in today's oil and gas industry. Especially after the tragic deep water horizon accident attention towards the oil and gas industry has increased substantially. In order to avoid such worst case scenarios, drilling companies face many challenges and in most cases invest heavily in advanced well control and kick detection systems as well as other preventative measures. Especially due to the increased complexity and harshness of the drilling environments maintaining a smooth and safe operation becomes more difficult. Conventional kick detection systems are often not up for the task and leave little time for the drilling crew to decide and react to well control events. A flow paddle and mud pit level sensors are nowadays the most commonly used indicators on conventional drilling rigs to detect such events. However, in the past years new sensors and kick detection approaches have been tested on rigs and proven their capabilities to not only detect inflows into the wellbore but to detect ballooning effects and mitigate false alarms. Such systems might not always be the simplest and cheapest solutions but in offshore operations or other very safety conscious operations under intense scrutiny the higher investments may be worth their money.

This thesis reviews the currently used surface devices for kick and loss detection on most rigs and looks into other possible types of surface devices that could be used as an alternative. Thereby the different kind of surface devices are compared in relation to their working principles accuracies as well as advantages and disadvantages.

For the practical part of this thesis flow simulations along the drill string and the drilling fluid return line are conducted with a state of the art CFD (computational fluid dynamics) software. Hereby the behavior of a drilling fluid is examined in an open drilling system. The outflow takes place in a partially filled pipe hence open channel flow conditions are present which differ significantly in some respects compared to so-called pipe flow. The behavior of drilling fluid height and velocity is studied under changing flowrates, fluid properties as well as return line drop angles to determine possible sweet spots for surface device placement.

The main objective of this work to gain an understanding on what factors drive the open channel detectability of influx or loss events in drilling applications. Based on these findings recommendations for optimal sensor placement without costly rig modifications are given as well as guidelines and directions for future simulation work in that area.

Especially onshore rigs are often technologically outdated years or even decades compared to state of the art, newly built rigs and safety could be increased tremendously if such rigs would get upgraded with more advanced kick and loss detection systems. However in a low oil price environment like we see right now cost reduction is the number one priority and gains in safety and operational efficiency have to come at a reasonable price.

Chapter 2 Flowmeter Types used on Drilling Rigs

Due to the nature of the measured liquid and the environment it is measured in only a handful of flowmeters are actually capable of handling such harsh conditions on the drilling rig and measure accurately. When flowrate is measured in the fluid return line the fluid is usually contaminated with cuttings form the drilling process as well as possibly small gas bubbles and wear material from the drill string or the casing. So the measured fluid can by no means be described as a pure fluid which brings some challenges in measuring its flow. In comparison to pure fluid measurement such as in oil and gas pipelines in chemical processing plants or water pipes the drilling fluid is a unpredictable mixture of a liquid with solid and gaseous components hence the application of some flowmeters is not feasible. In the subsequent chapters the most important types of flow measuring devices are described in detail. Important to note that all devices discussed use methods of obtaining the flowrate without obstructing elements in the flow path such as turbine or vortex flowmeters do. The high degree of contamination of the fluid especially during drilling would clog up such devices and would require constant maintenance.

Flow meter Type	Pressure Drop	Accuracy	Low Maintenance	Slurry Flows	Viscosity Independent	Non-Conductive Fluids	Non-Intrusive
Coriolis	limited	good	good	good	good	good	good
Differential Pressure	poor	poor	good	poor	poor	good	poor
Magmeter	good	limited	good	good	limited	poor	good
Positive Displacement	limited	good	poor	poor	limited	good	poor
Turbine	limited	good	poor	poor	poor	good	poor
Ultrasonic	good	good	good	limited	good	good	good
Vortex	good	limited	good	poor	limited	good	limited

good limited poor

Figure 1: Selection table for flow measurement technologies showing how well the different types fulfill the requirements for flow measurement on drilling rigs with regards to their capability of delivering accurate and effective measurements (modified from Emerson Process Management 2009).

In the subsequent sections the most suitable flowmeters for a drilling rig are discussed. As can be seen in Figure 1 the only three types that are capable of handling slurry flows well are the Coriolis, Electromagnetic and Ultrasonic flowmeters. The color – code provided by this chart gives a quick overlook on the capability of the different flowmeter types to handle flow measurements on conventional drilling rigs. 'Good' means that this property poses no limitation for the intended operation, if a property is however marked with 'limited' there are some limitations that are explained in more detail in the sections below but usually can be overcome. If a property is marked as 'poor' it is inherently not suited for outflow measurement on conventional drilling rigs. For each type the working principle is explained as well as their specific advantages and disadvantages and their limitations in regards to open and closed drilling systems.

As it is evident, about 90% of the worlds drilling rigs are onshore rigs and most of them are conventional drilling rigs, meaning that the drilling fluid circulation is an open loop and the drilling fluid flowing out of the annulus is at atmospheric pressure (Baker Hughes 2015). Due to the high cost and technical complexity of upgrading to a managed pressure drilling (MPD) system the application of such systems is rarely justified on onshore drilling rigs. Hence for at least the medium term future it can be assumed that the majority of drilling rigs will continue to be conventional open loop drilling systems. For this reason the open channel flowmeters of conventional drilling rigs are discussed as well.

2.1 Outflow Measurement in Drilling Operations

The outflow measurement in drilling operations is usually done in conjunction with an inflow measurement in order to determine the differential flow. The majority of inflow measurements today are still done by counting the strokes of the mud pumps. By knowing the displacement volume per stroke and the efficiency of the pump the inflow volume can be determined. Other more accurate methods that use Coriolis flowmeters are mainly used in offshore operations.

The outflow sensors which are discussed in this thesis are installed between the bell nipple and the shale shakers. The bell nipple is a large pipe installed on top of the blowout preventer (BOP) and acts as a funnel to guide drilling tools into the hole and the drilling fluid into the mud return line towards the shale shakers.

The mud return line is usually a large diameter pipe that is connected to the bell nipple outlet and acts as a conduit for the drilling fluid to the mud treatment equipment. Depending on the BOP height and rig layout this flowline has different inclinations which affect the mud flow and the flow measurement respectively.

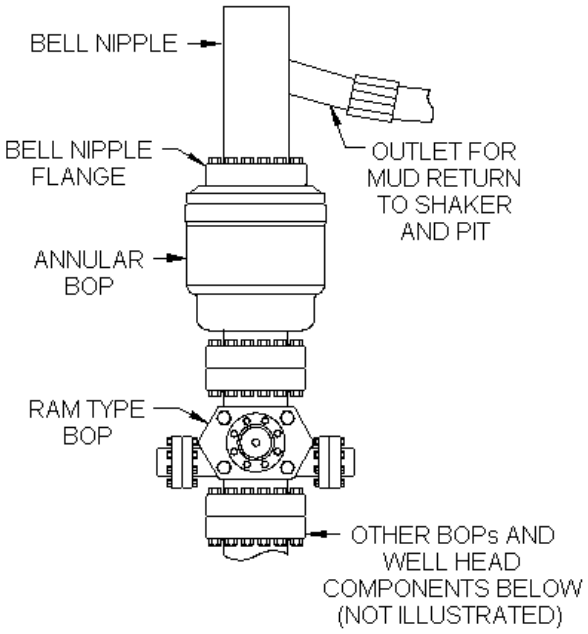

Figure 2: Typical bell nipple and flange installation below drilling rig floor (Woodco 2014).

2.1.1 Open and Closed Drilling Systems

Drilling systems can be divided into two major groups. Open and closed systems. Open systems are also often called conventional systems. The drilling fluid circulation is open to atmospheric pressure. This means the drilling fluid flows out of the annulus in atmospheric conditions into a flow line with usually open channel flow conditions. The bottom hole pressure (BHP) is determined by the effective circulating density (ECD). Hence it is controlled by the mud weight and the friction (friction is controlled by pump speed).

The more modern approach to drilling is a closed system also called managed pressure drilling (MPD). This approach brings several advantages but at a higher cost and complexity. MPD allows for (Robbie and Orbell 2016):

- Narrow margin drilling
- Better control of BHP
- Improved non-productive time (NPT)
- Improved response time in case of downhole events
- Better control of annular gradients for drilling through depleted zones

Unlike the conventional system in a closed system the BHP can additionally be controlled by the applied surface back pressure. The BHP can be increased and decreased instantly in case of a loss or a kick. This increases the safety and the well economics.

The types of flowmeters which are capable of measuring outflow in each system are different. While in the majority of conventional systems the outflow is measured by a flow paddle of a radar level meter closed systems need different types. In closed systems there is pipe flow at the surface opposed to open channel flow in conventional rigs. Hence Coriolis or electromagnetic flowmeters are used in such cases.

2.2 Coriolis Flowmeter

The Coriolis flowmeter is one of the youngest developments among the available flowmeters. Instead of measuring flow rate directly it measures the mass flow rate. Most commercially available flowmeters today even allow for the simultaneous measurement of mass flow rate, density and volume. Coriolis flowmeters are becoming increasingly popular due to their high accuracy, compact form, low pressure drop and their wide spectrum of applications. Generally the flowmeter comes in a pressure sealed housing in case the inner tube leaks and releases possibly dangerous fluids. Due to the undisturbed flow path of such a flowmeter it has a very low pressure drop and is almost maintenance free. The two most common failure types are fatigue of the inner tube because of the cyclic stresses acted on it and much more so corrosion failure. Failure due to cyclic stress fatigue can be prevented by proper mechanical design of the tube and is usually appearing very rarely. Corrosion failure however can have severe consequences since it is very dependent on the measured fluid and operating conditions. The correct choice of materials is critical for the corrosion resistance of the tube. In addition the vibrating part of the flowmeter has to be made of softer material to minimize cyclic stress failure. Typically stainless steel or titanium is used for the construction of the inner tube.

Coriolis flowmeters can be used for both systems, the MPD and conventional open loop drilling system. They can increase the accuracy of detecting kick and loss events, consequently more time will be available for the drilling crew to react before catastrophic events happen. Wellbore ballooning effects can sometimes cause false kick and loss alarms or kicks can develop undetected when assumed to be the ballooning effect. Hence another important application it is often mentioned in, is the identification and quantification of wellbore ballooning effects which is supported by its exceptional accuracy. Figure 3 shows the installation of a Coriolis flowmeter on a conventional rig. In order to improve the measurement accuracy it is important to install the device correctly. This makes it necessary to install it so that no cuttings and no gas bubbles can accumulate at low flow velocities and consequently impair the measurement. In order to overcome the small pressure drop of the flowmeter on conventional drilling rigs Micro Motion made an example calculation for such an installation. For example if the flowmeter needs an input pressure of 3 psi at full flow rates the minimum hydrostatic head required would be 6ft (1.8m) (Russel and Simons 2013). These requirements have to be taken into consideration when planning such an installation.

Figure 3: Installation of a Coriolis flowmeter on a conventional drilling rig using the Schlumberger flag kick detection system. It can be seen that the pipe coming out of the bell nipple splits into the measuring line and the bypass line used if the flowmeter is clogged or under maintenance. The switching between the lines can be controlled by the driller via the electric valves. The flowmeter is installed in a flag orientation to not allow accumulation of gas bubbles and solids in the measuring tube (Schlumberger FLAG Product Video 2015).

2.2.1 Working Principle

Although there exist different designs for the Coriolis flowmeter the general operation principle is explained with the U-tube design, because it is relatively simple to understand and the most widely used in drilling operations. In principle this device uses the Coriolis force acting on the fluid in the pipe to measure flow and density. The theory behind all models is the same and can easily be applied to other models once it is understood. The pipe is vibrated by an external actuator, usually in the form of an electromagnetic actuator. Considering an element of fluid flowing through the tube during the upward motion of the vibration this element has an angular momentum.

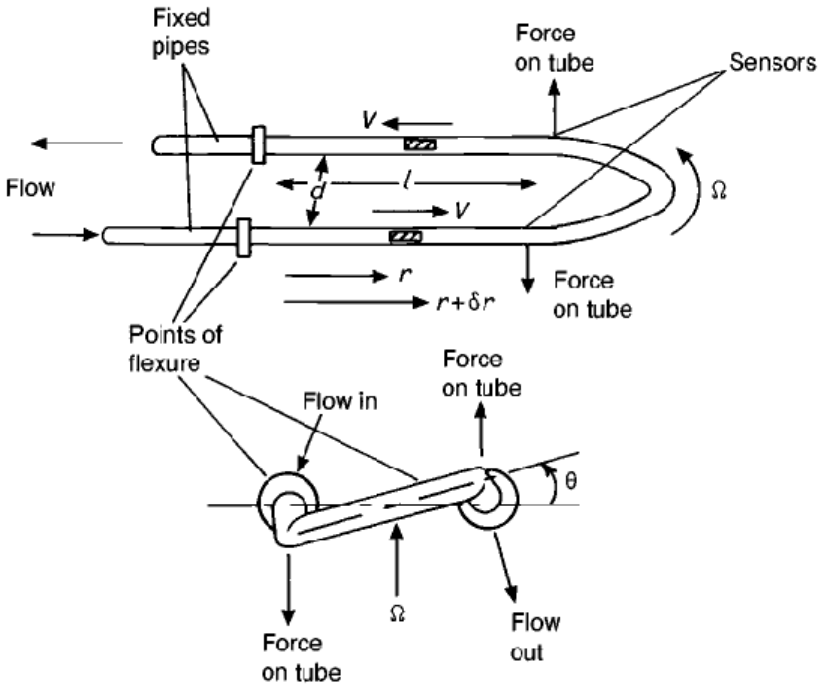

Figure 4: Sketch of a U-shaped Coriolis flowmeter showing the acting forces on the pipe during the upward movement of the pipe (Roger 2000).

As the fluid moves further out the angular momentum increases because the distance to the center of the rotation increases. The change in velocity results in a force which is acted onto the fluid, hence a counteracting force is acted onto the pipe. If this sequence is continued while the pipe is vibrated and fluid flowing through this results in a twisting of the pipe. Usually two sensors either optical or magnetic sensors are installed on the pipe and measure the motion of the pipe. From the frequency of the twisting and the phase shift between the two sensors the mass flow rate can be calculated. In addition Coriolis flowmeters are capable of measuring the density of the fluid (Figure 4, Figure 5).

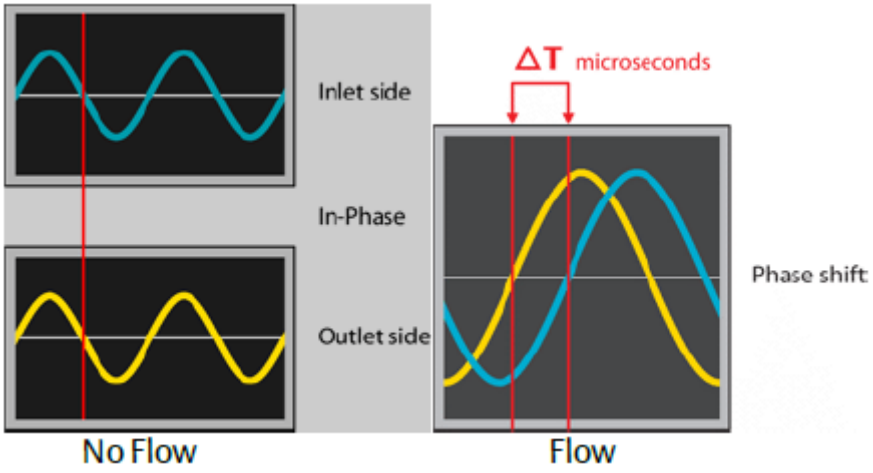

Figure 5: Phase change between the two sensors when flow occurs (Russel and Simons 2013).

Although there are a variety of different flowmeter designs available the straight tube design is becoming more and more common in certain scenarios due to their inherent advantages. Straight tube designs are the mechanically simplest design and therefore allow for easier installation and service. In addition it is very space saving compared to other designs and allows operators to replace old flowmeters with these ones in their facilities. Another major reason why straight tube designs are becoming increasingly popular among most industrial users is their low pressure drop. The pressure drop is almost negligible in most industrial processes because it only differs little compared to an ordinary straight piece of pipe however to date straight tube flowmeters capable of measuring such high flowrates used in drilling operations are not available and therefore larger U-shaped types have to be used. Figure 6 shows typical values of pressure drop for different pipe diameters compared to the mass flow rate. Advances in Coriolis flowmeters that happened in recent years allow diameters of up to 12″ diameter hence measure high flow rates accurately too. Typical pressure drop values range from 5 to 40 psi.

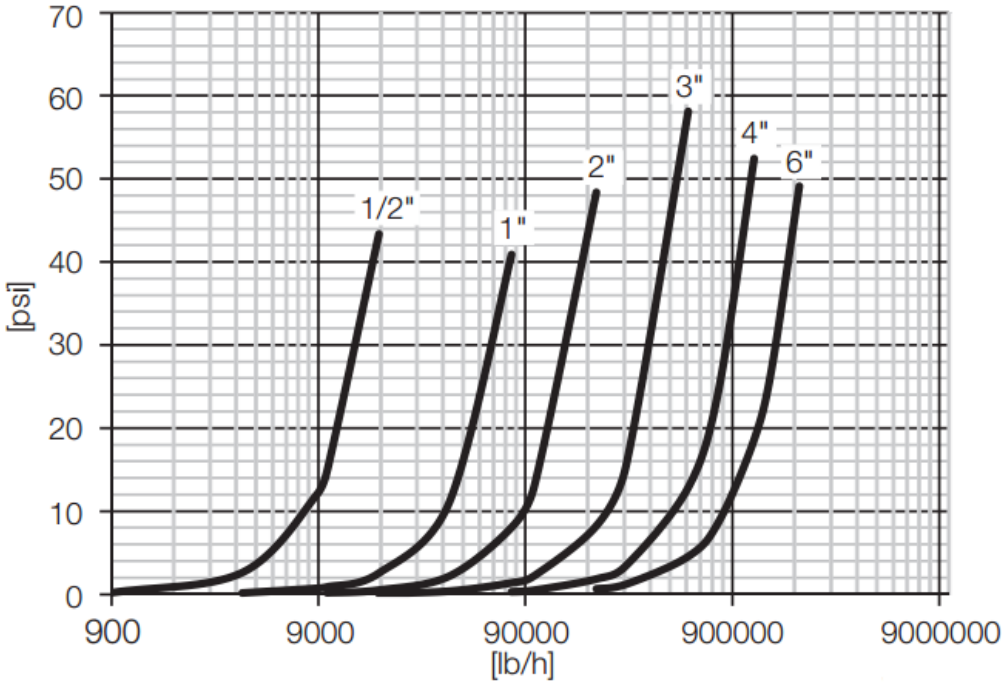

Figure 6: Typical straight tube pressure loss diagram measured with water (ABB 2015).

A graphical representation of the discussed equation below can be seen in Figure 4. With the time difference τ of the pipe displacement signal the mass flow rate can eventually be determined with the following equation below.

$$q_m = \frac{k_s * \tau * (1 - \frac{\omega^2}{\omega_s^2})}{2 * k * d^2} \quad (1)$$

q_m … $Mass\ flowrate$

K_s … $Spring\ constant\ of\ the\ U-tube$

τ … $Time\ difference\ between\ the\ two\ sensors$

ω … $Driving\ frequency\ of\ the\ vibrating\ tube$

ω_s … $Free\ vibrating\ frequency\ of\ the\ twisting\ motion$

K … $Shape\ dependent\ factor$

d … $width\ of\ the\ pipe$

This equation incorporates all relevant geometrical, material constants of the device as well as the readings from the sensors and actuator. The driving frequency ranges from 80 to 1100Hz to bypass the possible vibration frequency of the surrounding hence to minimize sensor noise. The displacement amplitude of the twisting pipe usually ranges from 60µm to 1mm and therefore require accurate optical or magnetic position sensors.

2.2.2 Advantages

- There are no obstructions in the flowmeter tube, which is very important because the fluid coming out of the hole carries solids that could interfere with the measurement. This requires less maintenance and cleaning.
- Due to the unobstructed flow path the pressure drop is very low. Under certain conditions a Coriolis meter can even be used in conventional drilling systems.
- The accuracy and the turndown ratio is among the highest of all flowmeter types.
- It can handle liquids, slurries, foams and gases as well as multiphase mixtures. The measurement is independent of fluid chemistry which makes it ideal for many applications even outside the oil industry.
- Density, mass and volume flowrates can be measured simultaneously.
- No requirements for certain flow regimes in the measuring tubes, therefore no special requirements for straight pipe sections before or after the flowmeter.

2.2.3 Disadvantages

- The biggest and most often mentioned disadvantage of Coriolis flowmeters is its high price compared to other flowmeters. This may often lead to investment decisions in favor of other cheaper flowmeter types, especially in facilities where lots of them are needed. In the drilling industry most Coriolis flowmeters are found on offshore units because the higher cost is worth the higher safety gained through higher accuracy.
- Some models that are no high temperature versions may show bad performance and decreasing accuracy at higher temperatures. This might become an issue especially in high temperature wells and geothermal drilling where temperatures over 200°C can be expected. Furthermore the measurement electronics are limited to an ambient temperature range between -40°C and +60°C which might become critical in arctic or desert environments.
- Cleaning of the flowmeter tubes can be difficult, therefore a bypass line has to be in place. Because the pipe is split into two smaller flow tubes in the Coriolis flowmeter they are also clogging more easily. This has to be kept in mind during drilling operations because of the high solids content in drilling fluids and the rheological behavior of the fluid after static conditions. Also during certain operations where bigger more problematic pieces of material are expected to come up the bypass line should be used.
- Flowmeters come with different materials for the inner measurement tubes. Because these vibrating parts are especially susceptible to corrosion the used materials have to be chosen carefully. This may be an issue while drilling sour gas wells or circulating out backflows of acid jobs.
- The necessary changes in the rig layout in order to install such a flowmeter can become complex and might in some cases be impractical.

- A big part why the installation might be a challenge is because the device does not work in partially filled pipes hence it requires a setup that ensures it is always filled with liquid such as in Figure 3.

2.2.4 Accuracy

Coriolis flowmeters for drilling rigs are mostly U – shaped, high capacity models. In the table below the performance specifications for a typical Coriolis flowmeter is shown. Most studies available about Coriolis flowmeters on drilling rigs use this series which represents the industry standard for high capacity Coriolis flowmeters.

Table 1: Flowmeter performance for liquids and slurries from the Micro Motion ELITE high capacity flowmeter series datasheet (Micro Motion Product Data Sheet 2015).

Performance Specification	Standard	Optional
Mass/volume flow accuracy	±0.10% of rate	±0.05% of rate
Mass/volume flow repeatability	±0.05% of rate	±0.025% of rate
Density accuracy	±0.0005g/cm^3 (±0.5 kg/m^3)	±0.0002g/cm^3 (±0.2 kg/m^3)
Density repeatability	±0.0002g/cm^3 (±0.5 kg/m^3)	±0.0001g/cm^3 (±0.1 kg/m^3)
Temperature accuracy	±1°C ±0.5% of reading	
Temperature repeatability	±0.2°C	

The first factor that can have a big impact on measurement accuracy is the measured flowrate in relation to the maximum flowrate capable of the device also called turndown ratio. Figure 7 shows an example curve how the device loses its high accuracy as is approaches the higher turndown region. The point until the device deviates from its specified accuracy is called the zero point stability. In the example below it would be at a turndown ratio of 20:1 or at 5% of nominal flow capacity. The zero stability point increases with the maximum flow capacity of the device therefore it is crucial to choose the appropriate dimension in order to prevent such inaccuracies.

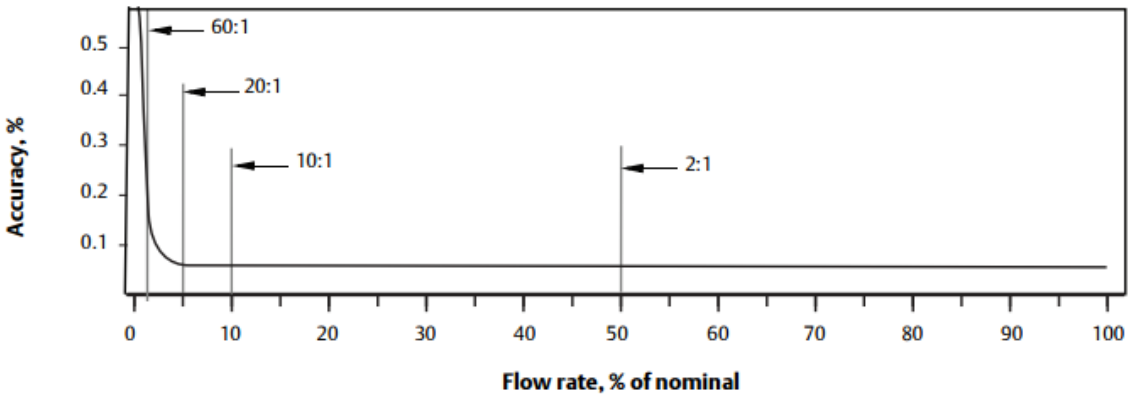

Figure 7: Change of the accuracy in relation to the percentage of maximum flow capacity (Micro Motion Product Data Sheet 2015).

This source of error is especially important at identification and quantification of wellbore ballooning as the measurements might take place at very low flowrates possibly inducing lots of errors. In order to prevent this and to increase measurement performance Micro Motion has used two Coriolis flowmeters each with different dimensions in one of their pilot projects. A higher capacity model for the upper sections of the wellbore where circulation is substantially more compared to the lower sections where a smaller flowmeter was used (Micro Motion, Emerson Process Management 2013).

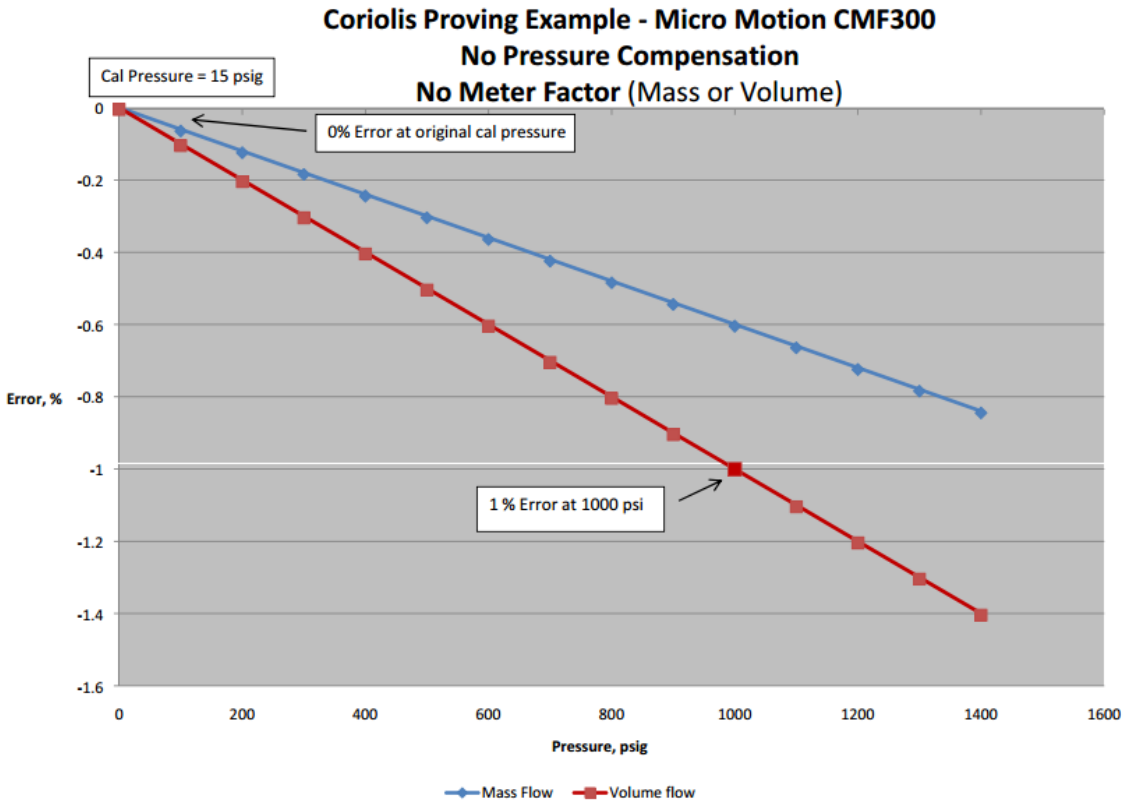

Figure 8: Example of how the measurement errors increase the further away the operating pressure is from the calibration pressure (Kuhny 2011).

A second source of error is the pressure dependent error of Coriolis flowmeters. This especially applies to higher capacity models. Figure 8 shows how the error increases with increased operating pressure if the device is not compensated for the higher pressure. This issue might be of no relevance for conventional drilling rigs as they work constantly at almost atmospheric pressure. On MPD rigs however this effect might become important to recognize. Dependent on the current formation with its corresponding mud pressure window operating pressures for Coriolis flowmeters at the surface might change regularly und therefore require constant compensation to the new pressures. Micro Motion states in a published paper that correction is recommended when the new pressure exceeds a 100 psi change (Kuhny 2011). Most new models have the function to compensate automatically and on the fly which is a necessary solution

for constantly changing pressures for many circumstances however a manual compensation might be sufficient as well.

Flowmeter orientation during operation is another important parameter to keep in mind when designing a system. Although Coriolis flowmeters are capable of measuring liquids, slurries, gases and multiphase flows for the different media certain peculiarities have to be considered. For measuring gases it is important to not install the flowmeter in a low point within the pipeline because fluid might accumulate and condensate may form and if the flowrate is low enough the accumulations are not carried out and increase measurement errors. The same issue occurs for systems predominantly measuring liquids. Here the devices shouldn't be installed on high points to prevent gas bubbles to accumulate and induce additional errors (ABB CoriolisMaster Operating Instructions 2015).

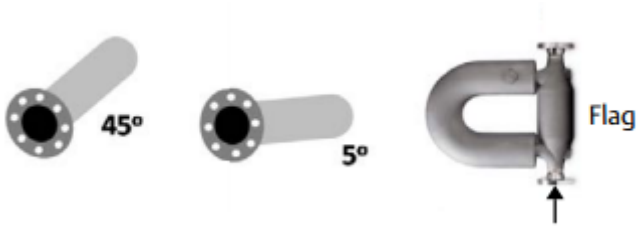

Figure 9: Most used device orientations on a drilling rig (Russel and Simons 2013).

In drilling operations the orientations in Figure 9 are used most often. Because the drilling fluid usually carries solid parts the device has to be placed in a way the solids can't accumulate in the U – part of the flowmeter to impinge measurement accuracy or possibly clog the device. When selecting a flowmeter the expected range of flowrates to be measured should be known and the model selected accordingly. For gas bubbles and cuttings to be efficiently entrained a minimum flow velocity in the measuring tubes has to be achieved. On the other side of the spectrum, if the flow velocities become too high in the flowmeter the liquid starts to corrode the inside of the flowmeter and will eventually damage it. As mentioned above it might be necessary to use more than one Coriolis flowmeter on a drilling rig each for a different section of the well to better fit the expected range of flow rates.

2.3 Magnetic Flowmeter

2.3.1 Working Principle

The electromagnetic flowmeter is based on the principle discovered by Faraday in 1832 where he discovered that a voltage is induced into a wire moving through a magnetic field. Figure 10 shows a wire moving through a magnetic field which flows perpendicular to the wire. Depending on the speed the wire is moved through the field a corresponding voltage can be measured at the wire. The same principle applies with a conductive liquid flowing through the field.

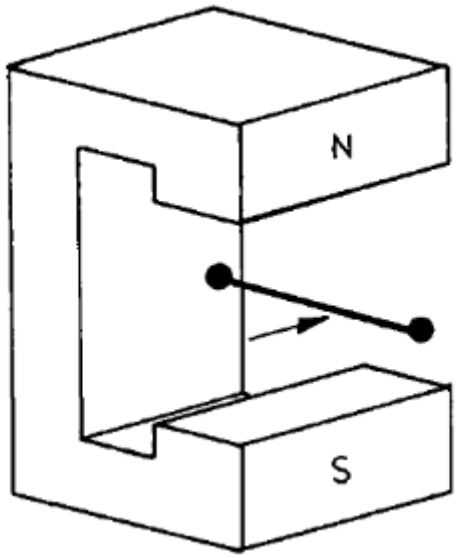

Figure 10: Wire moving through a static magnetic field (Roger 2000).

The equation below shows the proportional relationship between measured voltage, flow velocity and pipe diameter:

$$U_E \sim B \cdot v \cdot D \tag{2}$$

where B represents the induction, v the flow velocity of the liquid and D the diameter of the pipe. The flow velocity is linked to the flowrate with the relationship below:

$$q_v = A \cdot v = \frac{D^2 \pi}{4} \cdot v \tag{3}$$

An important requirement for an electromagnetic flowmeter to work the measured liquid has to be conductive. The minimum conductivity for the majority of devices is between 20 and 0.05µS/cm, additionally the pipe section where the measurement takes place has to be made of nonmagnetic material usually austenitic steel to allow the magnetic field to penetrate the pipe.

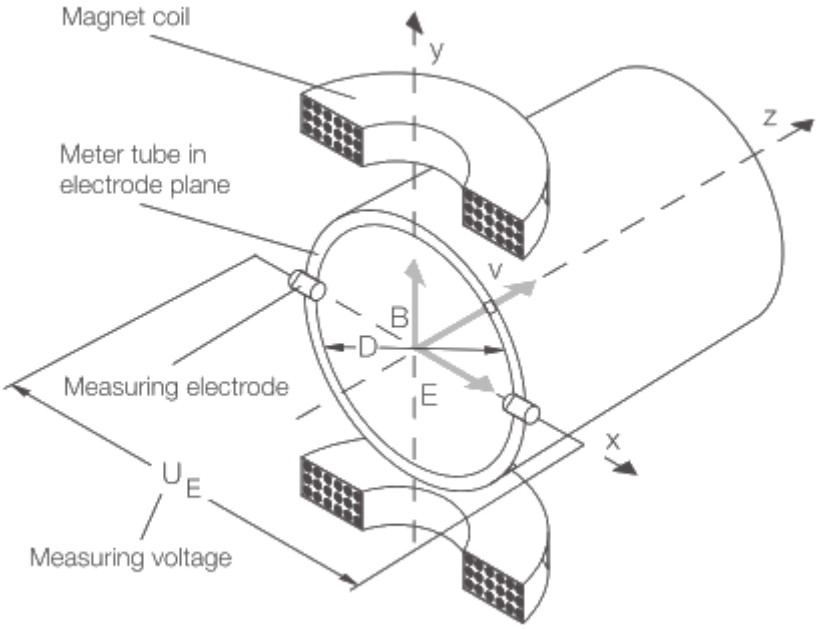

Figure 11: Schematic of an electromagnetic flowmeter continued from the figure above. instead of a wire the magnetic field is passing through a liquid which is flowing in the tube, voltage is induced at the electrodes on each side of the tube (ABB Electromagnetic Flowmeters Operating Instruction 2015).

To further improve accuracy and resistance to noisy environments as well as better zero drift performance manufacturers have applied innovative advancements in the way the magnetic coil works and interacts with the measured fluid. Usually the coil was energized with AC or DC current which led to poor measurement results especially in challenging industrial applications. The use of pulsed DC technology brought substantial improvements (Livelli 2008).

The pulsed DC excitation works at frequencies between 5-70Hz and excites the coil with an alternating square wave. In order to distinguish the noise from the signal between the alternating waves is a short period with zero volts so that the system can measure the noise and can use that in the DSP (digital signal processor) to calculate a measured value. Noise mainly arises from two sources, first the environment in which the flowmeter is located called the process noise and secondly impingement noise on the electrodes by solids carried in the liquid. According to Figure 12 it would even be better to increase the frequency even more, but as the frequency becomes higher the square wave resembles more and more the behavior of a sinus wave which makes it work like an AC drive. This phenomenon is called “drooping” of a signal.

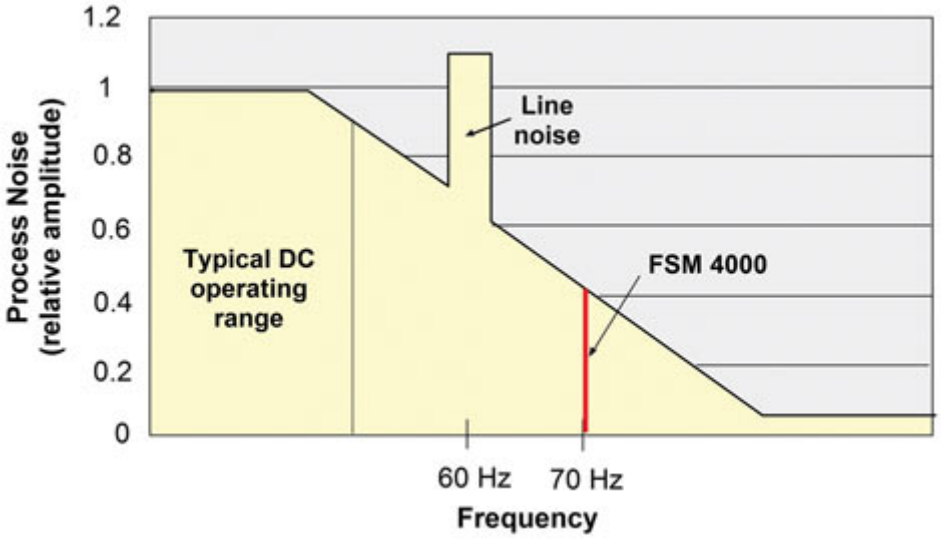

Figure 12: Typical frequency distribution in an industrial environment (Livelli 2008).

2.3.2 Advantages

- Similar to the Coriolis flowmeter electromagnetic flowmeters have high accuracies and turndown ratios.
- No obstructions in the pipe cause very low pressure drop barely different to a normal piece of pipe.
- No moving parts in the whole flowmeter causes low maintenance to be done.

2.3.3 Disadvantages

- The major disadvantage of electromagnetic flowmeters is that they can only measure conductive fluids. This makes them practically useless on drilling rigs where oil based mud (OBM) is used. And so that a rig is able to handle all kinds of drilling fluids this flowmeter is not suitable. In the past, attempts have been made to make OBM more conductive mainly for well logging reasons however no information was available for applications on drilling rigs with OBM and electromagnetic flowmeters (Carl Joseph Thaemlitz 2004).
- Gases also cannot be measured due to their lack of conductivity, however this should be of no concern for drilling operations.
- Flow distortions due to pipe bend, pumps or valves upstream and downstream can have an impact on measuring accuracy.
- It is more space saving than Coriolis flowmeters and is sometimes used for Schlumberger's FLAG service on offshore rigs where no sufficient installation space is available (Schlumberger FLAG Service Brochure 2015).
- Zero drift can be a big contributor to errors for measurements at very low flow rates.

- Chemical changes in the fluid and irregular flow patterns especially in slurries can cause measurement errors with DC measurements. Therefore the pulsed DC measurement method has to be applied.
- Likewise to Coriolis flowmeters electromagnetic flowmeters don't work in partially filled pipes.

2.3.4 Accuracy

Overall the measurement accuracies are in the same range of Coriolis flowmeters as they get sometimes substituted by electromagnetic flowmeters. However their serious shortcoming in measuring only conductive liquids makes their application very limited for drilling operations.

A typical electromagnetic flowmeter manufactured by Rosemount is specified with an accuracy up to 0.15% volumetric flow rate. The greater the turndown ratio gets the higher the measurement errors. At zero flow velocity an electromagnetic flowmeter can have a significant zero drift hence most models have a low flow cut-off function that is adjustable to a certain flow velocity. The expected flow velocity in such a device is important when choosing a size. Rosemount shows recommended flow velocities for electromagnetic flowmeters.

Table 2: Recommended velocities in electromagnetic flowmeters (Rosemount 8700 Series Data Sheet 2015).

Application	Velocity range (ft/s)	Velocity range (m/s)
Normal service	0-39	0-12
Preferred Service	2-20	0.6-6.1
Abrasive Slurries	3-10	0.9-3.1
Non-Abrasive Slurries	5-15	1.5-4.6

The necessity to choose a flowmeter size for the right velocity range could mean that the flowmeter diameter differs from the adjacent piping. For all kinds of slurries the recommended flow velocity is especially low because if the velocity gets too high the insolating liner on the inside may be damaged and eventually causing an electrical short circuit making the measurement unusable.

Electromagnetic flowmeters are especially sensitive to flow distortions from the piping system up or downstream. Therefore Rosemount recommends to have five diameters before and two after the flowmeter as a straight pipe. If such an installation is not possible the measurement will lose some accuracy, repeatability will stay the same however.

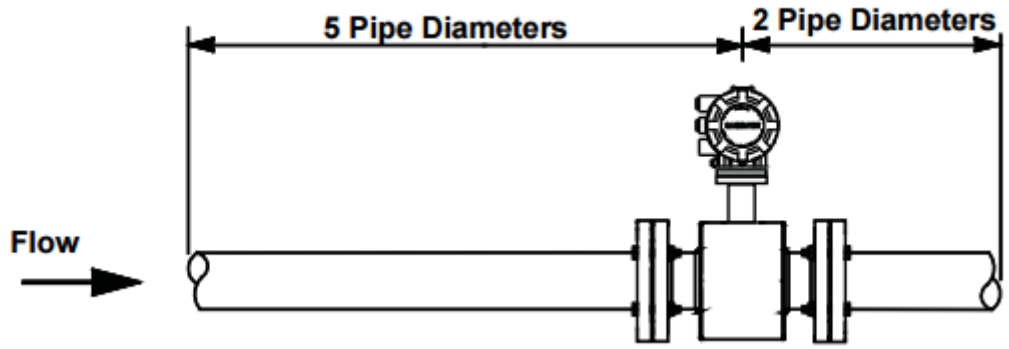

Figure 13: Recommended piping before and after an electromagnetic flowmeter (Rosemount 8700 Series Data Sheet 2015).

Although there are some models available that can measure flow in partly filled pipes it is recommended that the device is kept full at all times. Hence the manufacturer advises to install a flowmeter either horizontally in low pipe sections that are normally full or vertically with the flow going upwards through the device. If horizontally mounted it is important to keep the two electrodes as close to the horizontal plane as possible.

Under normal conditions an electromagnetic flowmeter delivers decent measurements under multiphase conditions. However Baker and Deacon reported that above a void fraction of 8% accuracy drops significantly (Baker and Deacon 1983).

2.4 Ultrasonic Flowmeter

Ultrasonic flowmeters use the principle of sound waves travelling through the measured fluid. Two general designs are available. The Doppler ultrasonic meter and the Transit-time meter. Each of these designs works best in its own specific applications. Doppler meters work best in dirty or aerated liquids like drilling fluids. The Transit time meter works best in clean fluids like water or natural gas. Hence this section discusses the principles of Doppler meters as they are more relevant for drilling operations. Ultrasonic flowmeters are available as standalone in-pipe devices or as clamp-on flowmeters. Clamp-on flowmeters are ideal for retrofitting old rigs have a lower accuracy however.

2.4.1 Working Principle

Doppler meters use the principle called Doppler Effect. They measure the frequency shift of an emitted sound wave that travels through a liquid. This works only in fluids that are not clean because the sound waves have to collide with particles in the fluids such as gas bubbles or solids in order to work.

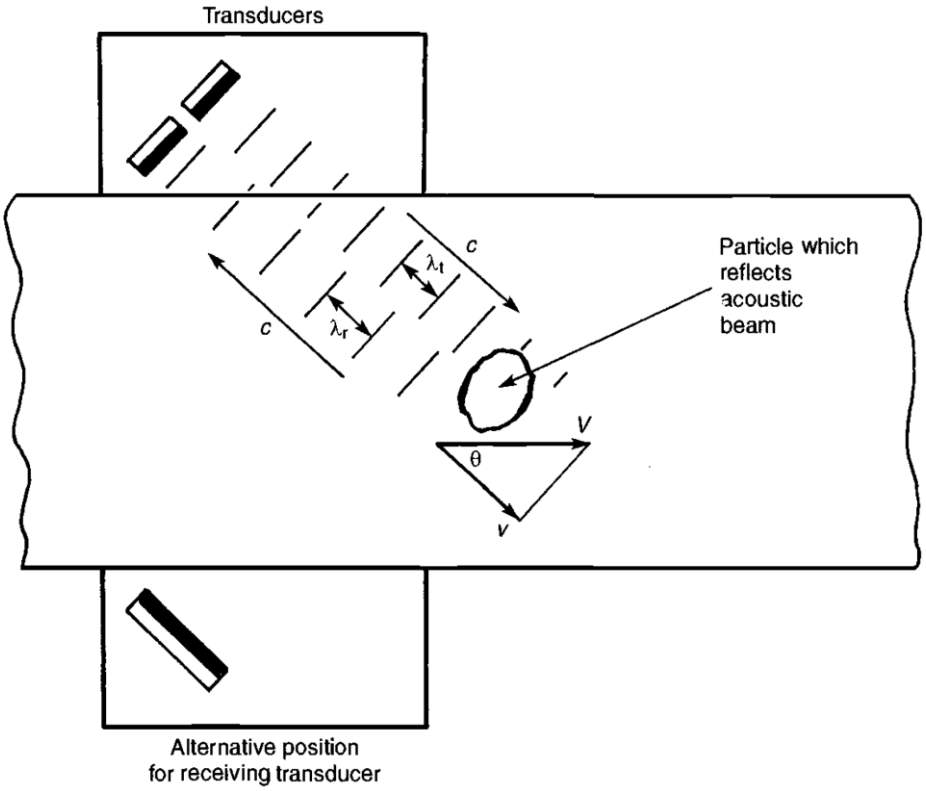

Figure 14: Schematic of a Doppler ultrasonic flowmeter (Roger 2000).

The flow velocity and the volume flow rate respectively can be determined with the equation below. The transmission frequency usually lies in the MHz range in order to prevent outside noise to harm the measurement.

$$v = \frac{c \cdot \Delta f}{2 f_t \cdot \cos\theta} \tag{4}$$

$c \ldots speed\ of\ sound\ in\ the\ fluid$

$\Delta f \ldots frequency\ difference\ between\ emitter\ and\ receiver$

$f_t \ldots transmission\ frequency$

$\theta \ldots relative\ angle\ between\ fluid\ flow\ and\ ultrasonic\ beam$

2.4.2 Advantages

- No obstructions in the pipe cause less problems during operation.
- In addition to in-pipe flowmeters there are clamp-on models available which are easy and fast to install and deliver accuracies almost as good as the inline models.
- No pressure drop makes it possible to use it also as outflow flowmeter on conventional rigs.

2.4.3 Disadvantages

- Lower accuracy than Coriolis or electromagnetic flowmeters due to a large dependence on temperature, fluid density, sonic conductivity and flow profile.
- Susceptible to surrounding vibrations, especially clamp-on models.
- Dependent on even flow profile, hence long straight pipe section before and after the device are required.

2.4.4 Accuracy

A clamp-on flowmeter capable of measuring drilling fluids produced by Expro is specified for a flowrate accuracy of 2 percent and a repeatability of 0.3 percent (Expro QEX1000 datasheet 2015).

Similar to electromagnetic flowmeters ultrasonic flowmeters are required to have a certain length of straight pipe before and after the flowmeter in order to have an even flow profile at the measuring point. The measurement accuracy is highly dependent on the flow profile, therefore some manufacturers build several transmitters into their devices to measure the flow velocity on different parts of the cross-section to get a more averaged flow velocity measurement.

Another issues that might have an impact on accuracy is the potential accumulation of cuttings on the bottom of the pipe. Hence the flowmeter is optimally placed on a vertical pipe.

The achievable turndown ratio is given with 100:1 however at low velocities cuttings and gas bubbles might induce more errors.

2.5 Open Channel Flowmeter

In the following section the most commonly used open channel flowmeters on drilling rigs are presented. Compared to filled pipe flowmeters open channel flowmeters have different requirements in terms of how to measure the passing flow. In many respects it can be considered more difficult to measure a liquid flow in an open channel with the same accuracy as filled pipe flowmeters. When taking a quick look and comparing the accuracies of Coriolis, Magnetic or Ultrasonic flowmeters to the widely used paddle flowmeter for example these challenges are obvious. Some advances have been made to measure accurately with the aforementioned flowmeters even in open drilling systems by resembling filled pipe flow but for actual open channel flow in partially filled pipes accuracy is more difficult to achieve.

2.5.1 Flow Paddle and Pit Level Sensors

Paddle flowmeters are the most used outflow sensors on conventional drilling rigs especially onshore. They are cheap and easily maintainable. However compared to more sophisticated flowmeters the accuracy is very poor. Another contributing factor is the constant oscillations on the flow channel surface inducing errors to the paddle reading. The achievable accuracy lies in the range of 5 to 10 percent (Chopty and Sardo 2011, Schafer, et al. 1992).

The flowrate that is measured cannot be quantified for the paddle alone. The output signal only gives the paddle position relation to full opening. Constant recalibration is required to keep measurements somewhat accurate. Mud particles can stick to the paddle making it heavier and therefore harder for the fluid to lift it. To get a somewhat accurate and quantifiable volume measurement level sensors in the mud tanks measure the height of the fluid which can then be converted to volume. These sensors are however prone to inaccuracies by foam, fluid oscillation in the tank and dirt.

The deflection angle of the paddle flowmeter is measured either by a potentiometer or a strain gauge. Generally flow paddles are very rugged and can handle harsh rig conditions very well. Many newer models are also made lighter and enable it to be installed and serviced by just one person.

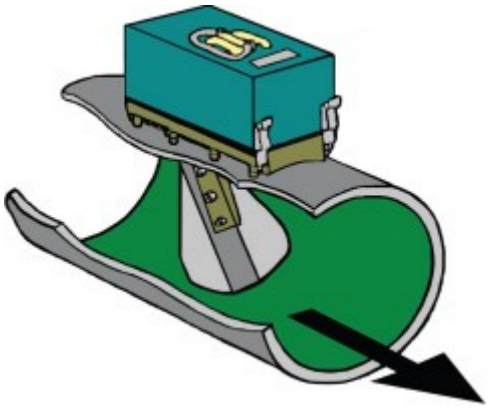

Figure 15: Typical paddle flowmeter in a partially filled pipe flow channel (Mitchell 2006).

As already mentioned the measurement from a paddle flowmeter is just of qualitative nature because it completely ignores the velocity of the passing flow, therefore makes it almost impossible to quantify flow accurately.

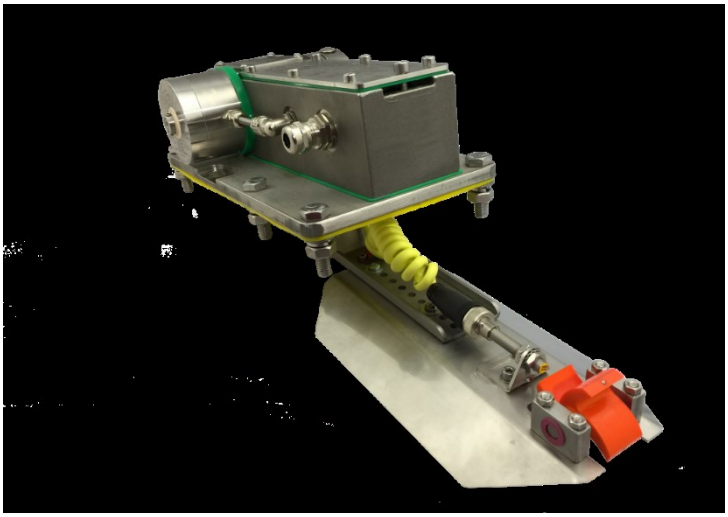

Figure 16: Paddle flowmeter with integrated velocity wheel by Rigminder (Rigminder 2015).

Figure 16 shows an attempt to incorporate a velocity measurement into the paddle meter with a small paddle wheel at the end. A hall sensor measures the revolution per minute (RPM) of the wheel and can get a velocity reading from that. Methods to combine height and velocity readings to measure flow rate are more deeply discussed in the later chapters especially in the practical part concerning flow simulations to measure flowrate cost effectively and accurately.

In addition to the paddle outflow meter most rigs have a pit volume totalizer (PVT). A PVT is a device that gathers pit level data from multiple mud tanks on the rig and gives an alarm if abnormal trends occur.

Figure 17: Typical PVT console informing the driller about mud tank volume and flow rate (pason n.d.).

Usually three different types of sensors exist to measure pit levels. It can either be done by radar, ultrasonic or by a swimming level meter. Radar and ultrasonic meters can also be used to measure the fluid level in the mud return line instead of a paddle meter.

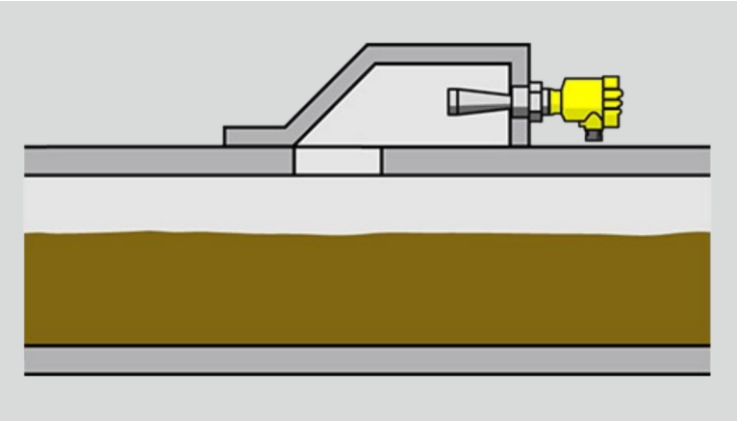

Figure 18: Typical installation of a radar level meter in a mud return line (Vega n.d.).

The accuracy given for a level meter seen in Figure 18 is given at ±2mm. Hence the accuracy in the mud return line depends on the position. The further down the pipe the shallower and faster flowing the drilling fluid becomes, hence the level measurement quality decreases. The sampling rate of level meters is typically greater than 10Hz which requires to average the signal over a duration of several seconds in order to reduce the effect of surface ripples and instabilities.

2.5.1.1 Advantages

- The relatively low price makes it attractive in an low oil price environment with tight budgets.
- The installation and maintenance is simple and can be done by one person compared to other flowmeters.
- Personnel is more likely familiar with these sensors and can fix issues without third party support.
- Radar and ultrasonic level meters are independent of fluid properties and do not interfere with the flow if installed in the mud return line.
- Radar and ultrasonic level sensors are wear-free.

2.5.1.2 Disadvantages

- The accuracy is the worst among the discussed flowmeters.
- The flow paddle gets easily worn by the solid material that is carried with the drilling fluid.
- Regula recalibration is required to maintain a reasonable accuracy.
- Pit level sensors are susceptible to foam, dirt, rig oscillation.
- Little time to react after kick event was detected.

2.5.2 Rolling Float Meter

Aside from the widely used paddle flowmeter several other designs have been developed over the last decades to not only improve open channel flow measurement but also to make it more accurate, repeatable and quantifiable. The obvious way to quantify flow in an open channel is to integrate the filled area of the channel cross-section and the flow velocity to be able to calculate a flowrate. One way to do this is the rolling float meter presented in this chapter. It works by means of mechanically interacting with the channel flow.

This flowmeter consists of a hinged arm and a wheel that is mounted at the end of this arm. The wheel is usually made of light plastic or foam material that swims on the liquid in the channel. The fluid height in the channel is usually determined by strain gauges or potentiometers. As the liquid level changes the hollow wheel is floating on it and affects the angle of the arm it is mounted to.

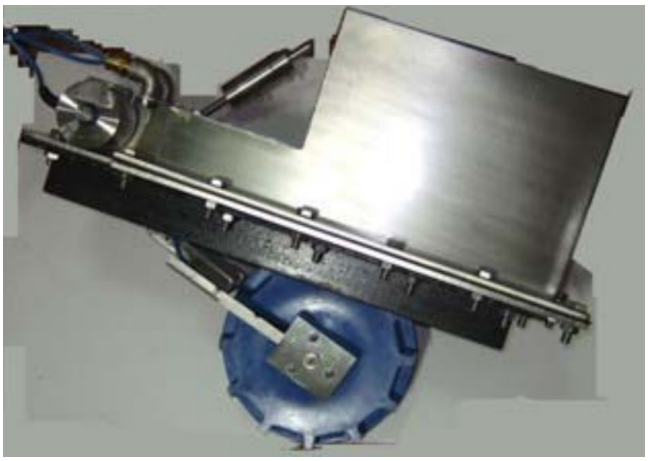

Figure 19: Example of a typical rolling float meter (Enertek 2012).

The floating wheel is made of a light high temperature resistant plastic material and is intended to roll over the free surface of the passing flow below it. The light weight is especially important for measuring low velocities and for a better reaction of velocity changes. The rotating velocity is measured with a tachometer. It can work either optically or magnetically. A defined number of shading stripes or magnets are incorporated into the wheel. The hall sensor of photodiode circuit produces a binary signal with a frequency linearly related to the rotation of the wheel hence the flow velocity. In the case of the model presented in the picture above the tachometer function is implemented redundantly to improve reliability in rough field conditions.

This flowmeter is intended to be used in partially filled pipes and open trough channels on rigs where minimal modifications are desired.

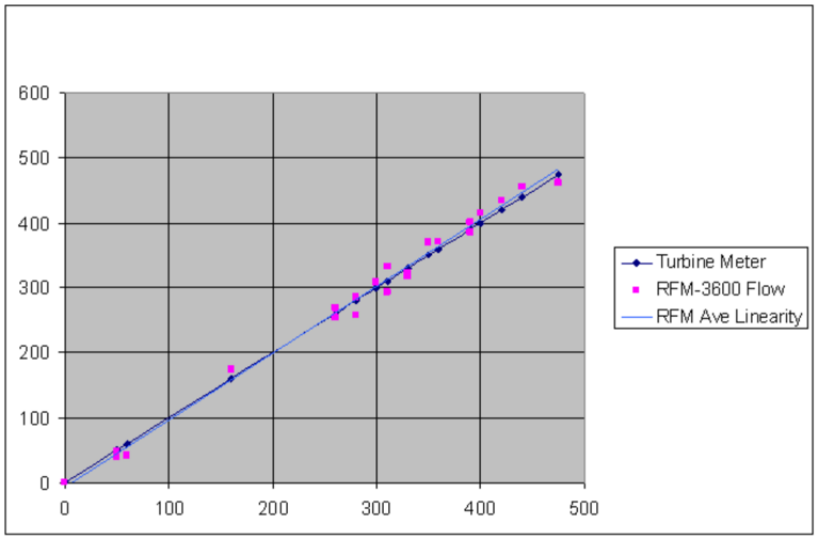

Figure 20: Linearity comparison of a turbine flowmeter to a rolling float meter (Enertek 2012).

Figure 20 shows the excellent linearity performance of such a rolling float meter. Originally this flowmeter was developed and tested by the Sandia National Laboratories for the United States Department of Energy and in their prototype report it also shows the remarkable similar performance to more expensive flowmeters (Loeppke, et al. 1992). This rolling float meter was estimated to cost just 1800$ at the time this report was written.

2.5.2.1 Advantages

- Easy installation in partially filled pipes or open trough channels by one or two persons. Newer models are relatively lightweight compared to more traditional models (25kg vs. 45kg) and can therefore be handled with less effort (Enertek 2012).
- Maintenance can be done by one person and it is also possible to inspect the device during operation. The relatively simple working principle makes it easy to troubleshoot malfunctioning flowmeters on a first look compared to other flowmeters.
- The rugged design makes is very favorable for harsh drilling rig conditions.
- The volume flow measurement which is derived from two separated measurements is surprisingly accurate compared to conventional flow measurements. In the prototype report published by the Sandia National Laboratories the rolling float meter could achieve an accuracy of 0.5 – 1% and was even able to detect minor lost circulation and influx events (Loeppke, et al. 1992).

2.5.2.2 Disadvantages

- The temperature rating of 135° for this flowmeter might become a problem for geothermal and high temperature drilling applications (Enertek 2012).
- A flowmeter like this is relatively rare on the drilling rig market and according to the literature research that has been done only one commercial manufacturer for this type exists. Hence there is a lack of actual application experience data.
- The seemingly low level of awareness towards this flowmeter might prevent widespread installation even with superior cost normalized performance.

2.6 Flowmeter Comparison

In the previous chapters a more detailed overview of the various flowmeter types was give and how they can handle harsh drilling rig conditions. When constructing a new rig or upgrading an old one it can be challenging to find the right flowmeter for the intended application. This is especially true for fluid outflow measurement of drilling rigs and even more so in open drilling systems that usually have open channel outflow.

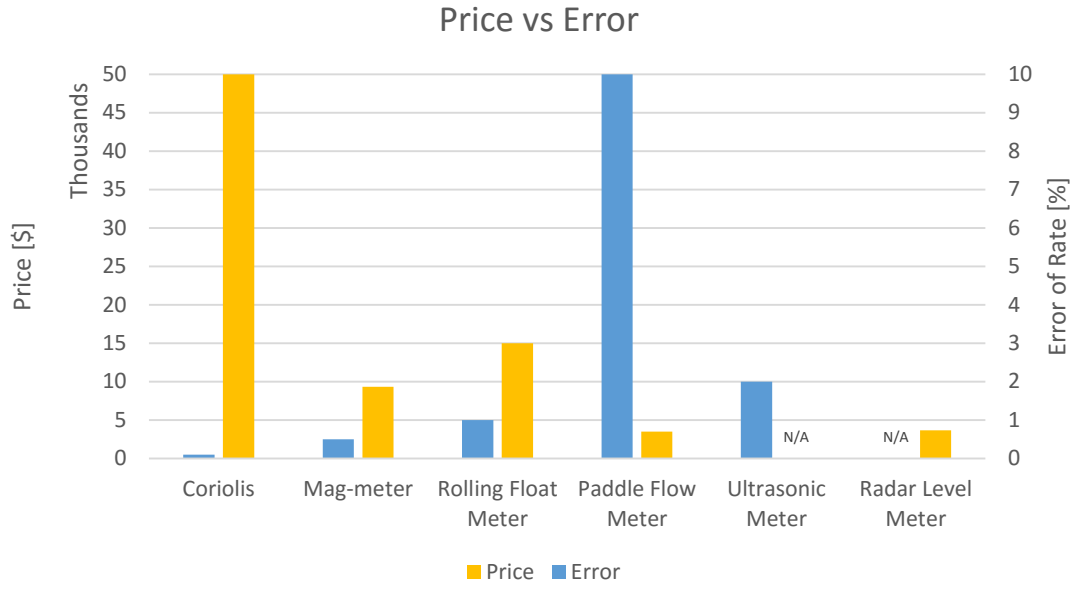

Figure 21: A price and error comparison of the major flowmeter types (M. /. Process 2015, R. /. Process 2015, 4runntertech 2016, VEGA 2016, Expro, ActiveSonar QEX1000 Flow Meter Datasheet 2016).

The figure above shows the most commonly used flowmeters compared in terms of their price and accuracy. The accuracy or error in this case is defined as the error based on the absolute value of change. On the one hand there is the Coriolis type with a very high price and exceptional accuracy and on the other side of the spectrum is the well-established paddle flowmeter with very low cost but poor accuracy and limited ability to quantify flowrates. Although both the Coriolis and the Magnetic flowmeter have the best accuracies in this comparison the rig modification effort should not to be overlooked. Both need the outflow line modified so that there is always a filled pipe at the device (Figure 3). To maintain their high accuracy under very low flowrates can even increase the price further. Those flowmeters are very dependent on fluid velocity in the device. Therefore a second flowmeter with a smaller diameter can be installed which would almost double the price. Additionally the Magnetic flowmeter has the huge disadvantage of being incapable of measuring non-conductive fluids which lowers the rigs versatility.

Taking latter statements in consideration the rolling float meter looks favorable in many ways. The price is reasonably low with good accuracy and the flowmeter can be installed

directly on the outflow line without additional modifications. The accuracy gain from upgrading from a paddle to a rolling float meter is much more significant in relation to cost and complexity that the other flowmeter types.

As largely known the rate of adapting new technologies in the oil and gas sector is very slow compared to other industries. The same is true for the adaption of the rolling float meters. According to Forerunner Technologies LLC the rolling float meter is underrepresented in the rig marked despite it being the most cost effective kick detection device. To date only 30 units have been sold which would only be 1.9% of the US onshore oil rig market at its height in summer 2014 (4runntertech 2016).

According to a leading manufacturer of ultrasonic flowmeter such flowmeters are very rarely used on their own for outflow measuring. Ultrasonic flowmeters face similar challenges as the Coriolis and Magnetic flowmeter in terms of rig modifications and are only of limited use in open channel measurement because the conditions have to be known and tightly monitored to maintain accuracy. However often passive ultrasonic sensors are used in combination with Coriolis and Magnetic flowmeters to calibrate those flowmeters for changing gas volume fractions hence improving their accuracy, reliability, possible range of operation and early gas kick detection (Expro 2016).

Chapter 3 Open Channel Flow

Liquid flow can take place in two general forms, a pressure driven flow which is also often referred to as pipe flow and open channel flow whose main driving mechanism is gravity. In this chapter the phenomena of open channel flow are explained in more detail because the simulations are based on conventional drilling rigs therefore open systems that have open channel outflow behavior.

Open channel flow takes place in natural channels such as streams and rivers but also in manmade structures such as sewer systems and irrigation canals. One major distinguishing feature of open channel flow compared to pipe flow is the presence of a free surface that is under atmospheric pressure conditions. Even though in this thesis a closed conduit is used for simulation, the pipe is partially filled all the time which means open channel flow conditions apply (Harlan H. Bengston 2011).

Figure 22: Examples of naturally occurring and manmade open channel flows (Freebigpictures.com 2009, Martin 2012, Ponce n.d., G. I. Inc. n.d.).

3.1 Flow Classification

Open channel flows can be classified according to several factors:

- Steady state / Unsteady state flow
- Laminar / turbulent flow
- Uniform / non-uniform flow
- Supercritical / subcritical / critical flow

Steady and unsteady state flow conditions refer to the change of flow velocity and magnitude over time. When velocity and flow rate remain constant over time steady state flow is present. For many open channel flow problems often steady state flow conditions are assumed with its corresponding formulas for simplicity reasons. However in practice most problems are of transient or unsteady state nature. Hence in the simulation the model was solved as a transient problem because flowrate was ramped up stepwise to study flow phenomena in the outflow line. Although between steps sufficient time was allowed to reach stead state condition in the channel it was not clear if oscillation would occur at some point and hence a more computational expensive transient simulation was necessary.

The classification into laminar and turbulent flow is another regularly used concept in fluid dynamics that is used in open channel and pipe flows. The major factor to predict whether a flow is laminar or turbulent is the widely known Reynolds number. Osborne Reynolds, born in 1842 conducted an experiment where he injected dye into a stream of flowing water and observed a behavior where the dye starts to deviate from its straight path and begins to oscillate and finally mix with the water.

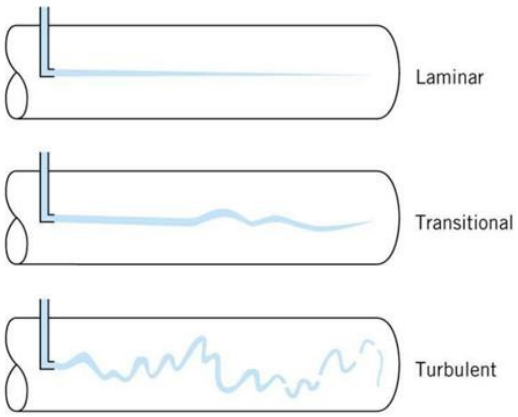

Figure 23: The Reynolds experiments showing the effects of dye mixture with increased flow velocity (Visavale 2014).

He discovered that this phenomenon was governed by a relationship between flow velocity, characteristic length and viscosity of the transport fluid. This relationship resulted in the famous Reynolds number which is used in many fluid mechanics problems today.

$$Re = \frac{inertial\ forces}{viscous\ forces} = \frac{\rho \mathrm{v} L}{\mu} = \frac{\mathrm{v} L}{\nu} \tag{5}$$

v ... $maximum\ flow\ velociy$

L ... $travelled\ length\ of\ the\ fluid$

μ ... $dynamic\ viscosity$

ν ... $kinematic\ viscosity$

ρ ... $fluid\ density$

For open channel flows below a Reynolds number of 500 flows are usually laminar and above 12500 they are turbulent. For the transition range between 500 and 12500 the flow is either laminar or turbulent which depends on other conditions such as upstream channel conditions and roughness of the channel wall.

In section of an open channel where cross sectional area, slope, flow rate and velocity are constant flow conditions tend to become uniform. In transitional zones of one of the above mentioned factors however open channel flow becomes non-uniform as seen in the figure below. The Manning equation which is explained in later sections only works for uniform flow conditions.

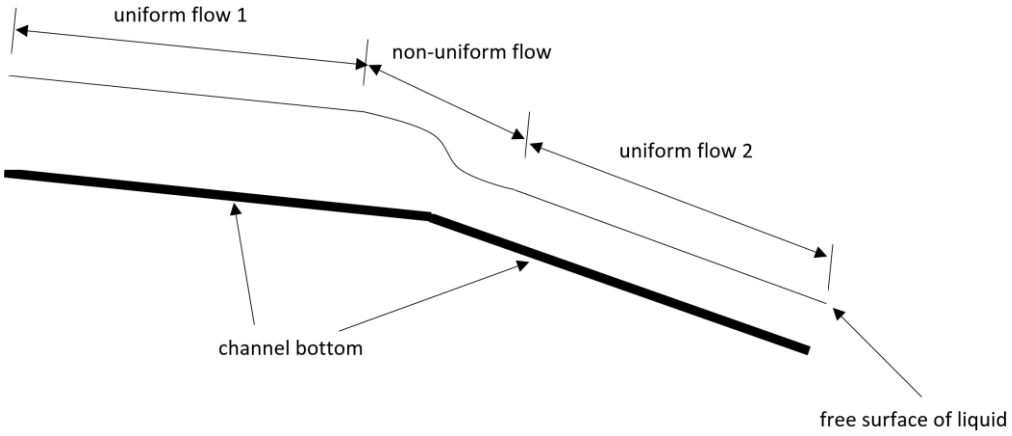

Figure 24: Difference between uniform and non-uniform flow (engineeringexcelspreadsheets.com 2012).

The last open channel flow classification factor is the supercritical, subcritical or critical flow. In comparison to the already discussed factors this one is less obvious and intuitive. The Froude number is used to determine the state of a flow. If the number is below 1 the flow is subcritical, if the number is above 1 the flow is supercritical and if it is equal to one it is defined as critical. Usually subcritical flows occur in relatively deep and slowly flowing channels whereas supercritical flow occurs in shallow fast channels.

$$Fr = \frac{\mathrm{v}}{\sqrt{gD}} \tag{6}$$

v ... $flow\ velocity$

D ... $hydraulic\ depth$

g ... $gravity$

The Froude number is a dimensionless number that describes flow regimen of open channels. It is derived as the ratio of inertial and gravitational forces. It is a measurement of bulk flow characteristics such as waves, sand bed forms and flow/depth interactions at a cross section or between boulders.

3.2 Specific Energy Concept

Specific energy is one of the most important concepts in open channel fluid mechanics. This concept is closely tied with the Froude number discussed above. It originated from Bernoulli's principle and assumes that for any given cross-section in a flow channel the specific energy of the fluid is the same, excluding the friction losses. This means that a flow has either a high potential energy and is therefore deep or it is fast flowing and shallow. Both flows can have the same energy but one is supercritical and the other one subcritical.

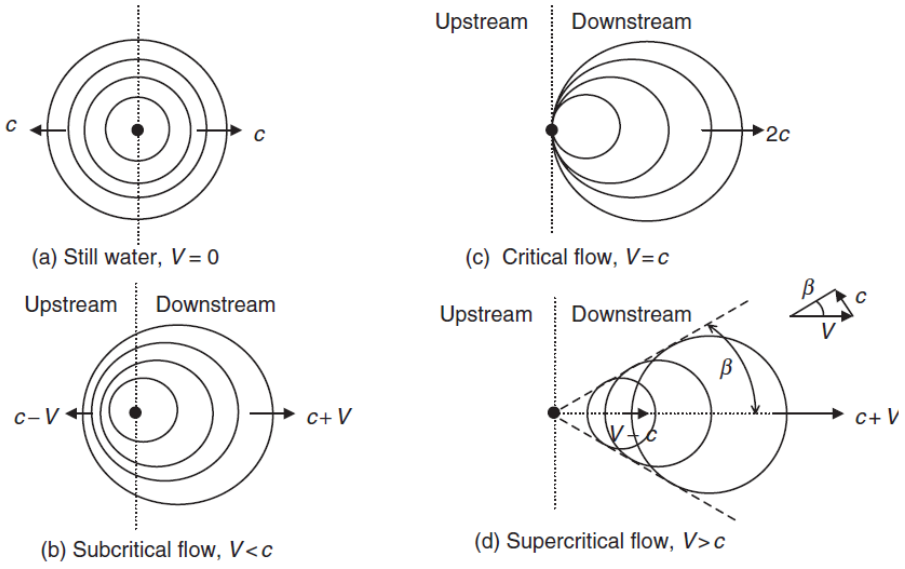

Figure 25: Explanation of different flows and their upstream disturbance behavior (Akan 2006).

The Figure above shows the difference between subcritical, critical and supercritical already mentioned in the previous section. It is the relationship between the flow velocity and the propagation velocity of a wave caused by a disturbance in the flow path.

At a certain flow velocity the disturbance can't carry any information upstream any more this point is defined as the critical velocity. The critical velocity also comes with a critical depth that corresponds to the specific energy of the flow. The relationship between those two can be seen in Figure 26 for increasing flow rates.

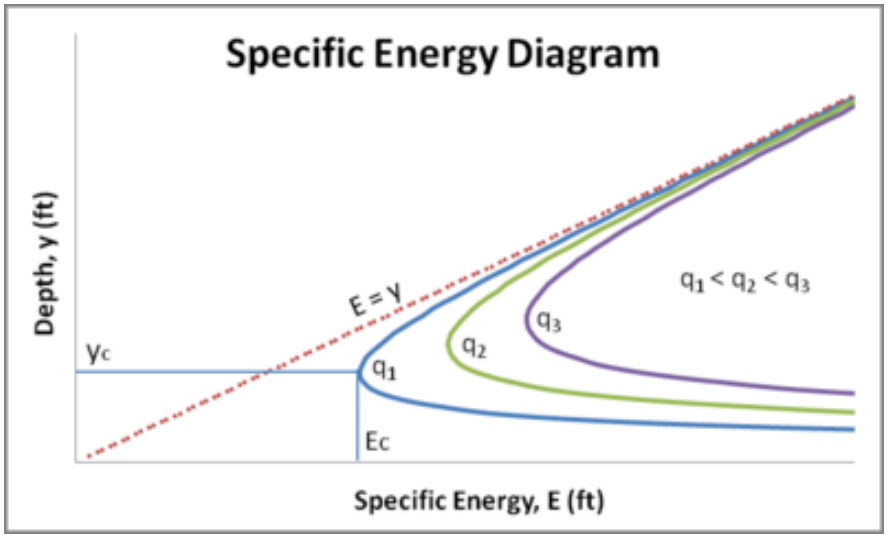

Figure 26: Specific energy diagram for three different flow rates (Lally and Hixon n.d.).

For fluid measurement in open channels this becomes important as it is not desired to have measurement influences by other downstream components. Below the equation of the specific energy is given showing the two components of potential and kinetic energy. As this concept applies to open channels the pressure term is everywhere the same and the friction losses are neglected. This relationship can be applied to all different shapes of channel cross-sections, however more complex shapes might only be solved numerically.

$$E = y + \frac{Q^2}{2gA^2} \tag{7}$$

E … $flow\ velocity$

y … $depth$

Q … $discharge$

A … $cross-sectional\ area\ of\ stream$

g … $gravity$

Chapter 4 Methodology

In this section the detailed steps will be explained how the model was built and how the simulation results were obtained. Basically a CFD (computational fluid dynamics) study consists of a series of steps that have to be worked through carefully in order to obtain a good result. Figure 27 shows a rough breakdown of the workflow. As fluid dynamics problems can become extremely complex and computationally expensive with small changes in the pre - processing phase it is generally recommended to start very simple and with each iteration increase the complexity of both physical properties as well as increased resolution of the mesh.

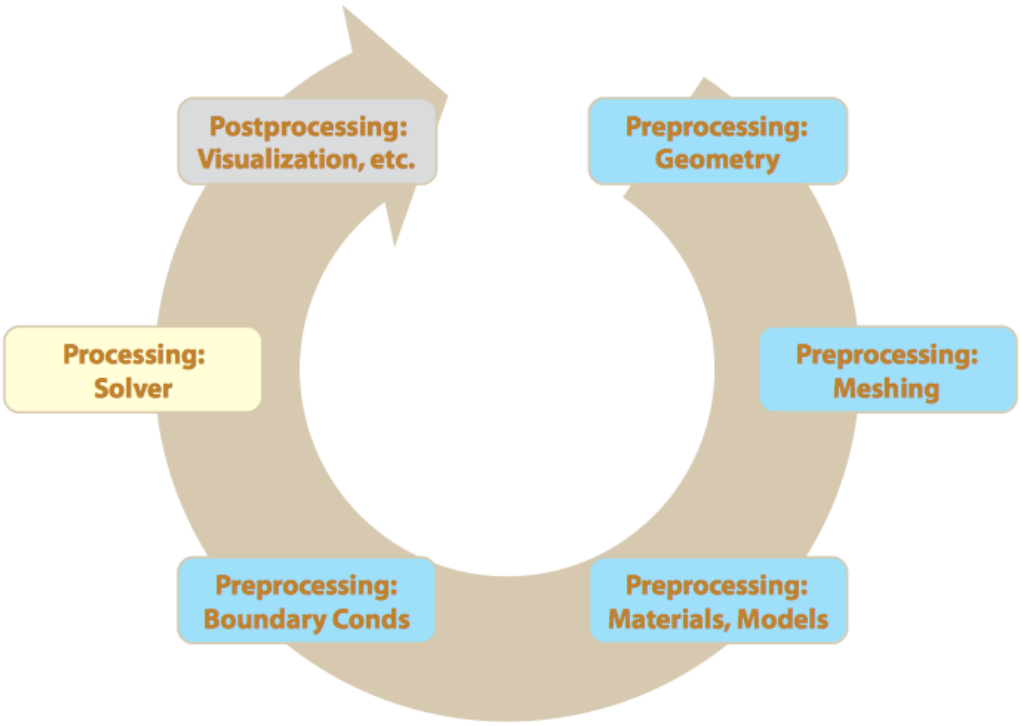

Figure 27: Schematic of a typical workflow in CFD studies (University of Illinois n.d.).

As mentioned before, accurate results demand an appropriate mesh resolution, according to the problem at hand, however simulations may quickly become computationally expensive. Therefore for the scope of this study a series of simplifications in form of assumptions had to be applied to keep the project within the intended timeframe.

4.1 Pre - Processing

This part of the CFD lifecycle is the most essential in order to obtain meaningful results that resemble reality as close as possible. Depending on what problem is to be solved the geometry and subsequent meshing have to be done carefully.

In this study the problem at hand is getting an understanding of the outflow behavior of a drilling fluid return line in an open drilling system. The main goal is to understand fluid height relationships in the flow channel on a macroscopic scale. Hence a turbulence model with standard wall functions approach was applied and the mesh adapted accordingly.

4.1.1 Geometry

For the purpose of the simulation a geometrical model of the flow domain was created based on actual rig data. The geometry consists of the bell nipple and a 10 m section of the fluid return line where the flowmeters are usually situated. The fluid return line of the base case has a drop angle of 30° and a circular cross-section. Both bell nipple diameter and fluid return line diameter are based on standard pipe sizes.

- Bell nipple diameter: 20″ (50cm)
- Fluid return line diameter: 12″ (30cm)

The geometry was created in the 3D design software Rhino 3D. For the geometry to be recognized as actual flow domain by Fluent it has to be completely watertight, which means that the elements of the model are solid shapes without openings in the outer surfaces.

Although more computational expensive a five inch cylinder cutout was included in the center of the well outlet to represent a static drill pipe as preliminary simulations have shown that the difference in the channel fluid levels was significant. Furthermore the model was cut in halve at the symmetry plane in order to save CPU time for the simulations and keep the results exactly the same.

The figure below shows the geometric model of the base case with a pipe slope of 30 degrees. The other two geometrically varying cases look similar but with the slope angels varied to 20 and 10 degrees respectively. Aside from that no further geometric changes were made in the simulation cases as the results would increasingly lack comparability as the model differs from the base case and for each new model a mesh independence study would have to be done in order to ensure limited simulation errors and consistency which would have gone beyond the scope of this project.

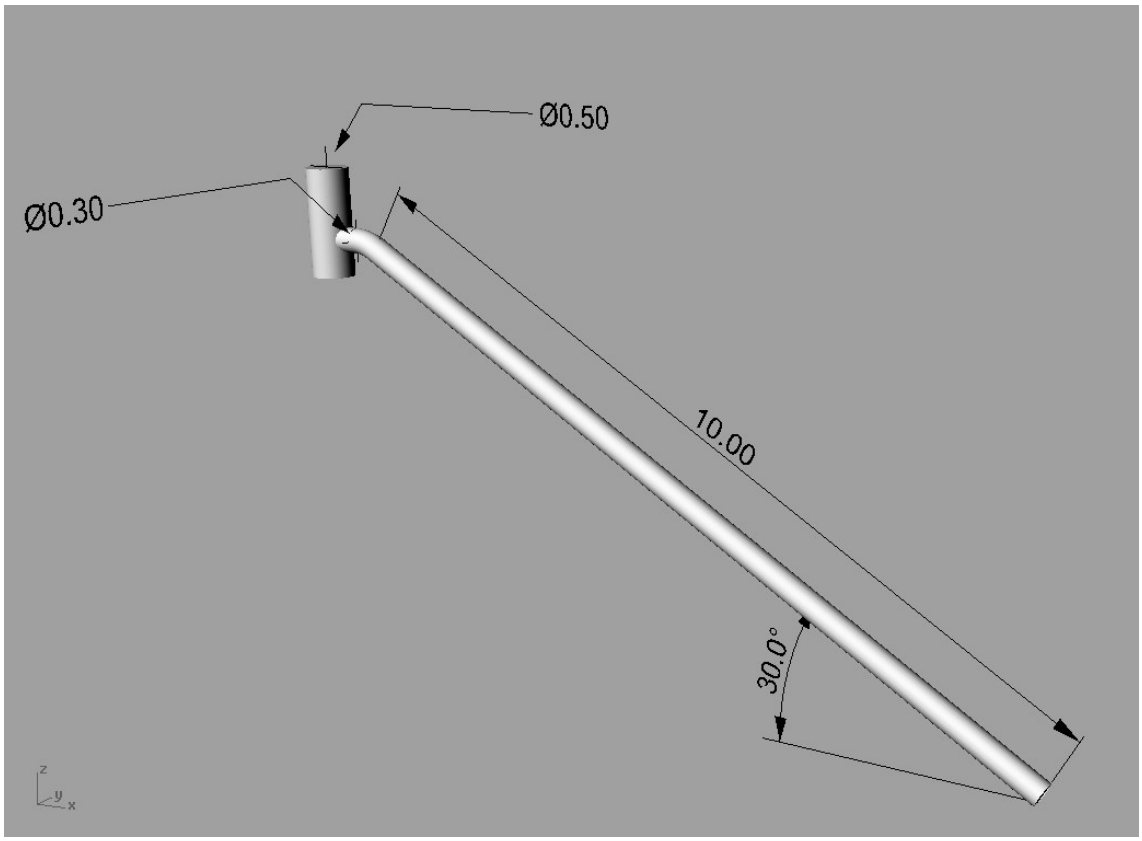

Figure 28: Geometry of the base case flow domain with the most important dimensions in meters.

4.1.2 Meshing

In the meshing process the watertight geometry of the flow domain is discretized into computational cells necessary for the subsequent simulation. This process is done automatically by the meshing tool. The provided model consists of three parts: the bell nipple, the pipe bend and the straight pipe section. The meshing tool has a variety of input parameters that control the meshing process such as the cell size. For the purpose of this simulation the goal was to have the model meshed in a sufficiently high resolution to show the intended flow phenomena.

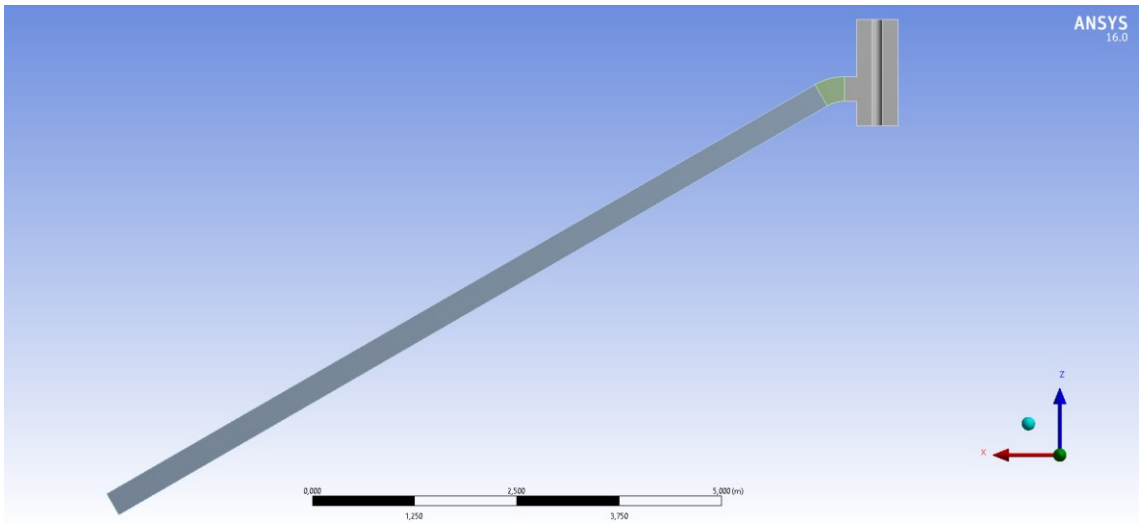

Figure 29: Cross-section of the model prior to the meshing process.

However from a certain point upwards there is no additional information gained by increasing the resolution. The only effect is an increased demand in processing power hence an increased simulation time. For this analysis the highest resolution part of the flow domain is the straight pipe section because this is the section of interest for this work. The two other sections have been given lower resolutions in order to minimize simulation time and to save unnecessary computational effort.

Figure 30 shows the different mesh sizes after the meshing process. It is important to make cell size transitions not too sudden and the size difference not too large because this could result in numerical instabilities later or artefacts in the results. Therefore the meshing of the pipe-bend acts as a transitional mesh from the rough mesh of the bell nipple to the high resolution part of the straight pipe section.

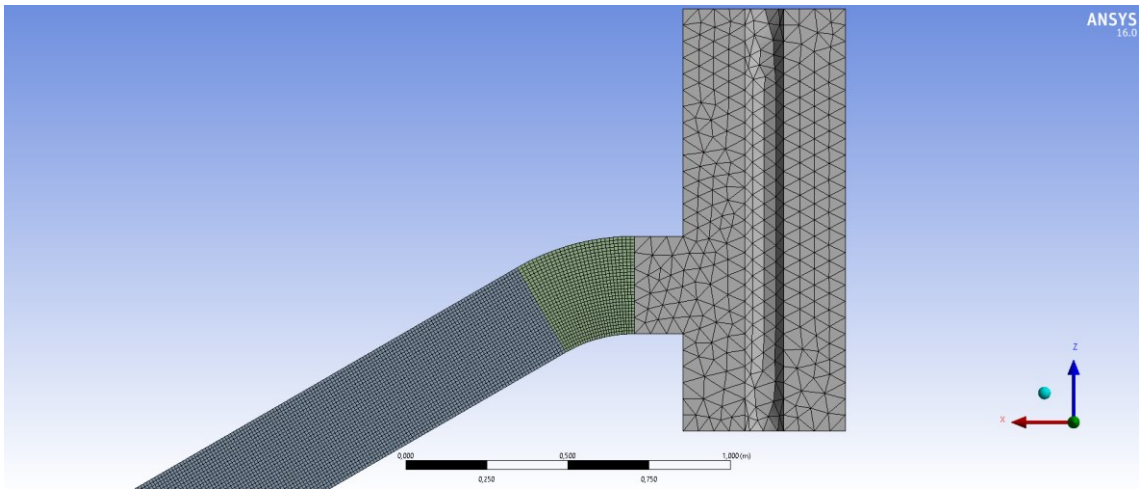

Figure 30: Comparison of mesh sizes of the three different flow domains.

In the figure below a cross section of the straight pipe section mesh can be seen. For this study the use of additional boundary layer cells was refrained from due to the mentioned limitations and the macroscopic scope of this project where boundary layer phenomena are likely negligible.

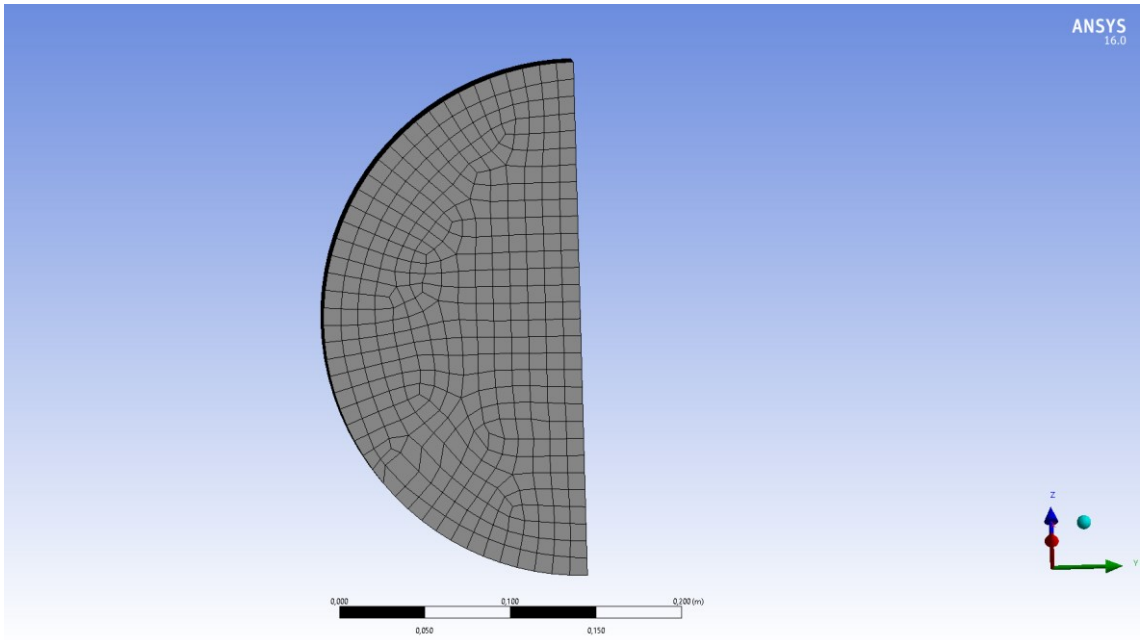

Figure 31: Meshed cross section of the straight pipe section.

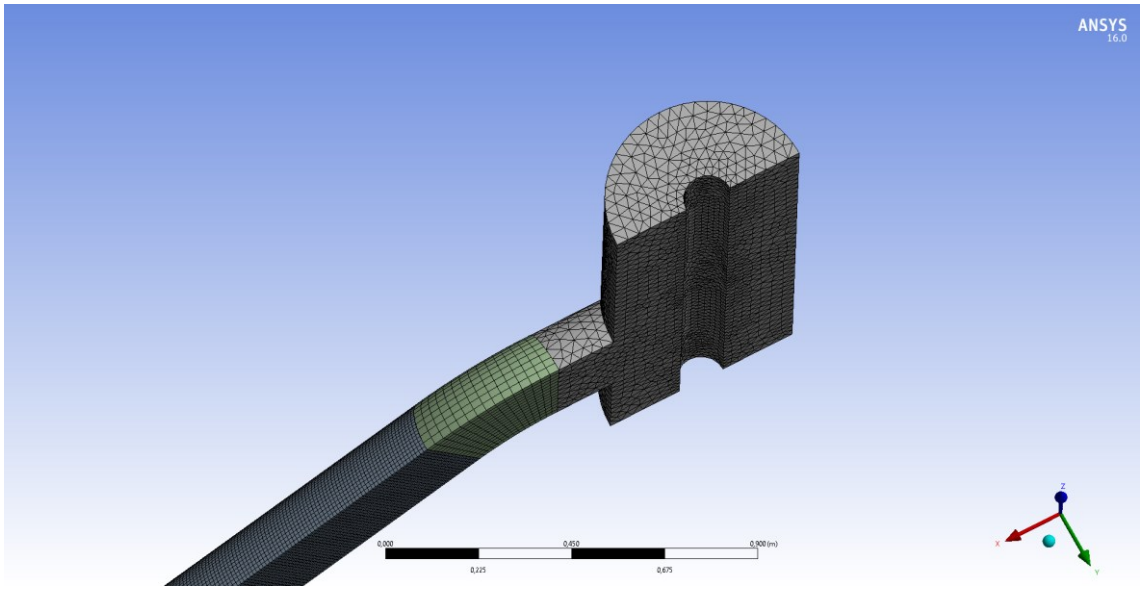

Figure 32: Final meshed model reduced to its symmetry half with the included drill pipe cutout.

4.1.3 Boundary Conditions

To further reduce the computational effort that has to be applied the model was reduced to its symmetric half. This particularly works for this model because it is symmetrical in

the XZ plane as seen in Figure 33. This measure saves about half of the needed simulation time. In the simulation software the areas in red were defined as symmetry planes instead of a wall boundary condition to take this into account (Figure 33). As another model alteration the top surface of the model was defined as a wall boundary instead of an "atmospheric" boundary condition because it made the simulation significantly more stable and resulted in a close solution.

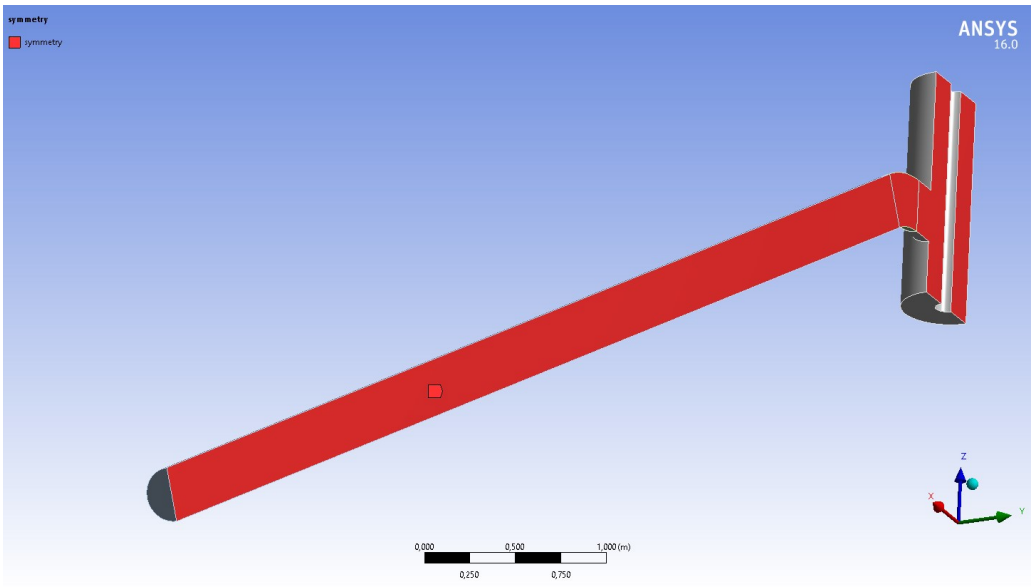

Figure 33: Symmetry plane of the model (red).

As the inlet boundary a velocity boundary condition was chosen where the velocity to the respective flowrate was defined. The direction of the velocity vectors is in Z-direction and uniformly distributed (Figure 35). Additionally the introduced flow is also assumed to have no turbulence when entering the domain because it can be assumed that drilling fluid flowing up the annulus is reasonably slow and laminar. The Reynolds number for the 1500gpm case was calculated at 1.5×10^{-5} which shows laminar flow for pipes.

The velocity boundary works in a way that it tries to hold the flow velocity at the defined value regardless of other flow properties. This makes it primarily useful only in incompressible flows because for compressible flows it would lead to nonphysical behavior due to the floating of stagnation conditions to any level.

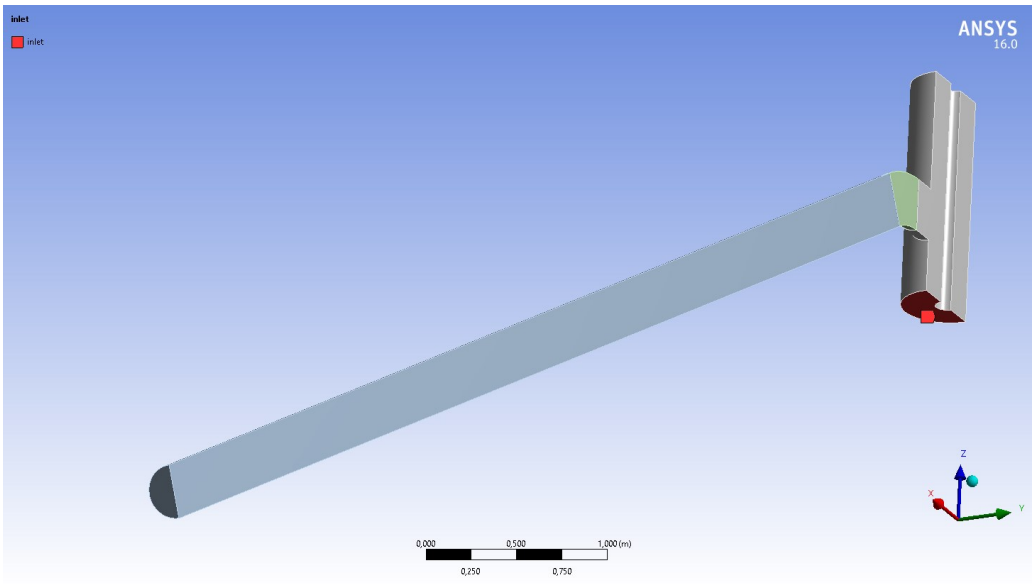

Figure 34: Inlet surface to the flow domain (red).

Figure 35 shows a cross-section of the model at its initial condition. The simulated fluid enters the domain from the bottom with a velocity marked by the vector arrows. It is also defined that only one phase enters the domain without other phases such as gas bubbles or solids. This input velocity is changed throughout the simulation to resemble a stepwise increasing scheme as shown in later chapters.

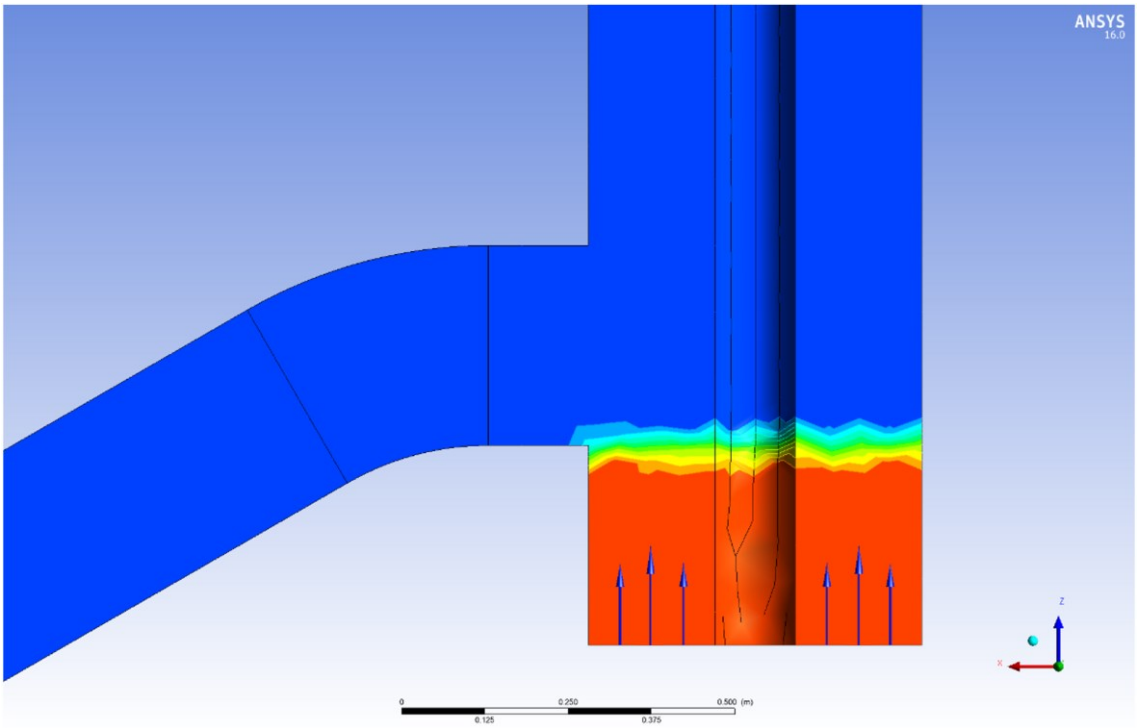

Figure 35: Initial conditions at the inlet boundary marked as velocity vectors.

In contrast to the inlet the outlet which is located at the far end of the straight pipe section is defined as a pressure outlet. This requires that a static gauge pressure is defined that this boundary tries to hold. For this particular case the gauge pressure was set to zero so that the fluid is "sucked" out of the domain. This may not be physically correct but it makes simulation more stable and is not causing unwanted upstream effects at the outlet.

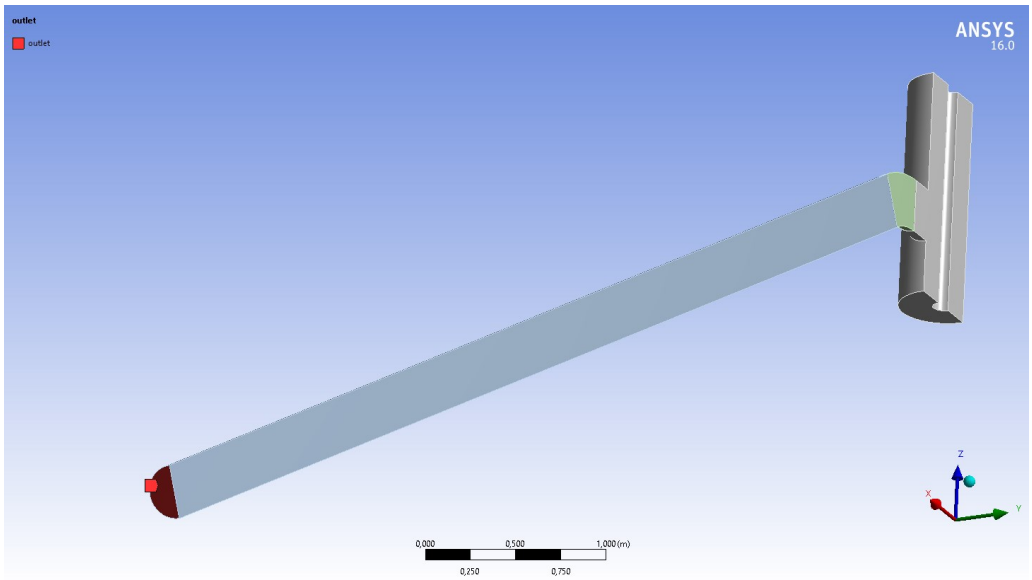

Figure 36: Outlet surface out of the flow domain (red).

In addition to the gauge pressure backflow conditions were defined for the outlet. This means the ability for phases to enter the pressure outlet if reverse flow occurs. In this case the only allowed phase to be able to enter the domain from the outlet was set to air.

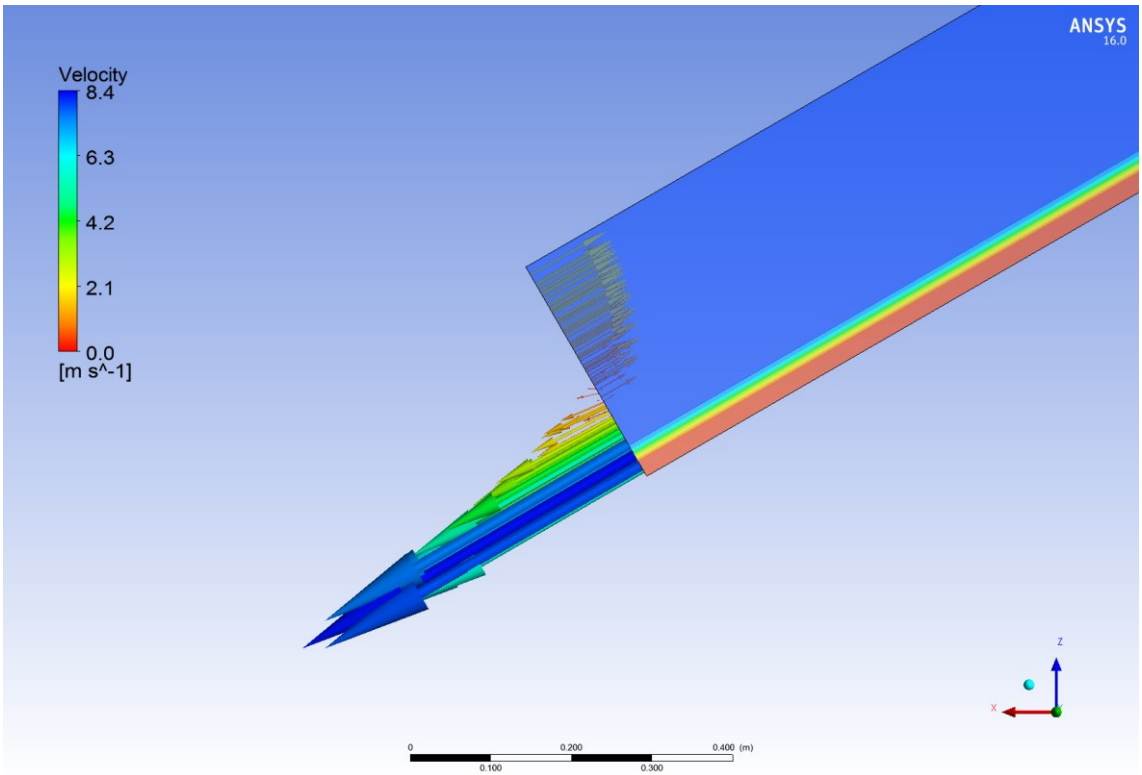

Figure 37: Velocity vectors depicted at the outlet boundary including backflow of air into the domain. The vector arrow size and color are proportional to the flow velocity.

All other surfaces of the model that lie on the outside were defined as wall boundaries. The shear condition was specified as a no slip condition and the wall roughness was assumed to be stainless steel (Table 3). Additionally the roughness variation distribution was assumed to be uniform.

Table 3: Pipe roughness values for different materials (Slurry Pipes Ldt. n.d.).

Surface	Absolute Roughness - k	
	10^{-3} (m)	(feet)
Copper, Lead, Brass, Aluminium (new)	0.001 - 0.002	$3.3 - 6.7\ 10^{-6}$
PVC and Plastic Pipes	0.0015 - 0.007	$0.5 - 2.33\ 10^{-5}$
Epoxy, Vinyl Ester and Isophthalic pipe	0.005	$1.7\ 10^{-5}$
Stainless steel	0.015	$5\ 10^{-5}$
Steel commercial pipe	0.045 - 0.09	$1.5 - 3\ 10^{-4}$
Stretched steel	0.015	$5\ 10^{-5}$
Weld steel	0.045	$1.5\ 10^{-4}$
Galvanized steel	0.15	$5\ 10^{-4}$
Rusted steel (corrosion)	0.15 - 4	$5 - 133\ 10^{-4}$
New cast iron	0.25 - 0.8	$8 - 27\ 10^{-4}$
Worn cast iron	0.8 - 1.5	$2.7 - 5\ 10^{-3}$
Rusty cast iron	1.5 - 2.5	$5 - 8.3\ 10^{-3}$

4.1.4 Export

For the data analysis and post processing after the simulation runs the relevant data had to be exported. For this study the most relevant data is the liquid level height in the straight pipe section. To do the calculations of height over distance along the pipe and height over time a cross-sectional surface in the center of the straight pipe was exported for each time-step. Therefore an artificial probing plane was created within the simulator that probes the interior of the flow domain and writes the data into output files. The probing resolution was set to a probing distance of one centimeter in a grid like fashion giving 1000 x 30 data points. This means that for each centimeter a volume fraction of fluid, absolute velocity magnitude and Reynolds number was exported in an ASCII format.

This export was done for every fiftieth time step, which means every 100 milliseconds a data point is available. This data density was considered to be sufficient for the purpose of this analysis without straining the data storage capabilities. The state of the complete simulation was also saved every 100 milliseconds of simulation time in order to prevent "data explosion" as a complete state demands significantly more storage space. The relevant data for this study was already exported which made the rest of all generated data unnecessary.

To further analyze the exported data processing scripts were developed using Matlab. This scripts imported previous mentioned data and generated the refined relevant data for this study. The most essential information gained by this transformation were:

- Fluid level over straight pipe length
- Fluid level over time
- Flow velocity over channel length
- Fluid level over pump rate

The chapter Post – Processing will cover the data manipulation of the imported simulation data in more detail.

4.2 Processing

In order to obtain good simulation outcomes the correct settings for the simulation software have to be set. Therefore it can be challenging to decide which models and exact sub - settings to use. Usually such knowledge comes with extensive experience of the simulator and with fluid dynamics in general. For this study a number of trail runs had to be made to determine the right settings for the job.

4.2.1 Model

For the sake of simplicity for this study a two phase gas – liquid flow was chosen as flow regime. The additional simulation of cutting particles was refrained from in order to not increase the simulation time and complexity further. For normal drilling operations the

cuttings concentration is usually relatively low and would likely have a negligible impact on the macroscopic flow phenomena in the outflow line.

In the outflow - channel a stratified / free - surface flow with a clearly defined interface is present. In CFD studies it is important to understand what flow regimes to expect in order to set up the software with the proper models as not all models are made for all flow regimes. Fluent offers the three multiphase models shown below. Each model has its own particular strengths:

- Mixture Model
    - bubbly flows
    - sedimentation
- Eulerian Model
    - bubble columns
    - risers
    - particle suspension
    - fluidized beds

For this study the VOF model was chosen as it handles free – surface flows with the lowest computational requirements well as well as it is the officially recommended model for free –surface flows. "The VOF model is a surface-tracking technique applied to a fixed Eulerian mesh. It is designed for two or more immiscible fluids where the position of the interface between the fluids is of interest. In the VOF model, a single set of momentum equations is shared by the fluids, and the volume fraction of each of the fluids in each computational cell is tracked throughout the domain" (Fluent Inc. n.d.).

4.2.2 Solver

Fluent allows to different kind of solvers to be used each with its pros and cons:

- Pressure – based
- Density – based

For this work a pressure-based solver has been used as it is generally more accurate than a density based solver for subsonic incompressible flows. The velocity field is obtained from the momentum equations and the pressure field is determined by solving a pressure or pressure correction equation which is obtained by manipulating continuity and momentum equations (Fluent Inc. n.d.). More specifically the pressure – based segregated algorithm was used instead of the coupled algorithm. The coupled solver would improve convergence of the solution but at the same time the memory requirement would double because all the continuity equations need to be stored in memory when solving for the velocity and pressure fields.

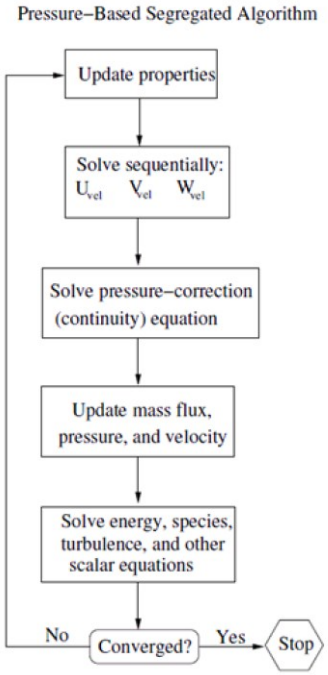

Figure 38: Overview of Pressure-Based solution algorithm used in the simulations (Fluent Inc. n.d.).

4.2.3 Fluid Properties

For the simulation cases of this study two different rheological models have been used. As described in the results chapter more closely for the cases that were simulated with water a constant viscosity was chosen and for the cases with varying fluid viscosities the Herschel – Bulkley Model has been used. In order to generate a Bingham plastic behavior for the fluid the input parameter n was set to zero.

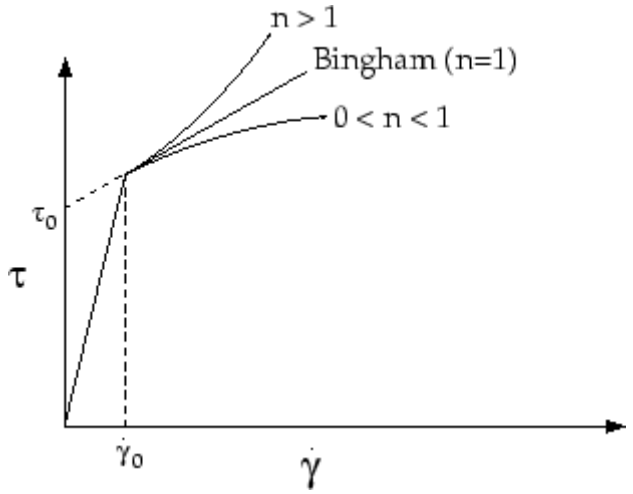

Figure 39: Variation of Shear Stress with Shear Rate according to the Herschel-Bulkley Model (Fluent Inc. n.d.).

The simulation software allows for more complex rheological properties for the chosen model but for this study they were neglected to generate the behavior of a Bingham plastic. In the subsequent simulation the yield stress and the consistency factor were varied separately to determine their influence on the results.

4.2.4 Convergence

A successful CFD simulation can't be done without a properly converging set of calculations. It essentially is a statement whether the residuals of the iterative numerical calculations are approaching a minimum or whether they are approaching infinity at which point the simulation becomes unsolvable and stops. Figure 40 shows an example plot of converging residuals of one of the transient simulation cases. A general rule of thumb is that the iterations for each time step should be able to reduce the residuals by three orders of magnitude. For this study the simulator was given a limit of 50 iterations which was sufficient to allow for proper convergence.

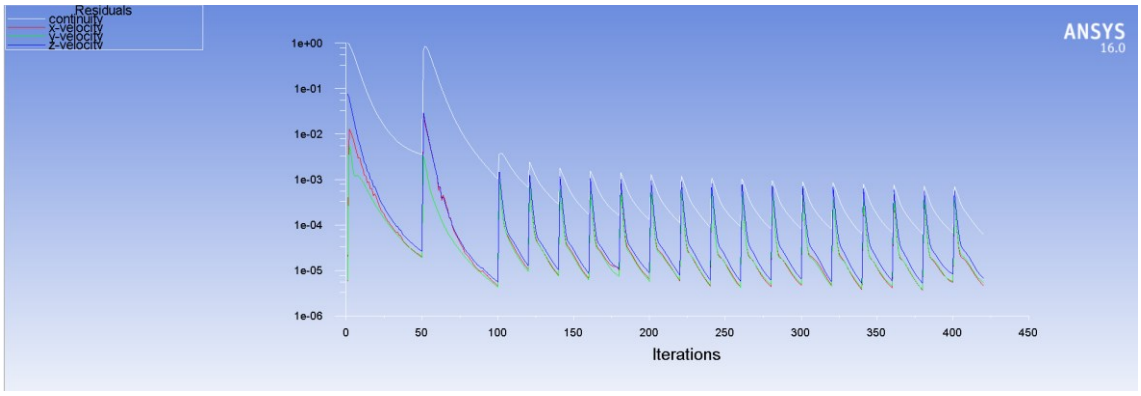

Figure 40: Residuals plot during a transient simulation run.

Residual plots are a useful tool to detect possible problems in the simulation and can be used to take the necessary divergence recovery steps if the plot shows a diverging trend. This is especially important in high performance computing where CPU time is mostly rented and if a simulation crashes due to divergence in the solver the rented hardware sits idle and can therefore increase costs substantially.

There are a number of steps that can be taken to keep the simulation stable and maintain good results. However the proper application of those steps is necessary as it can become a delicate balance between simulation stability and simulation time hence this steps play a huge role in cost effectiveness of large CFD studies.

4.3 Post – Processing

For the post – processing stage it was necessary to make some data manipulation on the exported output data to generate useful output graphs. In the center of the long straight pipe section parallel to the symmetry plane a monitor plane was created that acted as probing plane. This plane has probing points in a grid like fashion. For the planes'

dimensions of 0,3m x 10m there were probe points every centimeter hence 1000 x 30 points. Every 100 milliseconds an output data file was written which included the coordinate of every probe point with its corresponding fluid volume fraction and velocity magnitude.

Below an overview of the post – processing steps can be seen that were taken for each case. The source codes for each script can be found in the Appendix section.

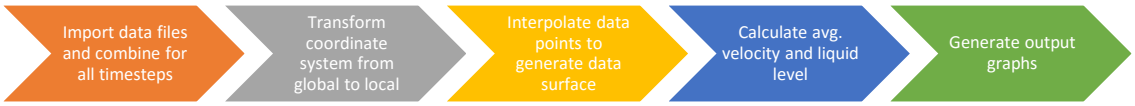

Figure 41: Overview of post – processing steps.

For the second step it was important to normalize the coordinates for all data points in order to compare different geometrical models in terms of fluid height. Therefore the global coordinates were transformed into new local coordinate system specific for each new geometrical model. Figure 42 shows the results for the base case. This transformation made it possible to compare flows in terms of their height relative to the channel bottom and channel slope as well as to the length of the straight pipe section.

The next step was to interpolate the data points over a predefined mesh to make later stage data analysis easier. The exported data point already came in a grid like structure but rounding errors in the fluid simulator and in the coordinate transformation make them not always align up perfectly. For the subsequent fluid height calculation this is essential. This method can also be used if the exported data comes in a more scattered fashion for example when data points are taken at mesh cell centers. This makes it also possible to use different meshing algorithms that don't create equidistant meshes (Figure 43).

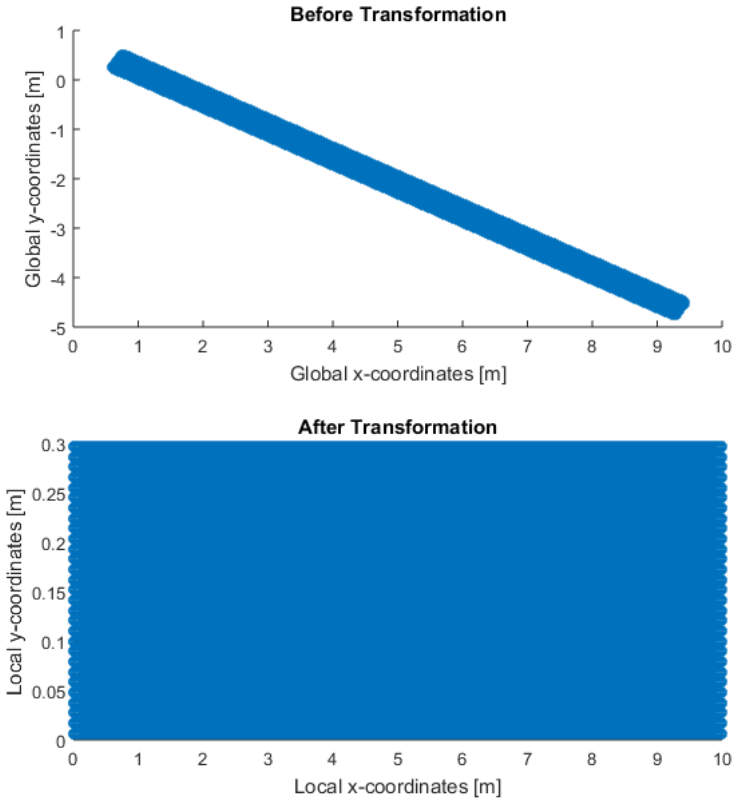

Figure 42: Probing points plotted before and after transformation of coordinate systems.

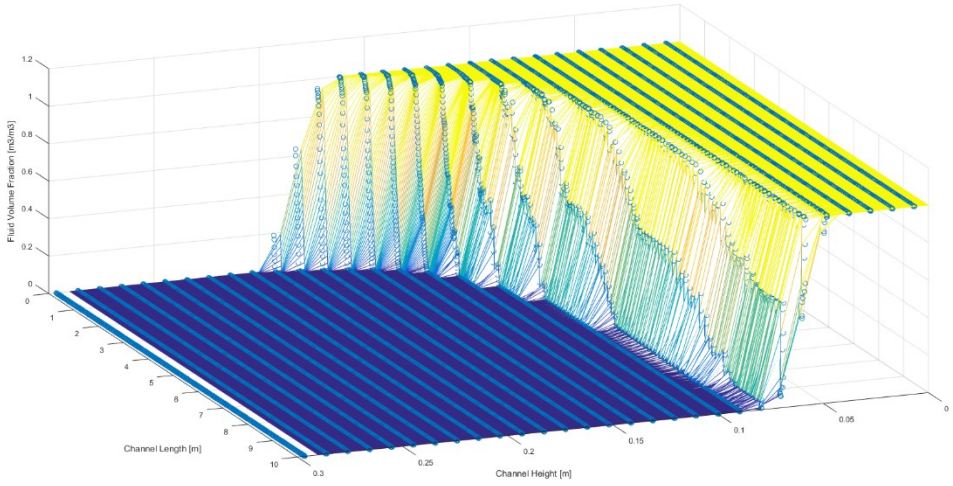

Figure 43: Example time slice with data points and interpolated mesh.

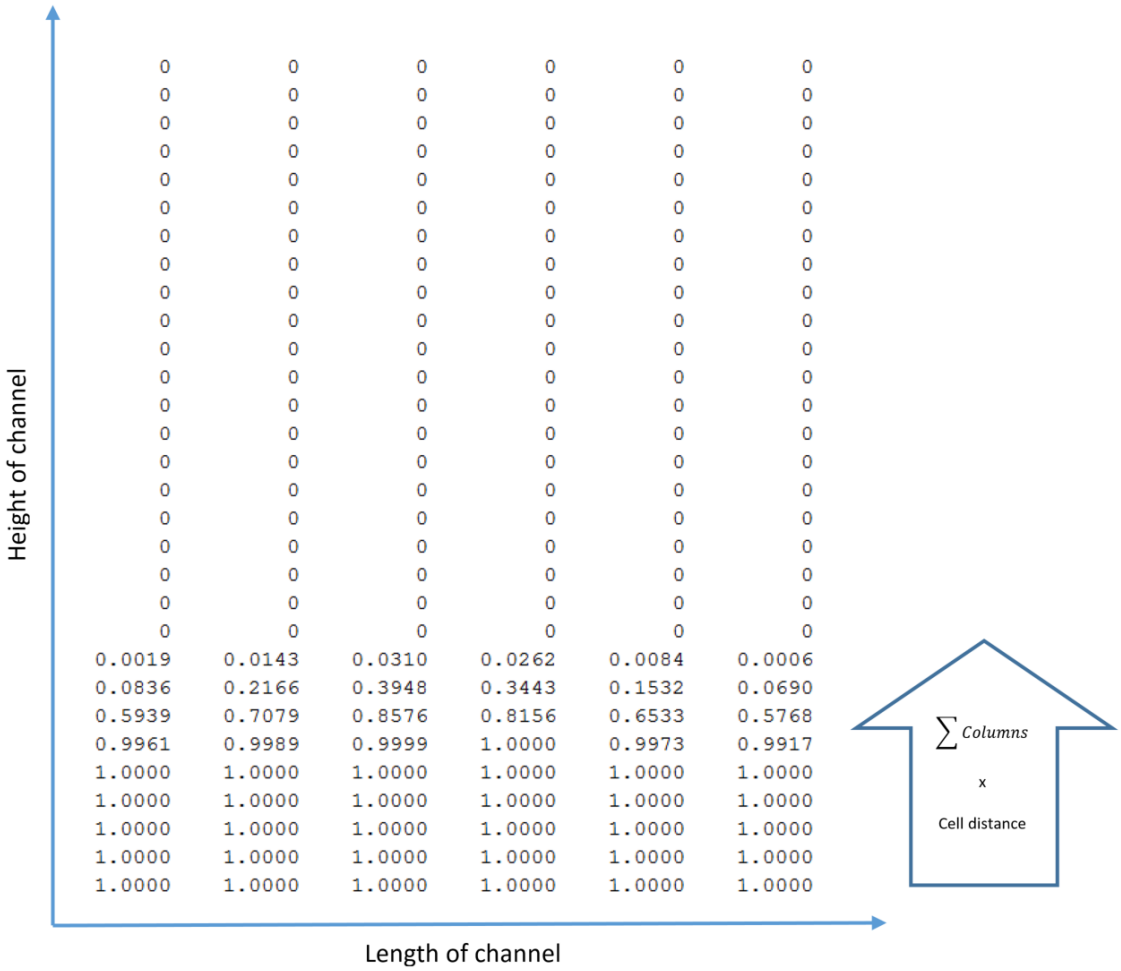

Figure 44: Example of how fluid height is calculated by the interpolated data.

The final step to determine the fluid height was to take the data of the finished interpolated mesh from Figure 43 and integrate the volume fraction values for each column as depicted above. This step is a standard practice among CFD professionals in order to extract the fluid height from simulations and use it for further data analysis. Then the sums are multiplied with the predefined grid resolution value, in this case one centimeter to determine the actual fluid height at each location in the channel. The results from the example above can be seen in the figure below.

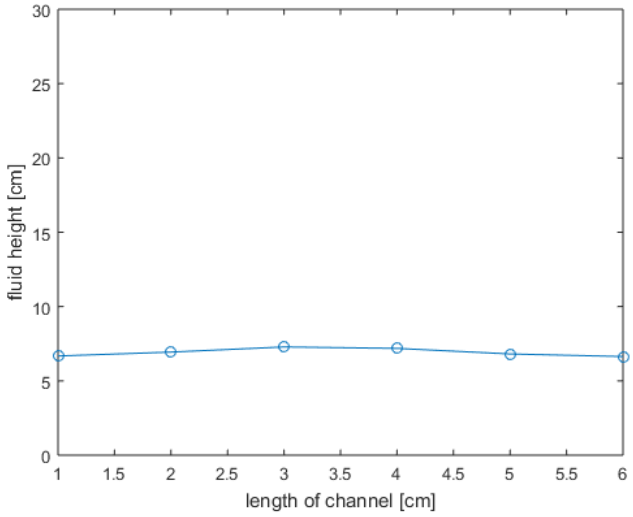

Figure 45: Result of the example calculation above.

For the calculation of the velocity a similar approach was taken. The simulator exported the values of velocity magnitude for each cell. To determine the velocity value the maximum was taken from each velocity profile along the pipe. The figure below shows a typical velocity distribution along the channel length and height. The velocity values were taken from the hump on the bottom of the channel as these are the cells with liquid. This approach was taken to minimize inconsistency due to the relatively low resolution of the velocity profiles. This approximation was assumed to be reasonably accurate for velocities measured by means of a rolling barrel or a radar/sonar velocity meter.

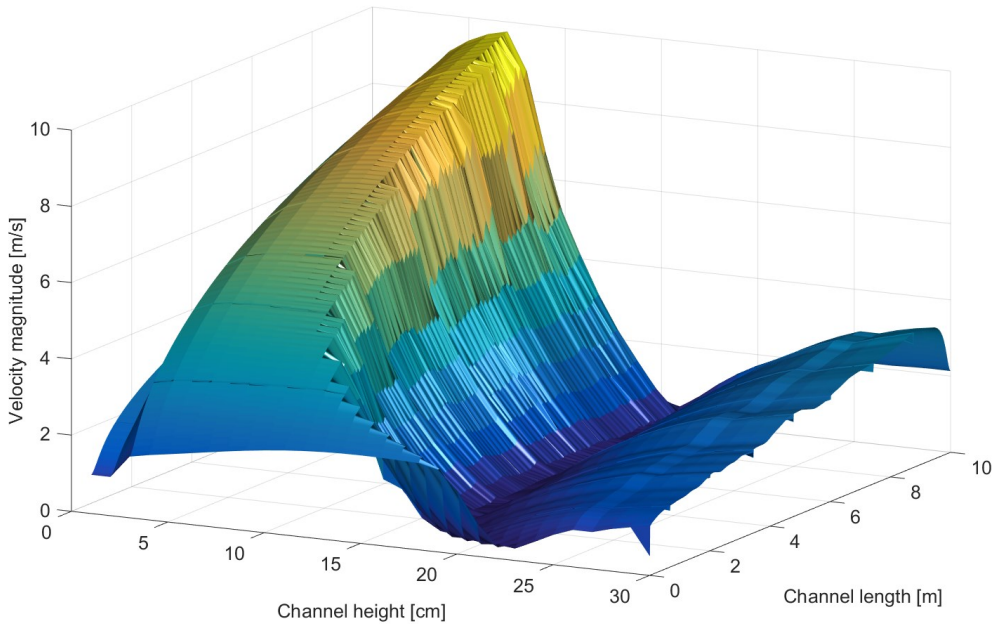

Figure 46: Example plot of velocity profiles along the channel length. Base case, 15000gpm, simulation runtime 15 seconds.

4.4 Mesh Independence Study

A first major step in the actual simulation work was the conduction of a mesh or grid independence study. The purpose of such a study is to find the optimal solution to a flow dynamics problem with the least amount of computational effort. As the resolution of a flow domain increases hence the cell element sizes becoming smaller and smaller the simulation solutions tend to converge to the actual solution. From this convergence point upwards in terms of resolution there is no improvement in the solution results to be expected.

Nine cases have been simulated each with an increased amount of total cell number in the model (Figure 47, Table 4). The case setup was kept very general because the purpose of this analysis was to compare grid independence and not fluid dynamics model independence. Each case was set up with the same models and initial conditions with the exception of the grid density. The flowrate was instantaneously set to 1500gpm and the simulation runtime was limited to 5 seconds as the model reaches its steady state by then.

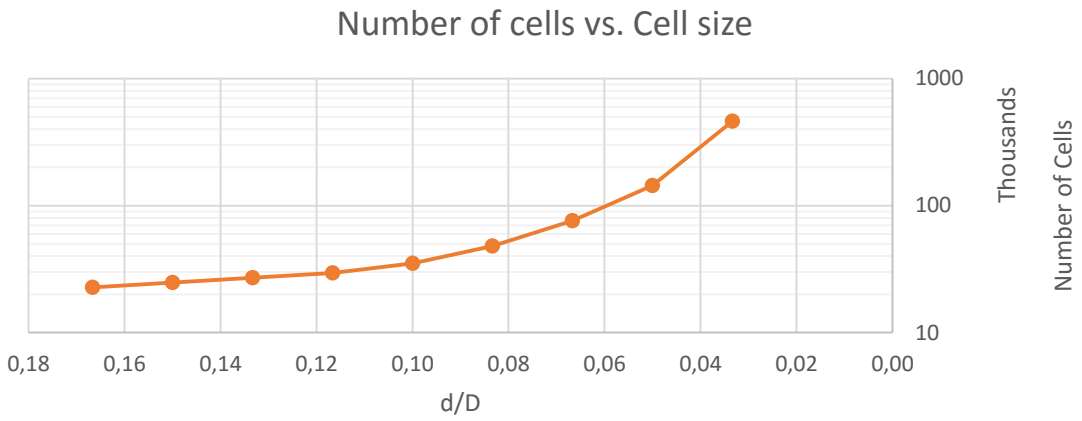

Figure 47: Relationship between the maximum cell edge length and its total number of cells in the model. Labelled from 1 through 9 are the cases simulated for this grid independence study. The horizontal axis is showing the ratio between maximum cell edge length (d) and total pipe diameter (D).

The results of all cases were compared with each other to get a feeling of how the model and the simulation outcome behaves with different mesh densities. Based on this the optimal mesh density for the subsequent more thorough simulations could be chosen. Usually grid independence studies and their outcome can be quantified based on the value of a certain parameter at a point in the model (such as temperature or pressure) and compared to measurements in the real world. This approach was not possible for this study because there was no real world model to compare it to and moreover the purpose of this thesis it to study free surface behavior in a partially filled pipe which is turbulence dominated and the computational resources were heavily limited. As shown

in previous chapters turbulent flow is expected in the observed part of the flow domain, hence a turbulent flow model was applied in these simulations.

Table 4: Cases and its exact number of cells in the model.

Case	Number of cells
1	22740
2	24742
3	27090
4	29506
5	35155
6	48078
7	75940
8	144015
9	460069

The following comparison was therefore more of a qualitative nature than usual based on the reasons stated above. Figure 47 shows a comparison of the velocity profile along the center line of the straight pipe section with the velocity profile derived from the Bernoulli equation for smooth pipes for each case and corrected to the inflow velocity into the observed section.

$$v = \sqrt{2 \cdot g \cdot l \cdot \sin(\alpha)} \tag{8}$$

v ... $flow\ velocity$

l ... $distance\ from\ inlet$

g ... $gravity$

α ... $channel\ drop\ angle$

It can clearly be seen as the grid density increases the velocity profile of the simulation converges more and more to the calculated profile. Starting around case 5 the model starts to show the turbulent ripples in the lower part of the pipe section where the velocity is the highest and the fluid height the lowest. Continuing the increasing grid density this unstable velocity phenomenon becomes more and more visible. In case 9 the difference to the theoretical profile is minimal and is likely to decrease further as the grid density is increased. It should be noted that the comparison to the formula based profile was merely used to compare cases, the derived profile likely does not represent the exact solution.

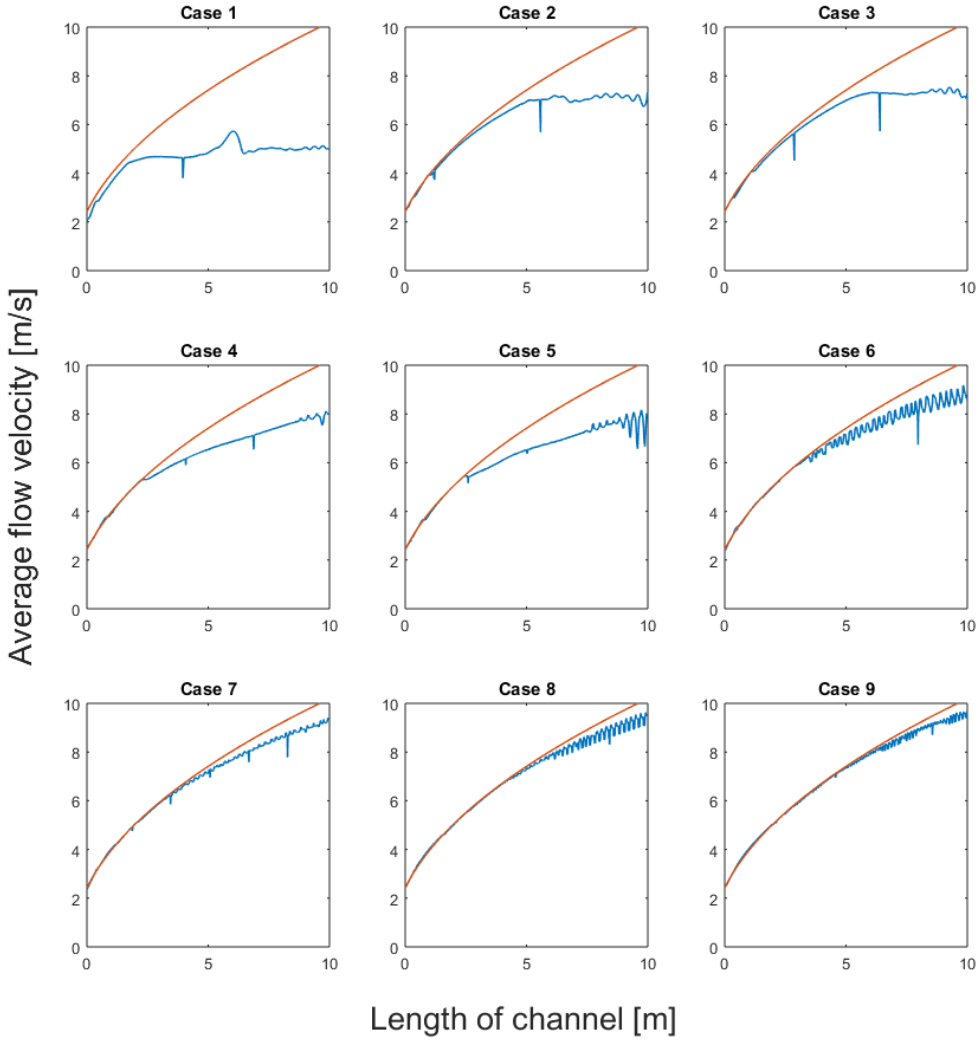

Figure 48: Comparison of average flow velocity along the main pipe section (blue) to the derived velocity profile for a smooth pipe according to the Bernoulli equation (orange) for each case. The x-axis refers to the length of the channel after the bent pipe section, hence 0 is at the bell nipple side and 10 is at the shale shaker side.

Figure 49 shows the estimated deviation compared to the number of cells in each case. When the trend is extrapolated for lower deviations then the model would need to have following densities:

- < 1% deviation → > 900.000 cells
- < 0,1% deviation → > 22 Mio cells

As mentioned before such high densities were not possible for this projects due to computational hardware limitations could however be a hint for future projects in that area.

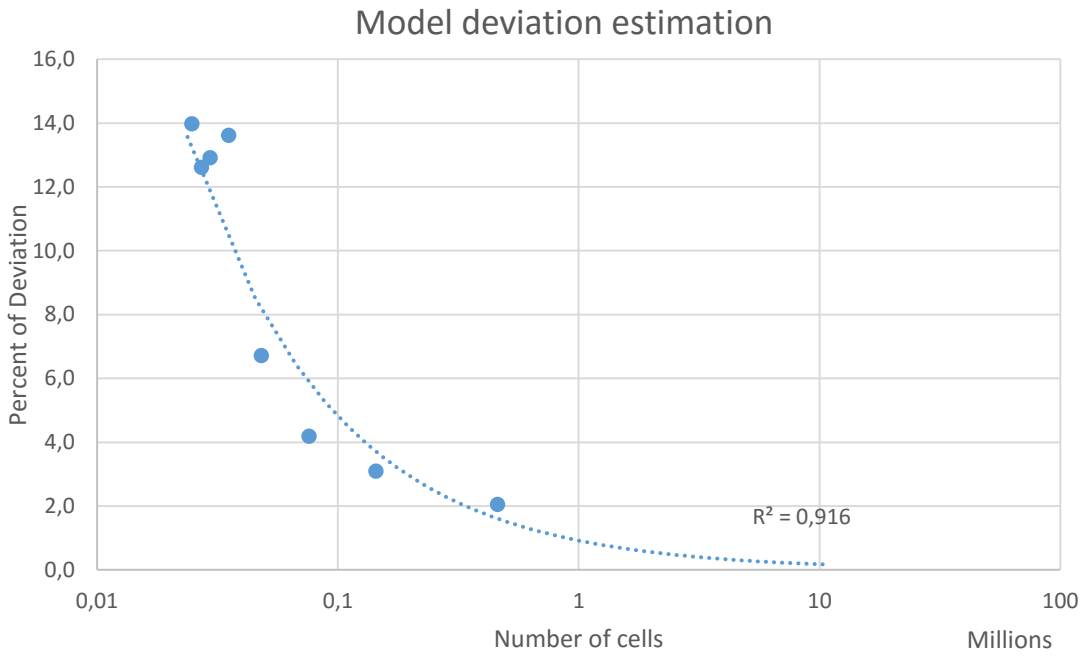

Figure 49: Relationship between simulation deviation and mesh cell number.

A more detailed look at the velocity deviations in Figure 50 shows that there seems to be an anomaly from case two to five where the deviation stays essentially unchanged despite increased mesh density. As mentioned above there is no real straight forward way to estimate the mesh independence of a model without real world laboratory measurement to evaluate simulation data correctly.

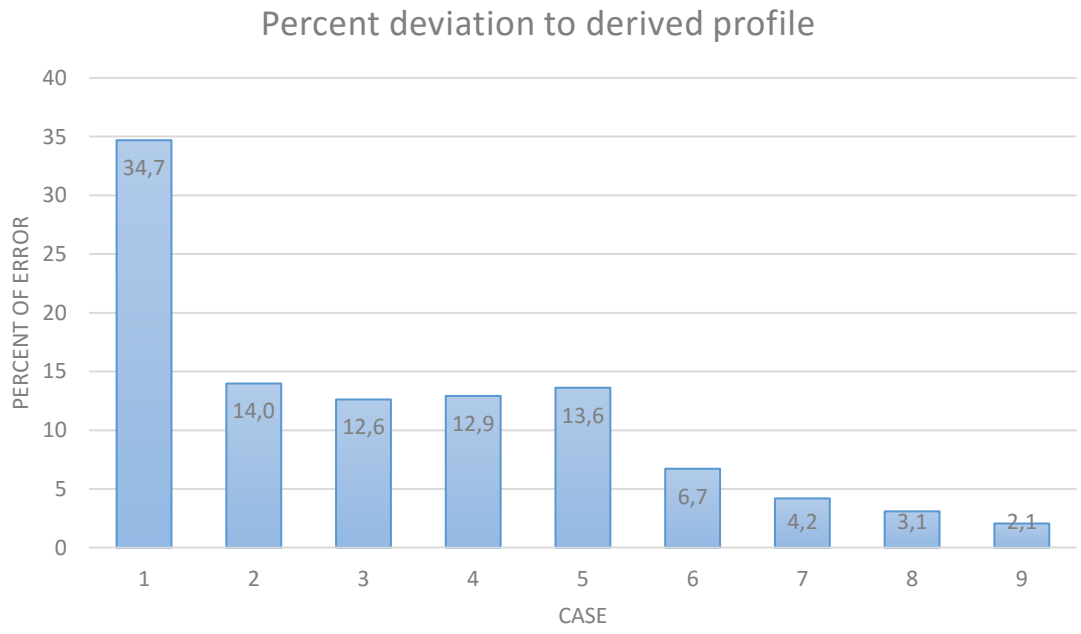

Figure 50: Deviation from derived velocity profile for each case.

Chapter 5 Study Results and Discussion

In the final chapter of this thesis the simulation outcomes are presented and how their results have been interpreted. Due to the lack of sufficient computational resources the number of cases had to be limited to the most meaningful scenarios for further analysis.

5.1 Cases

Table 5: Overview of the simulation cases.

Case #	Angle	Liquid properties	Density [SG]	Comment
1	30°	water	1	Base case / turbulence model
2	30°	water	2	turbulence model
3	30°	water	3	turbulence model
4	20°	water	1	turbulence model
5	10°	water	1	turbulence model
6	30°	drilling fluid	1	PV = 1cP, laminar model
7	30°	drilling fluid	1	PV = 3cP, laminar model
8	30°	drilling fluid	1	PV = 6cP, laminar model
9	30°	drilling fluid	1	PV = 12cP, laminar model
10	30°	drilling fluid	1	PV = 120cP, laminar model

The cases for the simulation and their main variables have been chosen according to the overview in Figure 51. This selection of cases covers a wide range of scenarios and gives a good initial understanding of outflow behavior on drilling rigs and a valuable insight for future projects in that area.

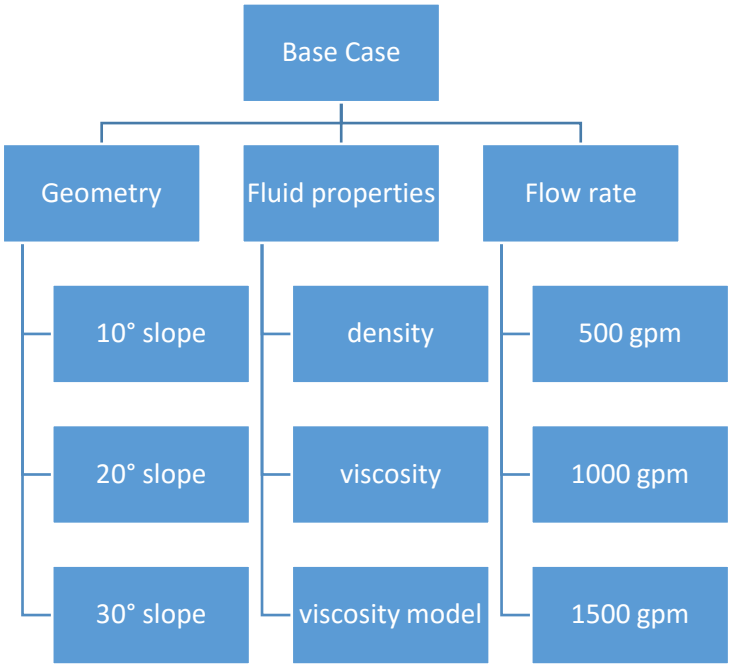

Figure 51: Overview of major case variables.

Geometry – wise the change was confined to changes in the drop angle of the straight, long pipe section because of limited comparability and unknown mesh independence error. Would the outflow pipe diameter change also the mesh cell number would change substantially hence the mesh independence error difference between the models would likely increase. As the cases presented here are already just partially mesh independent changing the pipe diameter was refrained from.

The effect on changing flow rates on fluid levels was likely the most important variable in the simulations. The variation was done stepwise in three steps as seen in Figure 52. After each flow rate change there was kept a 5 second constant flow rate to let the flow channel fill appropriately and to allow for the flow to stabilize. Should by that time some unusual effects occur like oscillations the boundary conditions could be changed accordingly to analyze this effect further as seen specifically in one case below.

To accommodate for these changing flow rates it was not necessary to set up a new case for each rate. The simulator allows for user defined functions that can act as boundary conditions where the user can define at which flow time the velocity of the incoming fluid has a certain value. For future projects in that area such a user defined function can be used to program more complex flow rate changes for kick or ballooning detection for this study however the profile was kept relatively simple with a step profile.

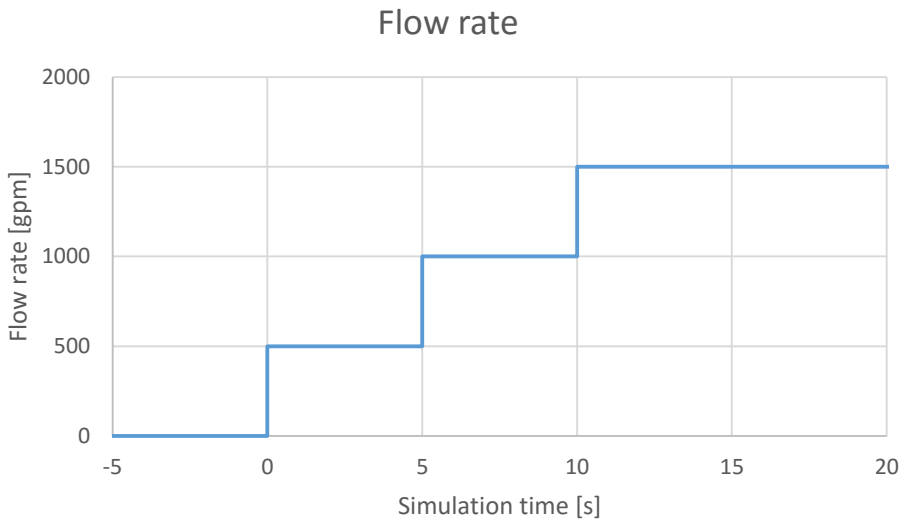

Figure 52: Flow rate function at the inlet boundary of the model.

For the variations in the liquid properties two different viscosity models have been used. All cases that were simulated with water a constant viscosity was applied. All other cases that studied the viscosity impact of a drilling fluid were set up to use the Herschel – Buckley model and to resemble different Bingham plastics.

In summary following assumptions have been made for subsequent simulations:

- The top of the bell nipple is defined as a wall boundary to increase numerical stability. It is assumed that the changed pressure situation does not affect the results significantly
- The incoming fluid from the annulus is assumed to be laminar. The incoming velocity profile is undeveloped due to the coarse mesh of the bell nipple and the assumption that it will not alter the results.
- The outlet boundary was defined as a pressure outlet because of the substantially increased numerical stability and the assumption that it is not affecting the results.
- The geometry was assumed to be axisymmetric to save computational effort.
- The wall material was defined as stainless steel with a homogenous roughness distribution.
- The simulation was done without the simulation of solid particles hence the effects of cuttings settling were not considered in this study.

5.2 Simulations

All simulation cases are variations of the base case. The data for the subsequent analysis is mainly derived from the fluid height and velocity raw data. The two 3D plots below show this raw data for the base case. Those 3D plots are a convenient way to view results along the length of the channel and the changes over time. Figure 53 shows the fluid height and there can clearly be seen the three steps of the changing flow rate and how the fluid height is behaving along the channel's length. Also noticeable is the increasing free surface instability towards the lower end of the channel.

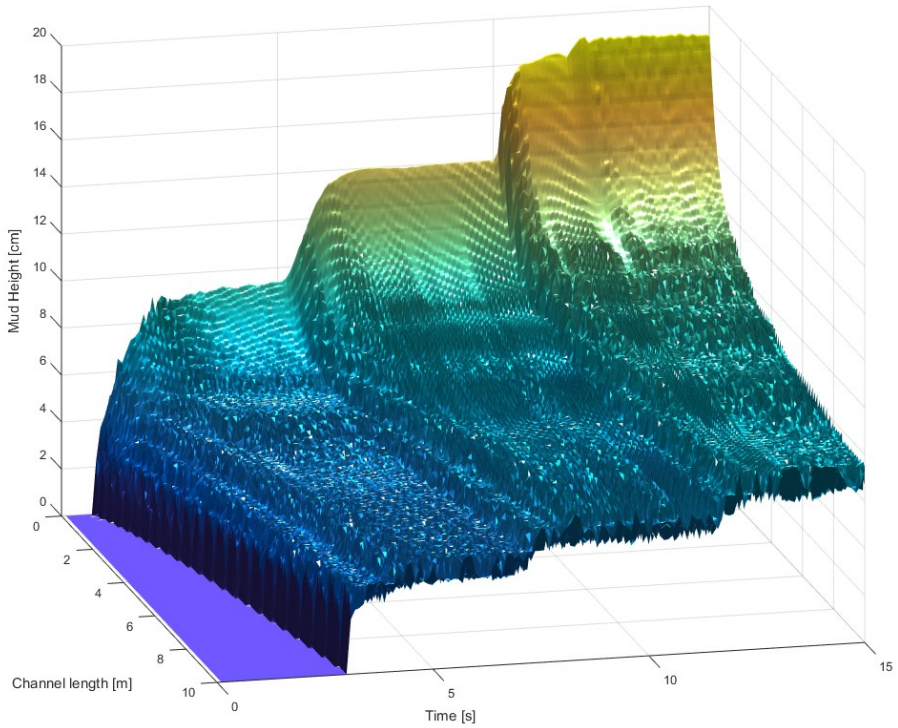

Figure 53: 3D plot of the fluid height across channel length and over time. The graph above shows the results of the base case.

The velocity data looks similar but is increasing with channel length. The average velocity changes along the observed pipe section due to flow rate changes are relatively small because the velocity is mainly a function of the height. For the cases with different channel drop angles the velocities are significantly different. The reason it still changes with flow rate is the different fluid height at the inlet of the channel which increases the potential energy hence the velocity towards the end slightly.

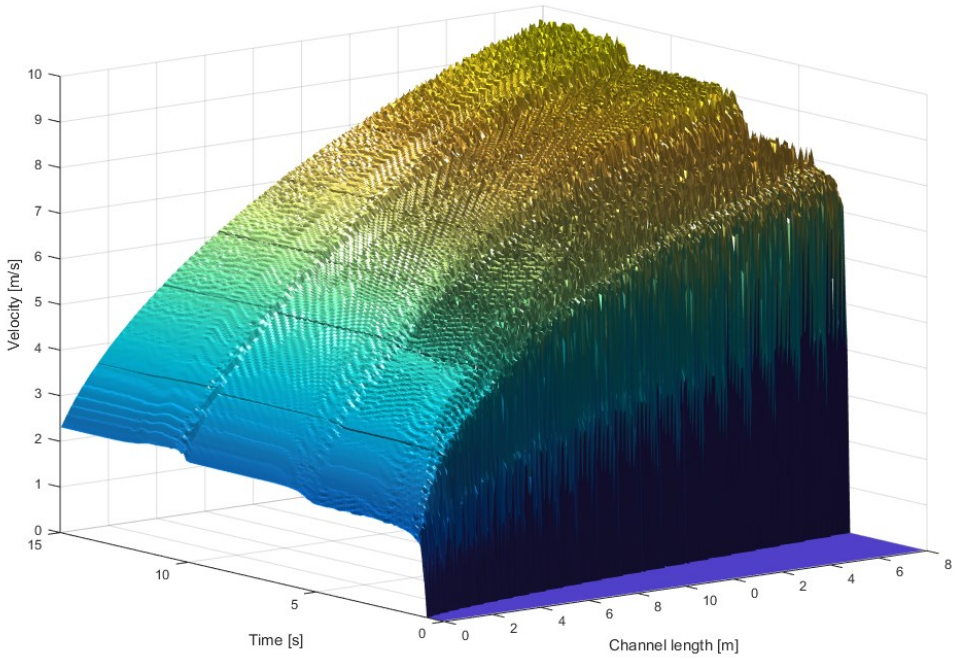

Figure 54: 3D plot of the flow velocity over channel length and time. The graph above shows the results of the base case.

Figure 56 shows a cross sectional view of the base case during all four flow stages. At the highest rate of 1500gpm the upper pipe section completely fills and might in some cases induce sloshing. Free surface instabilities and ripples develop differently at different flow rates also shown in Figure 57. The Figure below shows the Froude number along the channel for the base case. Along the whole observed section the Froude number is above 1 making the flow supercritical in the entire straight pipe section.

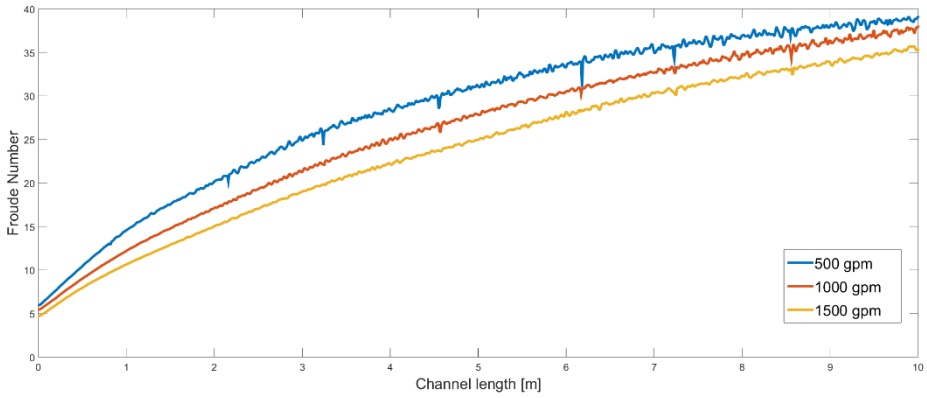

Figure 55: Froude number along the channel for each flow rate.

The velocity profile of the partially filled pipe develops a heterogeneous pattern with changing degree of pipe filling hence flow rate. This requires more sophisticated methods to determine the actual flow velocity in the pipe especially for radar, ultrasonic

and laser velocity meters. This becomes particularly important when trying to measure small influxes into the wellbore where every bit of accuracy counts.

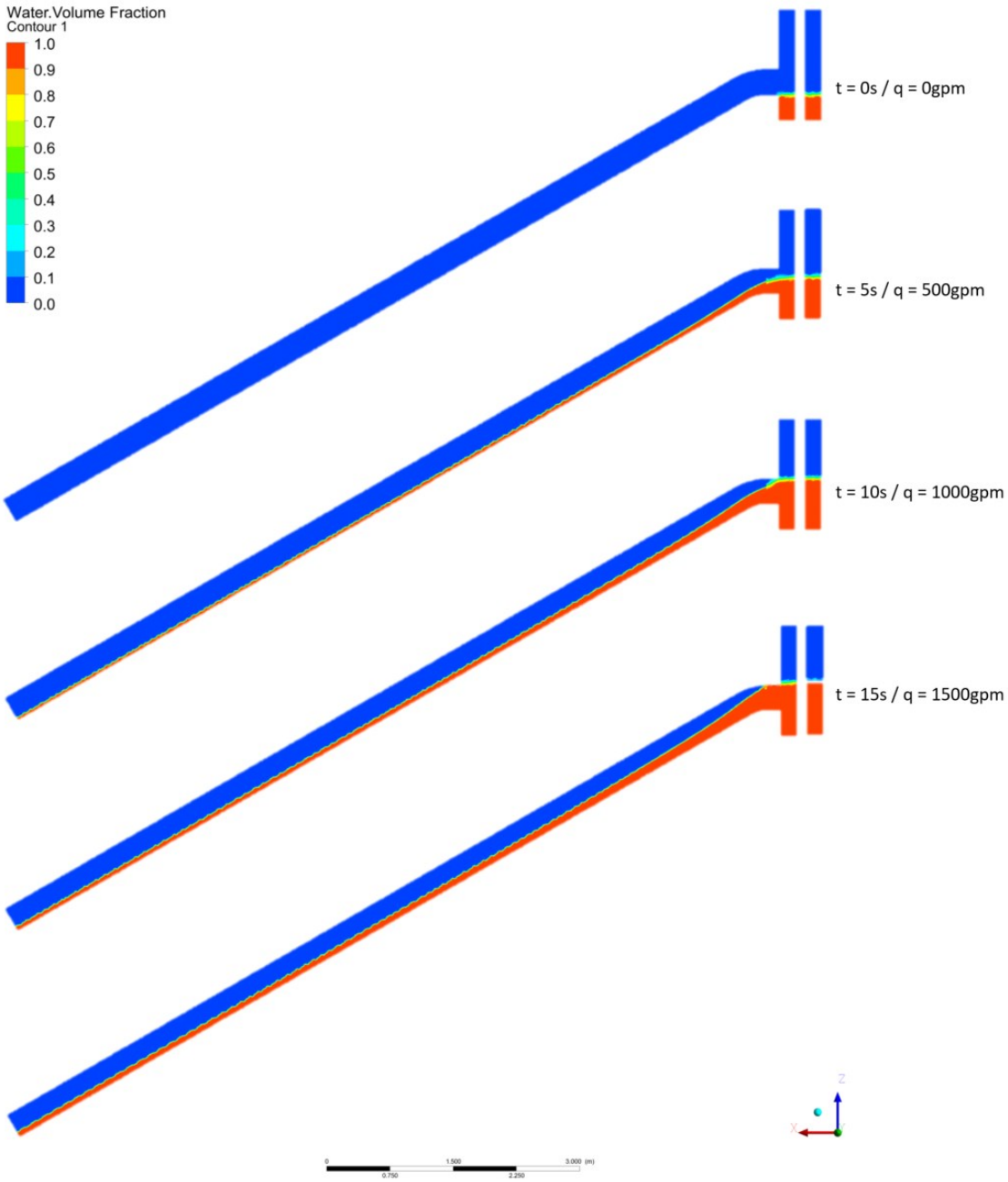

Figure 56: Cross – section of the base case model for each flow rate.

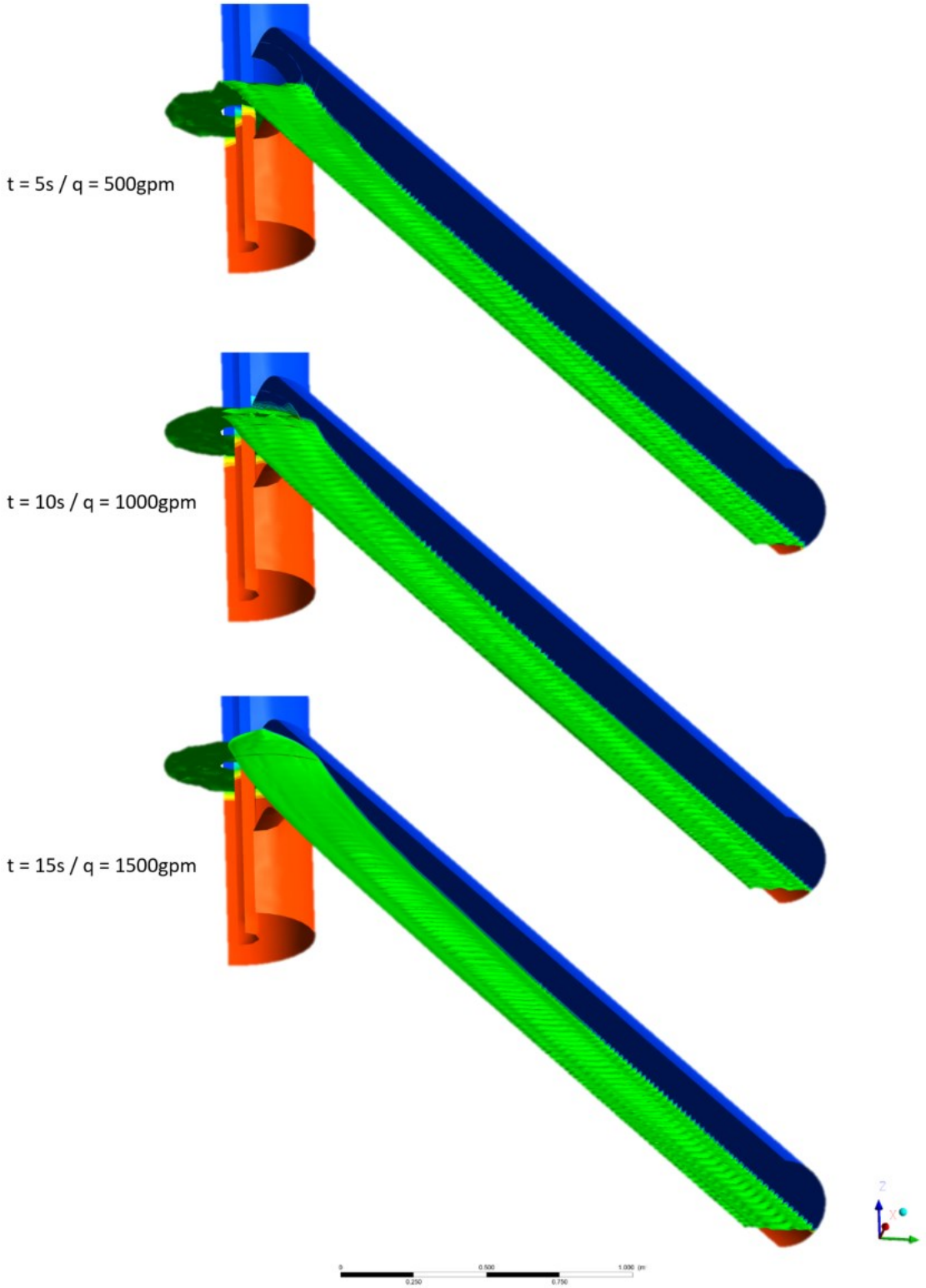

Figure 57: Detailed view on free surface ripples for each flow rate (base case).

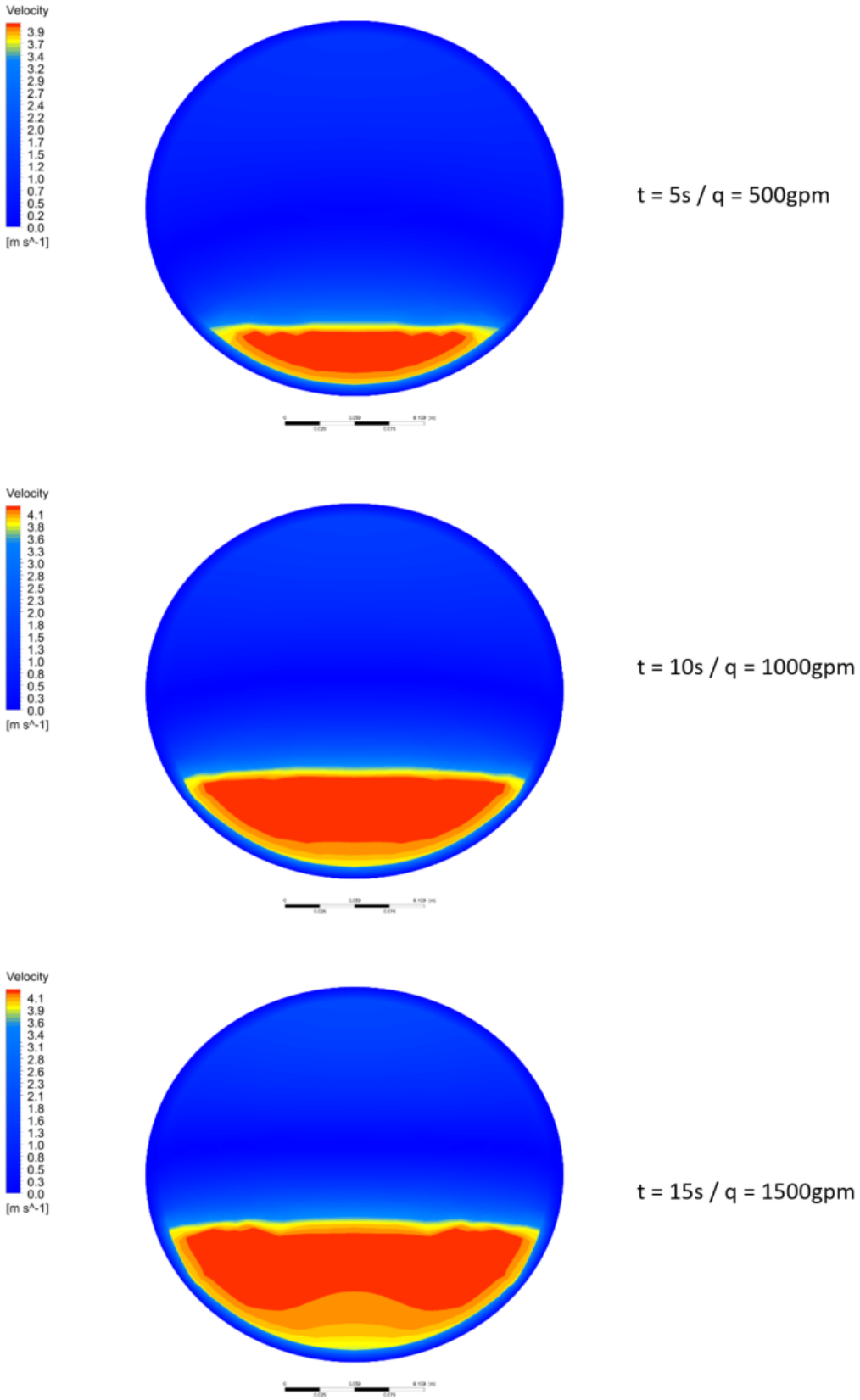

Figure 58: Velocity profile 2 meters after the outlet for each flow rate (base case).

5.2.1 Density Influence

The cases for variations in fluid weight to values double and triple the weight of water show no significant effect on fluid levels or velocity profile. This is expected as the density should have no effect in gravity driven flows where it cancels out of the Bernoulli equation. The results in the figures below confirm that statement (Figure 59 and Figure 60). The slight variations in the outlet data points (red) are likely occurring due to interactions with the pressure outlet boundary surface.

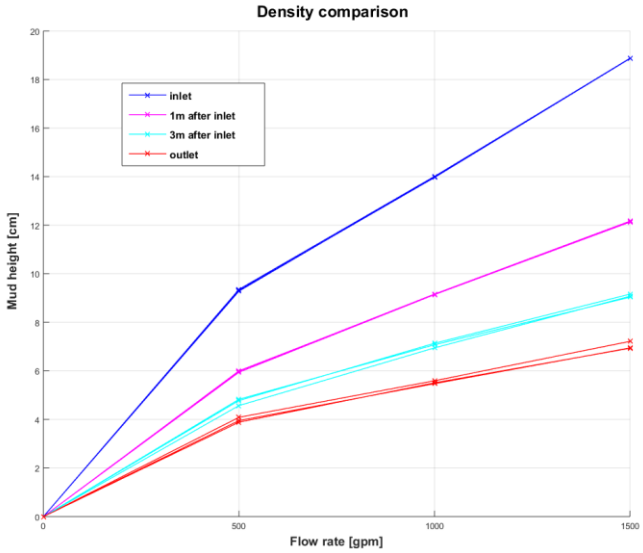

Figure 59: Comparison of different densities on the fluid height.

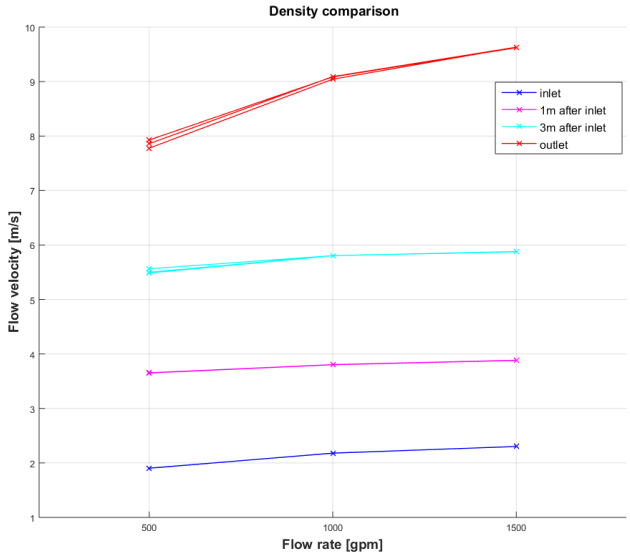

Figure 60: Comparison of different densities on the flow velocity.

5.2.2 Drop Angle Influence

For the series of cases with angle variations it could be observed that with increasing distance from the inlet which also means increased velocity and decreased fluid height that the sensitivity for flow rate changes decreases as the flow becomes more supercritical. Comparing the angles directly shows that the sensitivity decline is less severe in the shallow drop angle case (Figure 64).

When observing the fluid height cross section along the channel the extent and intensity of the free surface ripples becomes obvious. Figure 65 shows that these surface disturbances are more distinct in steeper flow channels and lose some intensity the shallower the channel becomes. As noted before some cases have been simulated with different turbulence models to evaluate the surface behavior of the fluid as it travels along the pipe. The next subchapter analyzes this differences in more details. In general however it could be observed that those surface ripples are similar in intensity and extent with different turbulence models.

The analysis of the time to fluid height signals a level meter would receive shows substantial signal quality decline over the length of the channel. This becomes especially obvious when the received signals are normalized and compared (Figure 66 - Figure 71). The noise due to increased surface instabilities increases along the channel. Signal quality improvements could likely be achieved with the application of certain filters but the question on the impact of flow rate quantification remains and is an opportunity for future research work.

In the case with a 10 degree channel drop angle it could be observed that the pipe diameter chosen for this case with high flow rates (~1500gpm) was not sufficient to maintain linearity in the fluid height function at each position in the channel (Figure 63). The pipe begins to fill completely and slowly moves the wave front downstream in an oscillating fashion (Figure 72, Figure 73). From the simulations here it is not clear if the wave front works its way all the way down the channel or if it will eventually reach a stable point. Based on this observation it can be concluded that the balance of pipe diameter, drop angle and expected flow rates have to be taken under careful consideration when designing a drilling rig.

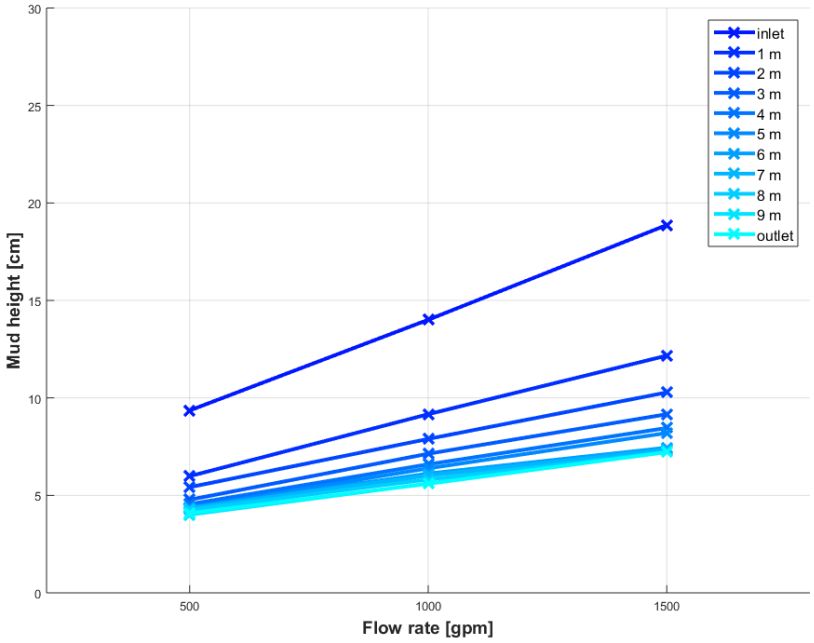

Figure 61: 30° sensitivity.

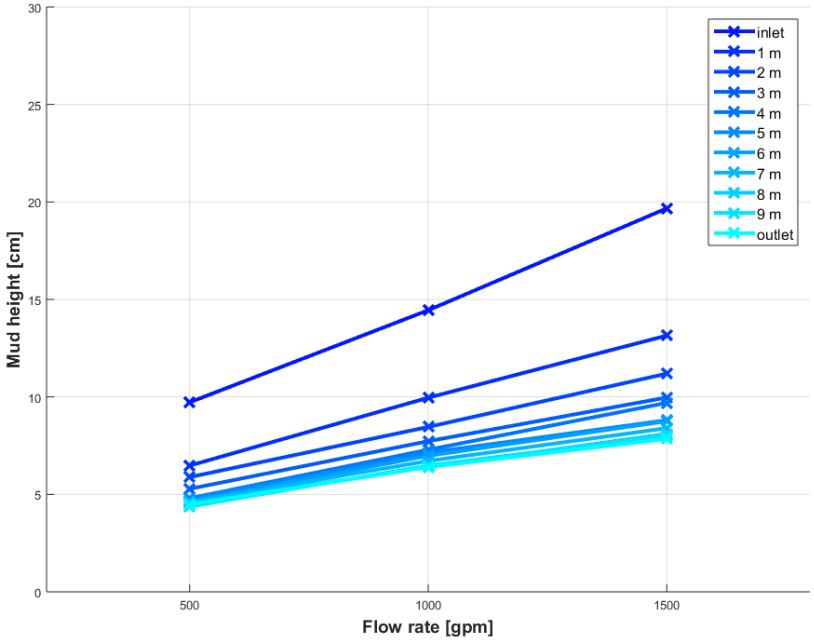

Figure 62: 20° sensitivity.

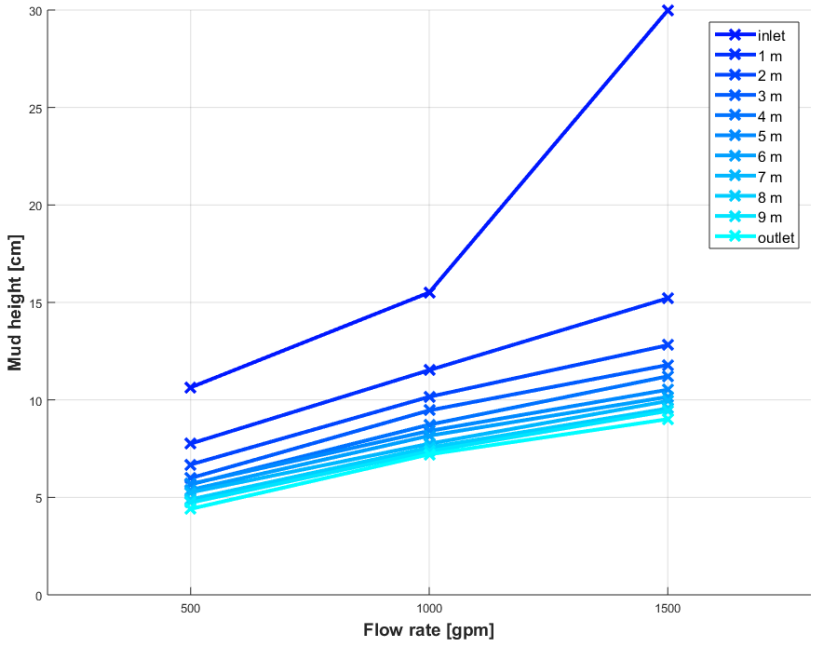

Figure 63: 10° sensitivity.

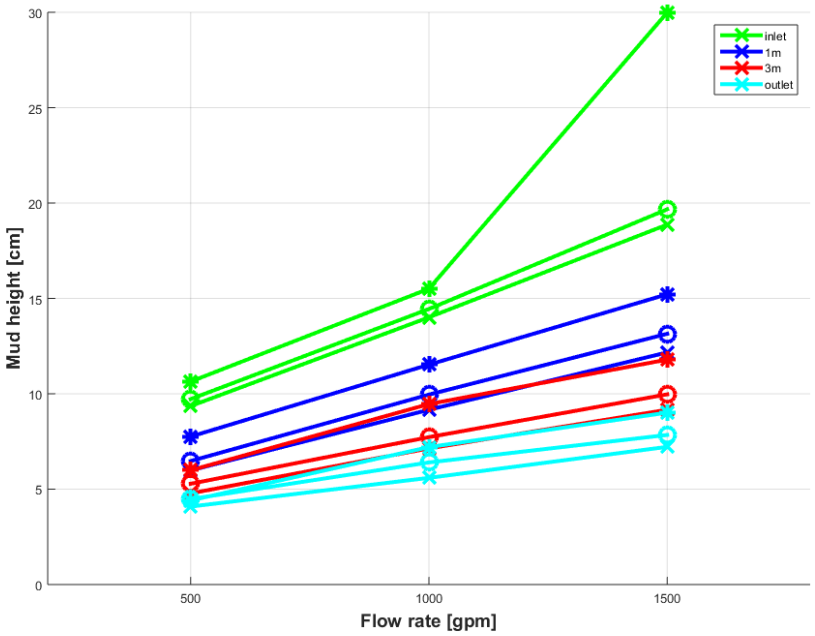

Figure 64: Sensitivity comparison of 30° (x), 20° (o) and 10° (*) drop angle.

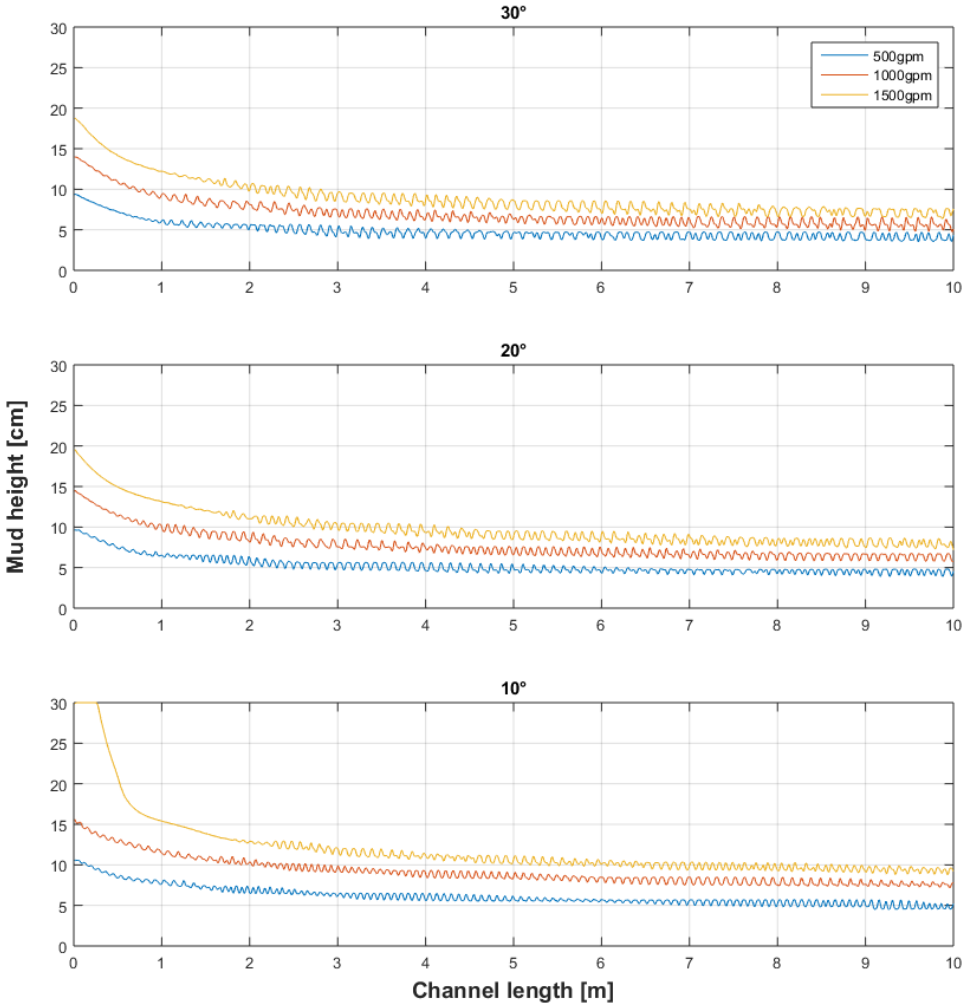

Figure 65: Fluid height along the channel length for different drop angles and flow rates.

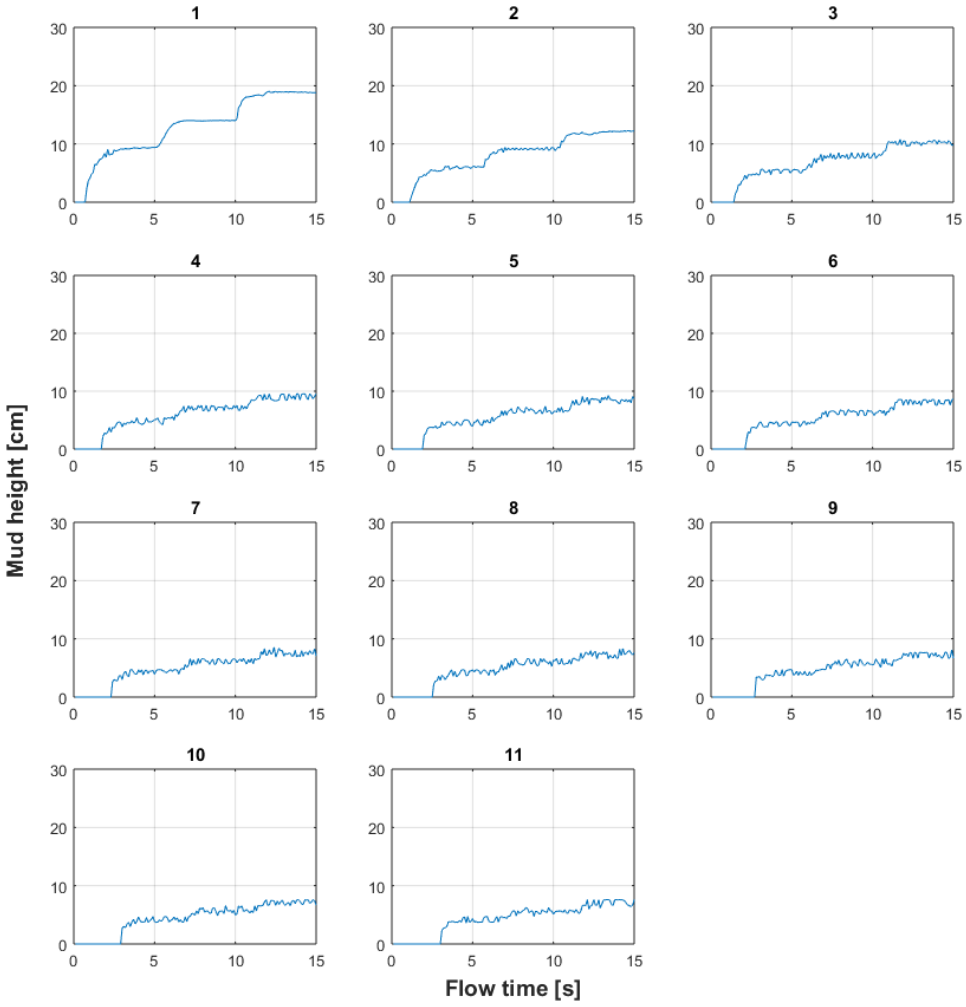

Figure 66: Absolute fluid height vs. time for different locations in the channel, 30° case. 1 = inlet, 11 = outlet, 2-10 are one meter steps between inlet and outlet.

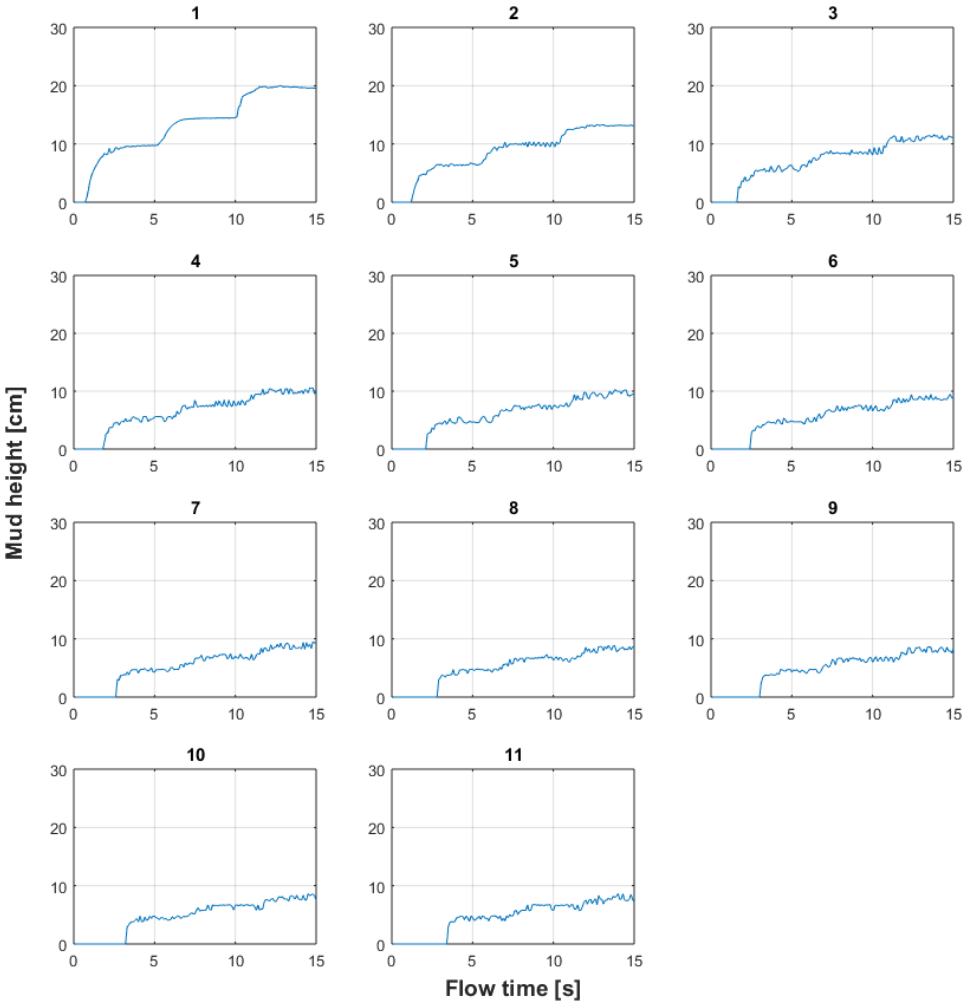

Figure 67: Absolute fluid height vs. time for different locations in the channel, 20° case. 1 = inlet, 11 = outlet, 2-10 are one meter steps between inlet and outlet.

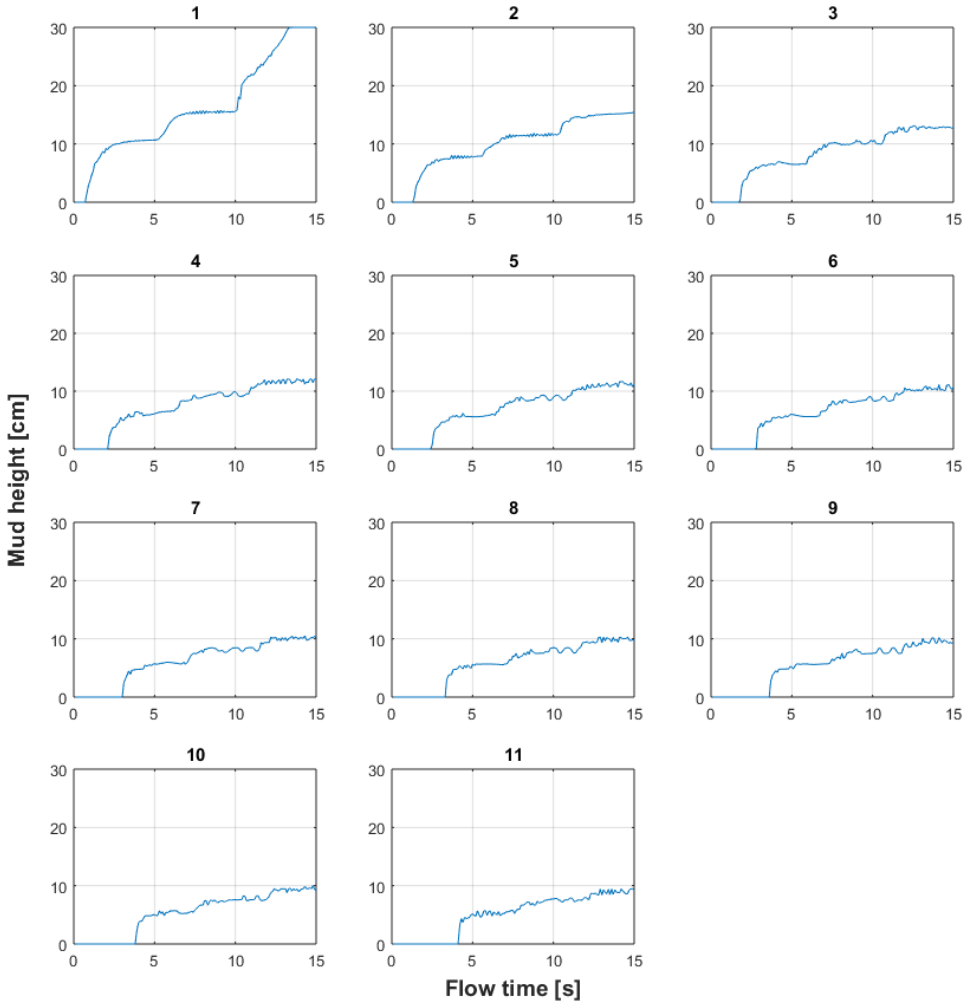

Figure 68: Absolute fluid height vs. time for different locations in the channel, 10° case. 1 = inlet, 11 = outlet, 2-10 are one meter steps between inlet and outlet.

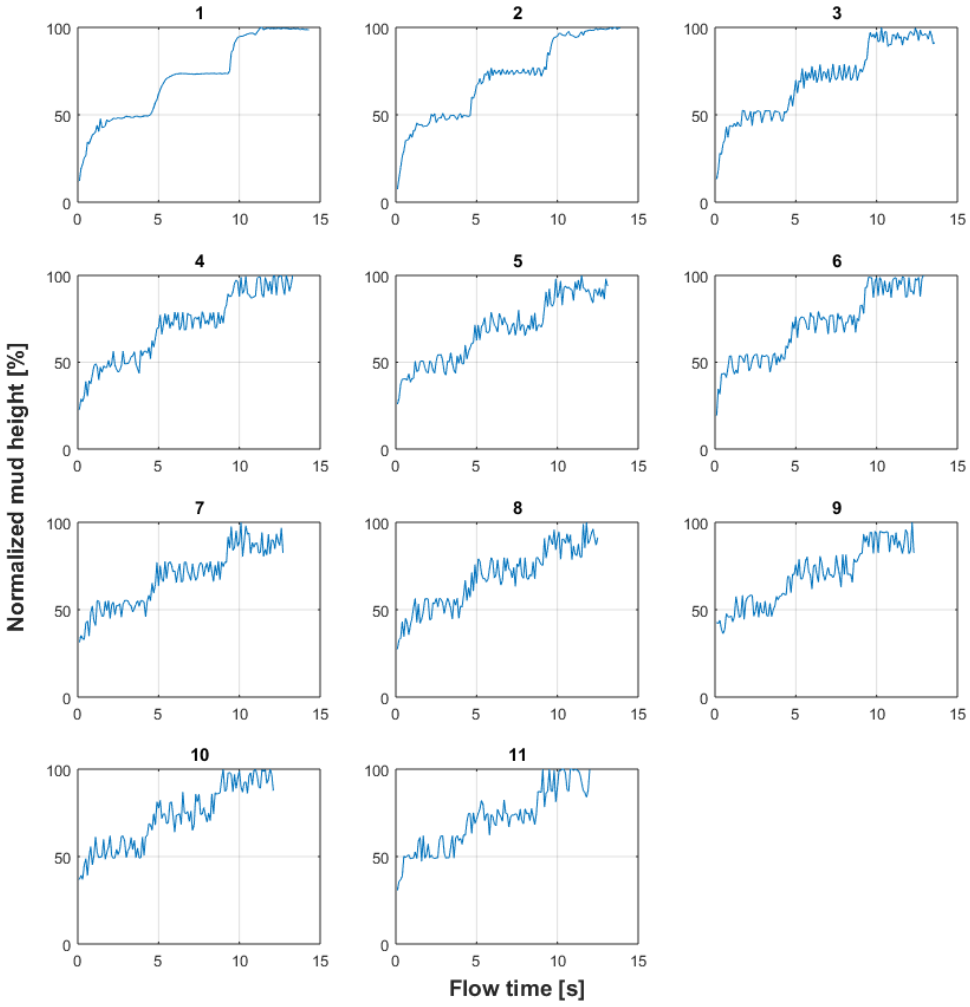

Figure 69: Relative fluid height vs. time for different locations corrected for the time delay, 30° case. 1 = inlet, 11 = outlet, 2-10 are one meter steps between inlet and outlet.

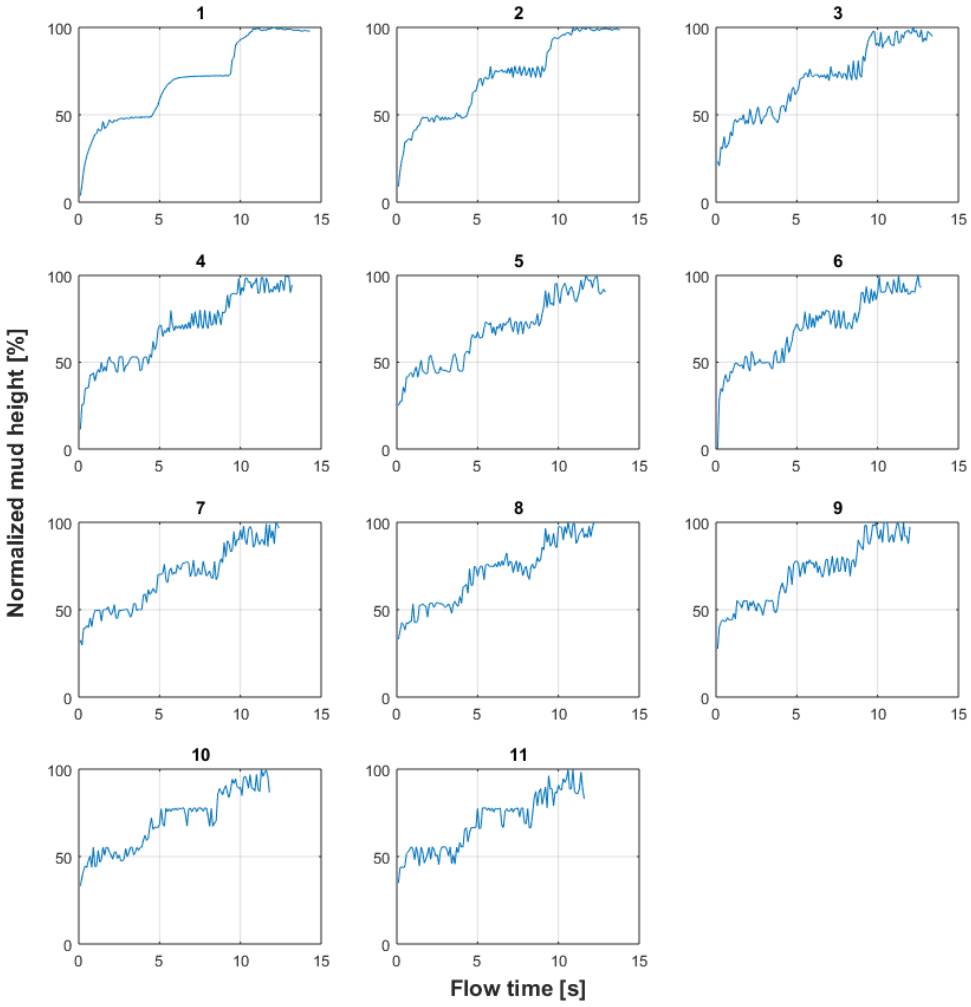

Figure 70: Relative fluid height vs. time for different locations corrected for the time delay, 20° case. 1 = inlet, 11 = outlet, 2-10 are one meter steps between inlet and outlet.

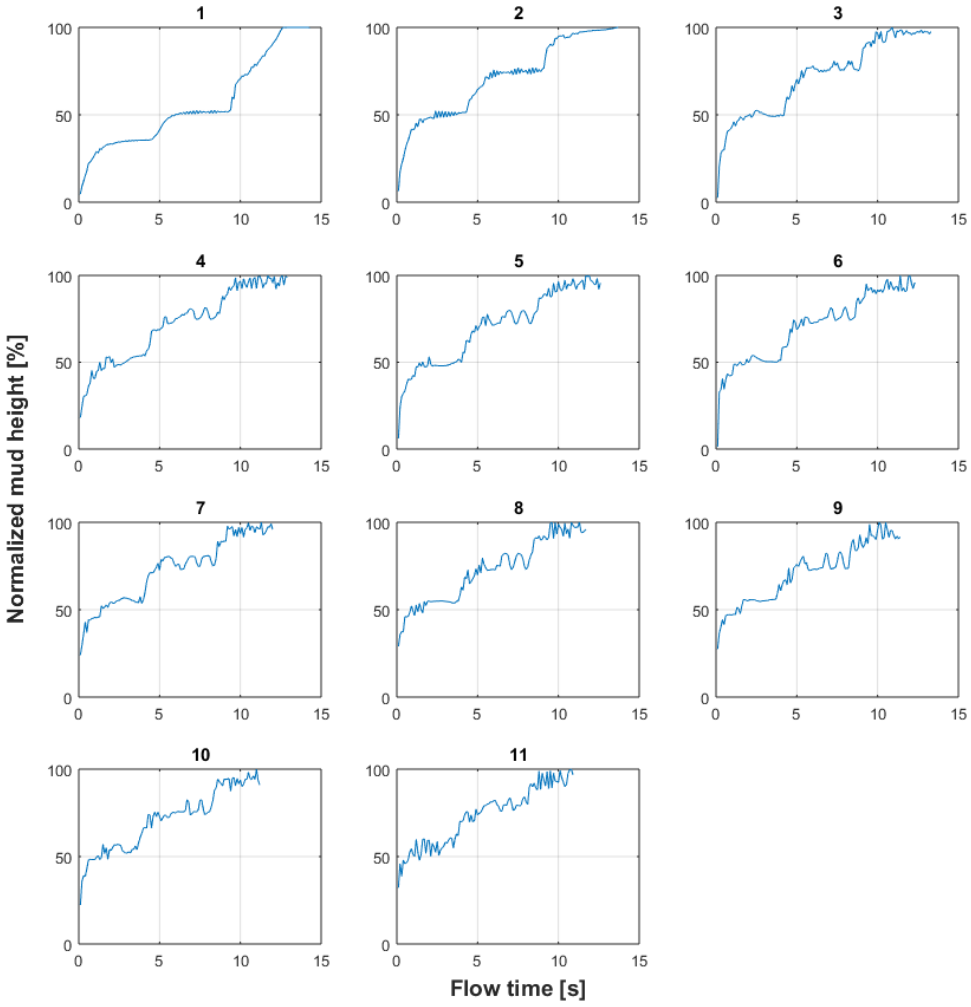

Figure 71: Relative fluid height vs. time for different locations corrected for the time delay, 10° case. 1 = inlet, 11 = outlet, 2-10 are one meter steps between inlet and outlet.

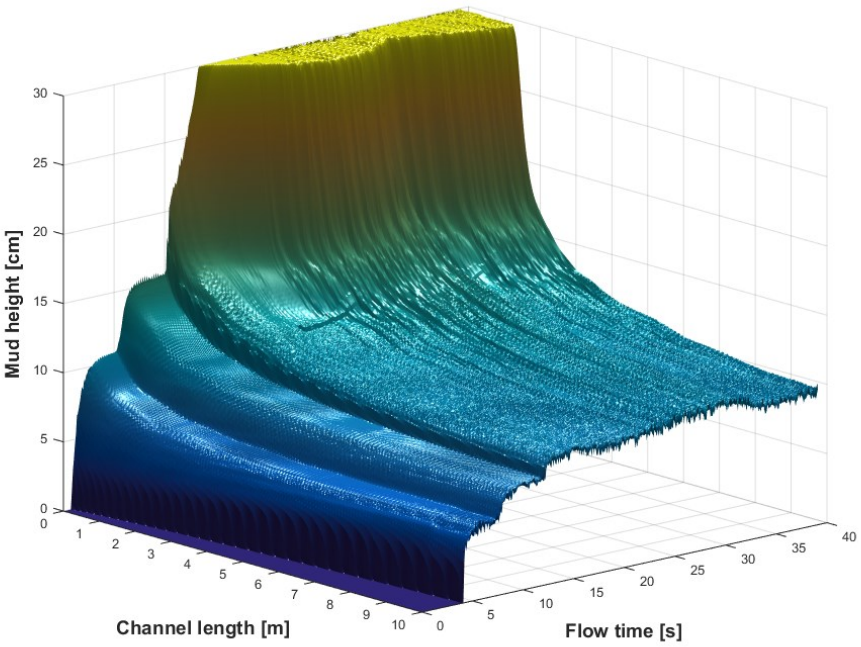

Figure 72: time vs. channel length vs. fluid height plot of 10° showing pipe fill.

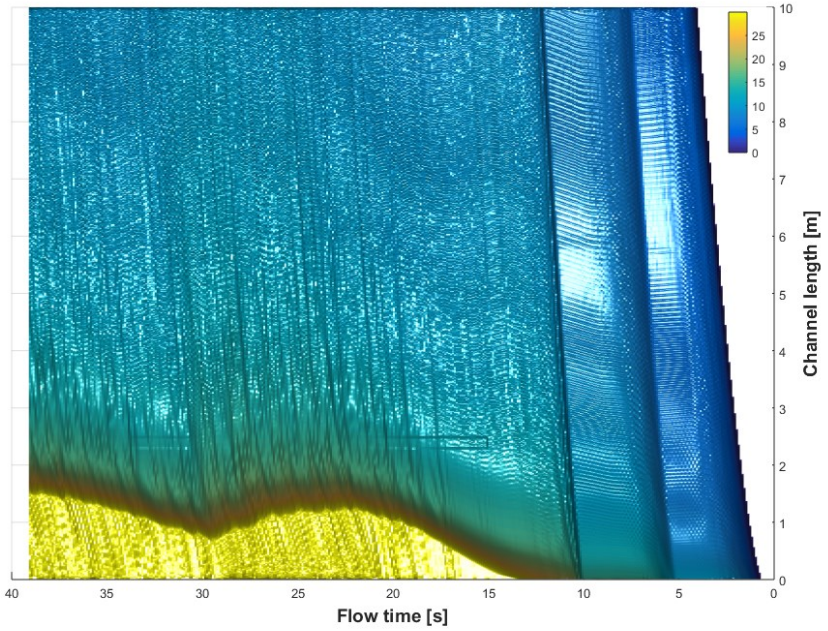

Figure 73: Top view of the figure above.

5.2.3 Viscosity Influence

To vary the fluid properties in terms of Bingham rheological properties the model was required to be switched to a laminar flow model.

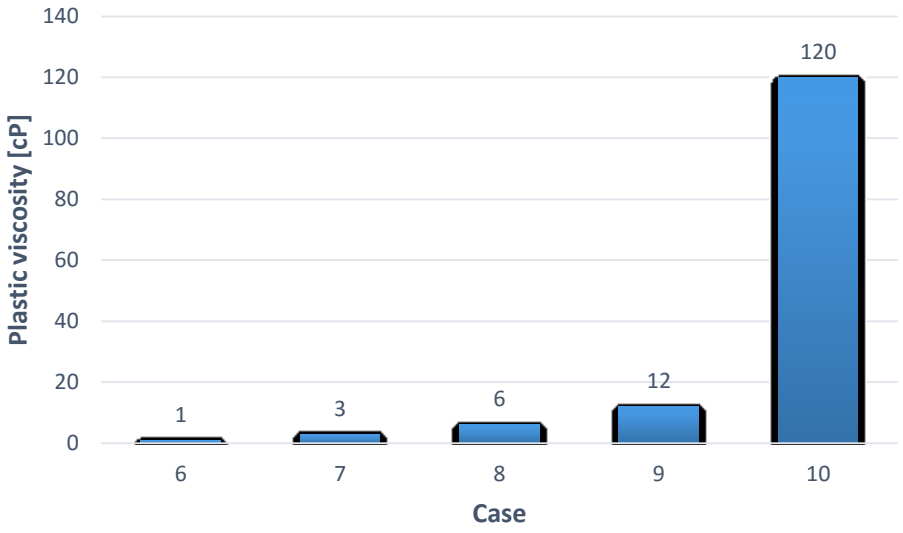

Figure 74: Plastic viscosity values used for each case.

Above the plastic viscosity values are shown which were used in the simulation runs. When fluid levels of these cases are compared no distinct trend in relation to increased viscosity could be observed. Figure 76 shows this comparison with the range of occurring surface disturbances. Over the range of used viscosity values no obvious relationship in terms of ripple intensity or location could be found. Surface tension will likely play a more prominent role at higher viscosities. The study of the surface tension influence on such flows could be a viable candidate for future CFD studies.

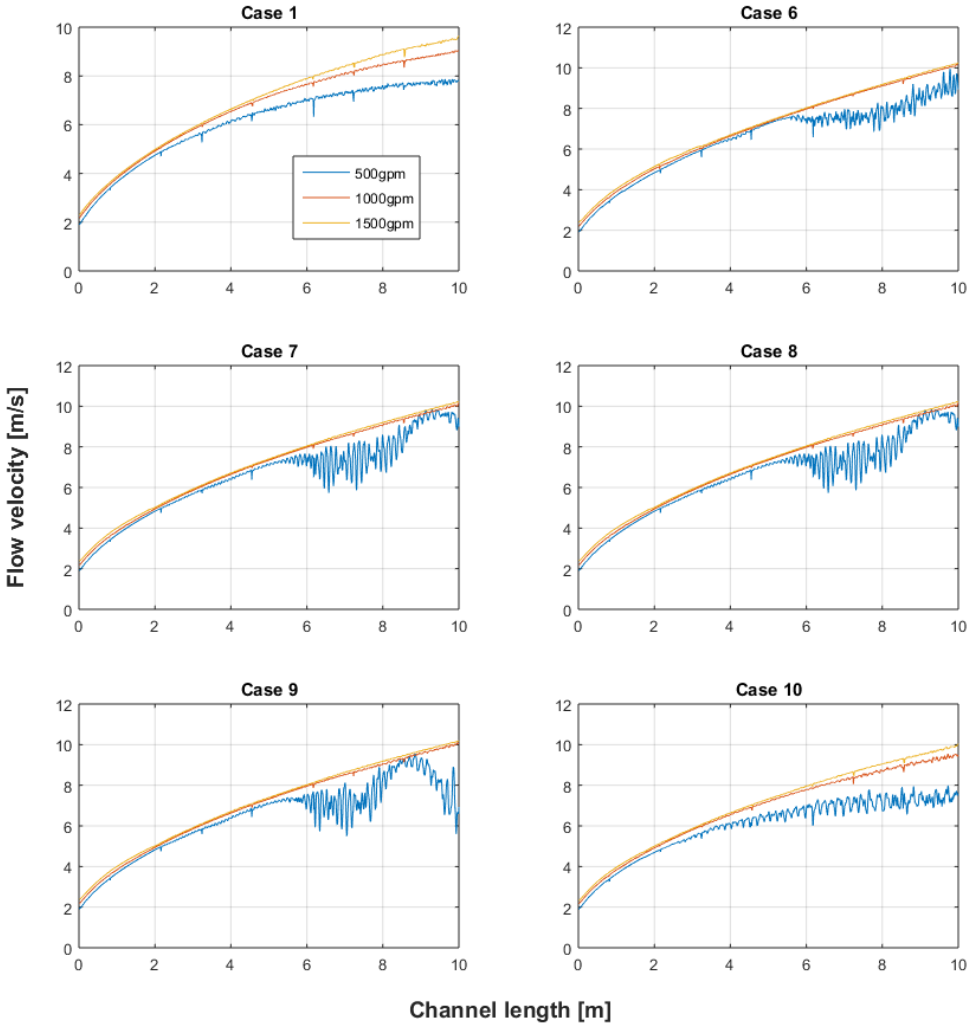

Figure 75: Velocity profiles for different fluid properties and flow rates.

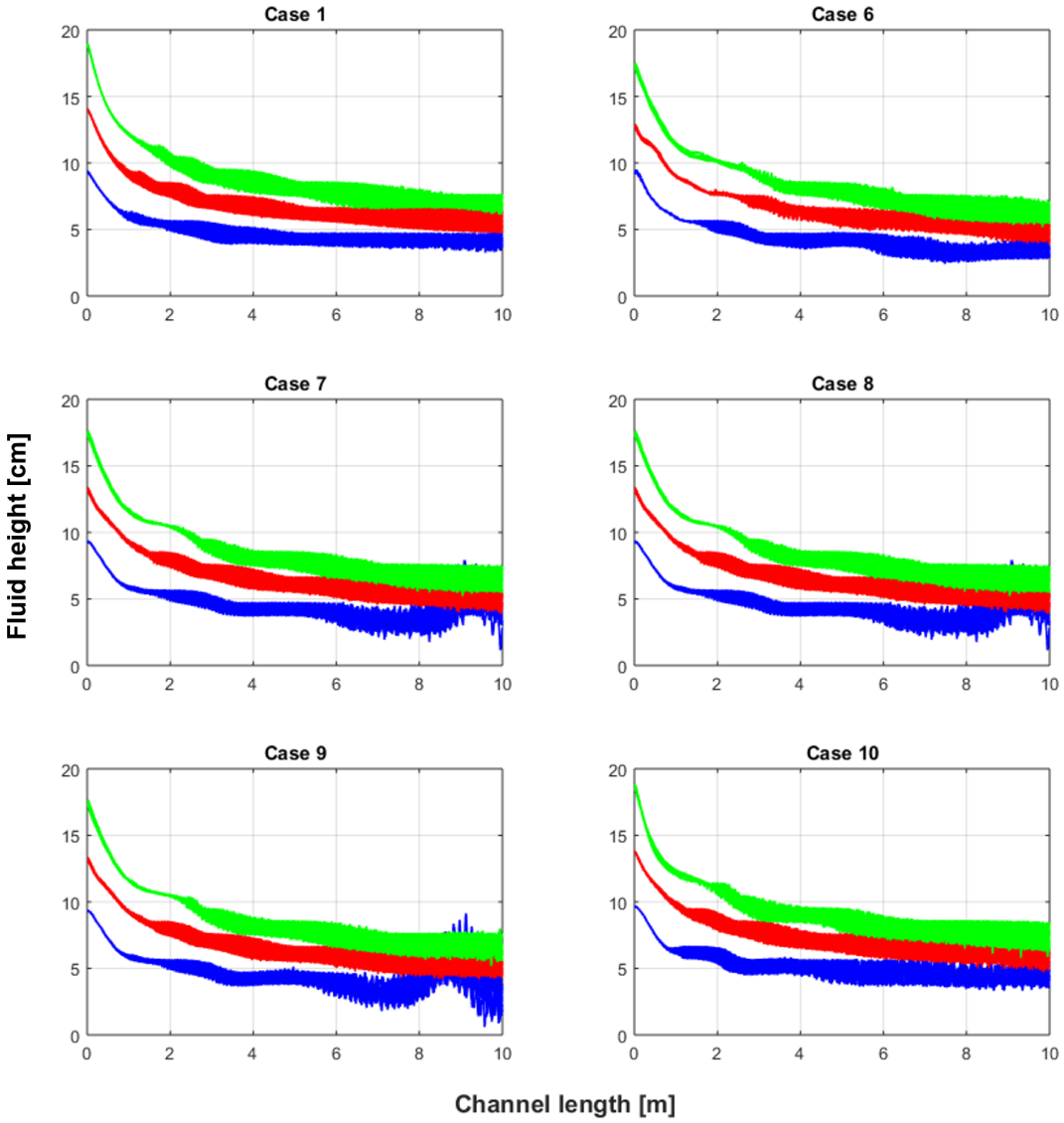

Figure 76: Fluid level range for different fluid properties and flow rates. 500gpm (blue), 1000gpm (red), 1500gpm (green).

Chapter 6 Conclusion

To gain a comprehensive understanding of fluid flow measurement on drilling rigs the most commonly used flowmeters were reviewed and assessed based on their advantages and disadvantages and their usefulness in the application of drilling fluid outflow measurement in open drilling systems particularly without costly and complex rig modifications. Based on data provided by numerous flow meter manufacturers and suppliers, the cost and accuracies of different flow meters were compared. The more expensive and accurate flowmeters showed to require complex rig modifications. In a cost benefit perspective the rolling float meter clearly showed its comparable accuracy to a magnetic flowmeter at a reasonably low price and not requiring any rig modifications.

A state of the art CFD software was used to run simulations in order to understand the governing factors of open channel flow rate measurement on drilling rigs better. Accurate open channel flow measurement is more complex due to the many factors contributing to a change in free surface phenomena. Beginning with a base case for the model different scenarios have been simulated with changing channel drop angle, fluid weight, viscosity and flow rate to observe their changing impact on a potential flow rate measurement.

The initial analysis of the base case shows that the cross section velocity profile along the channel length behaves as expected and resembles the theoretical profile derived from the Bernoulli equation. It could be observed that with increased distance from the inlet the fluid height sensitivity decreases with changing flow rates likely making it more difficult to measure fluid levels accurately. The faster flowing and the shallower the flow becomes the more free surface instabilities and surface ripples could be observed which may require more complex signal filters for fluid level measurements in order to keep measurements precise.

Varying the fluid weight by doubling and tripling the water density showed no particular effects on fluid levels or velocity which is as expected as in gravity driven flows mass cancels out of the Bernoulli equation and fluid height is a function of flow velocity.

Changing the pipe drop angle showed similar results as the base case. Fluid height sensitivity decreases but the shallower the drop angle the less sever this sensitivity loss becomes. At shallow drop angles it has been observed that at a certain point especially with high flow rates the pipe begins to fill completely and that this filled front is slowly moving downwards in an oscillating fashion. It can be concluded that the pipe diameter likely plays an important role and that there is a delicate balance between pipe drop angle and pipe diameter. This ratio should be selected diligently to allow for accurate measurements of the intended range of flow rates.

To simulate cases with different Bingham fluids the flow model was switched from turbulent to laminar. The variation of the fluid viscosity in a reasonable range showed no significant changes in outflow behavior. To evaluate these results a real world experiment is recommended. For future simulations in such a transitional flow regime

it might be necessary to split the model and use different viscosity models that fit the current conditions best. Based on the simulation setup used in this study there could be no distinct trends in terms of surface instability intensity and location observed with increasing plastic viscosity.

Overall the simulations showed that the outflow measurements done by measuring the fluid height are able to detect instant influxes into the system. However the ability to detect such events likely decreases with steeper pipe angles especially if the sensor is placed in the lower section where the fluid height is low and the velocity is high. This combination increases the measurement noise significantly and makes accurate measurements impossible even with signal processing. For more accurate measurements it is recommended to keep the flowline at a shallow angle and place the flowmeter closer to the well where the flow velocity is slow and the fluid height is deep.

For smaller instantaneous flowrate changes or incremental changes the measurement of fluid height might be insufficient to detect certain influx or loss events accurately. For future work it is recommended to establish the detectable limits of those parameters by varying the inflow function at the inlet boundary. Typical gain and loss scenarios could be simulated that way and the measured signal at the flowline could then be studied whether the simulated event would have been detectable.

Chapter 7 Future Work and Recommendations

Fluid dynamics and its research is a wide and complex field. This thesis was intended to gain an initial understanding of outflow behavior in open drilling systems with open channel outflow. In the drilling engineering field and in the oil and gas field in general there are many fluid dynamics research opportunities that could be picked up by students and researchers but are left aside due to the high barriers of entry into this field. Aside from the main purpose of this study it should also act as a foundation for future CFD related research work done by students at the chair of Petroleum Engineering.

As already stated a couple of times in this thesis this study was severely limited by a number of factors and had to be contained to a relatively narrow focus in order to keep the scope of this project reasonable. One major factor was the limitation of computational hardware for the simulation runs. Fluid dynamics simulations are immensely computational expensive especially if high resolution mesh models and transient simulations are applied. The simulations for this thesis were done on an ordinary desktop PC. For future CFD studies it is strongly recommended to either use a dedicated CFD cluster or rent CPU time in the cloud from a supported HPC (high performance computing) service provider which is likely more cost effective for occasional CFD studies.

The second important factor was the lack of a real world model to perform experiments in. CFD simulating is often referred as a form of art because there are so many different models that can be applied and a vast amount of controls for the user to be changed. To get a result often won't mean that the result is reflecting the real world behavior of a fluid dynamics problem. Therefore it is favorable to evaluate the simulation results with a real world experiment to compare if the applied fluid models brought the same results as the experiments before further simulation cases are run. A promising opportunity for this could be the proposed research drilling rig at the Erzberg if it will be an open drilling system.

A big issue of flow measurement in conventional drilling systems is the effect of cuttings settling in the flowline that can substantially compromise measurement results and lead to unnecessary safety hazards. Due to the hardware limitations cuttings were not simulated in this study but could be a potential object for future research in this area.

Appendix A User Defined inlet Function Source Code

```
#include "udf.h"

DEFINE_PROFILE(inlet_function,th,i)
{
 face_t f;
 begin_f_loop(f,th)
 {
     if(CURRENT_TIME <= 5)
         F_PROFILE(f,th,i) = 0.17;                          //  500gpm
     else if(CURRENT_TIME <= 10 && CURRENT_TIME > 5.001)
         F_PROFILE(f,th,i) = 0.34;                          // 1000gpm
     else
         F_PROFILE(f,th,i) = 0.51;                          // 1500gpm
 }
 end_f_loop(f,th)
}
```

Appendix B Post – Processing Scripts

B.1 Importing Raw Data into Matlab

```
function fluentImport
    clc
%%%%%%%%%%%%%%%%%%%%%%%%%%%%%%%%%%%%%%%%%%%%%%%%%%%%%%%%%%%%%%%%%%%%%%%%%%%%
    colX = 1;                                                                % Column
where X-Coordinates are in output files
    colY = 3;                                                                % Same with
Y-Coordinates
    colWater = 6;                                                            % Same for
Water Volume Fraction
    colVelocity = 4;                                                         % Same for
Velocity Magnitude
    colRe = 5;
    prefix = 'SYS-';                                                        % Prefix of
the output files followed by timestep (Can be changed in Fluent)
%%%%%%%%%%%%%%%%%%%%%%%%%%%%%%%%%%%%%%%%%%%%%%%%%%%%%%%%%%%%%%%%%%%%%%%%%%%%
    path = [uigetdir '\'];                                                   % Getting
Output files path
    nfiles = length(struct2cell(dir(strcat(path,prefix,'*.'))))              % Number of
to be imported files, hence datapoints
    filelist = struct2cell(dir(strcat(path,prefix,'*.')))';                  % Creating
list of filenames, which are used below

    filelist(:,2:5)=[];

    for i=1:nfiles
       filelist{i,2}=sscanf(char(filelist{i,1}),'SYS-%d');
    end

    filelist = sortrows(filelist,2);

    maxrows = length(dlmread(char(strcat(path,filelist(1,1))),',',1,1))      % Getting
number of rows in the output files
    globalX = dlmread(char(strcat(path,filelist(1,1))),',',[1 colX maxrows colX]);  %
Extracting coodinates seperatly
    globalY = dlmread(char(strcat(path,filelist(1,1))),',',[1 colY maxrows colY]);

    assignin ('base','globalX',globalX);                                     % Assign
global variables to global workspace so the other functions can access them
    assignin ('base','globalY',globalY);

    WaterFraction = zeros(maxrows,nfiles);                                   %
Preallocating arrays for increased speed
    VelocityMagnitude = zeros(maxrows,nfiles);

    tic
    h = waitbar(0,'Importing');
    for i = 1:nfiles
        WaterFraction(:,i)=dlmread(char(strcat(path,filelist(i,1))),',',[1 colWater
maxrows colWater]); % Writing data from each output file in one variable
        VelocityMagnitude(:,i)=dlmread(char(strcat(path,filelist(i,1))),',',[1
colVelocity maxrows colVelocity]);
        remaining = toc*((length(filelist)-i)/i);
        waitbar(i/length(filelist),h,['Importing file ' num2str(i) ' / '
num2str(length(filelist)) ' (' num2str(floor(remaining/60)) ':'
sprintf('%02d',round(mod(remaining,60))) 'm remaining)']);
    end
    close(h)

    assignin ('base','WaterFraction',WaterFraction);
    assignin ('base','VelocityMagnitude',VelocityMagnitude);
    assignin ('base','filelist',filelist);

end
```

B.2 Transforming Coordinate System of Imported Data

```
function fluentTransformCoordinates

    clc
    % Function to transform the data from the global to the local
    % coordinate system, defined in the meshing tool. Origin and Axis
    % vector can be extracted from there.

    globalX = evalin('base','globalX');                                    % Fetching
global coordinates from global workspace
    globalY = evalin('base','globalY');
    globalZ = zeros(length(globalX),1);                                    % Dummy Z-
coordinates for transformation

    localOrigin = [0.61148; 0.24333; 0];                                % 3D, round
outlet, 30
    localAxes = [0.5 0.86603 0; 0.86603 -0.5 0; 0 0 1];
%     localOrigin = [0.70228; 0.27355; 0];                                % 3D, round
outlet, 10
%     localAxes = [0.17365 0.98481 0; 0.98481 -0.17365 0; 0 0 1];
%     localOrigin = [0.67204; 0.25203; 0];                                % 3D, round
outlet, 20
%     localAxes = [0.34202 0.93969 0; 0.93969 -0.34202 0; 0 0 1];

    globalCoordinates = [globalX';globalY';globalZ'];                      % Prepare
global coordinates for transform function
    localCoordinates = global2localcoord(globalCoordinates,'rr',localOrigin,localAxes)';
% Transform coordinates
%     assignin ('base','localCoordinates',localCoordinates);

    localX = localCoordinates(:,2);                                        % Splitting
up transformed coordinates in single variavles again
    localY = localCoordinates(:,1);

    assignin('base','localX',localX);                                      % Assigning
back to global workspace for further use
    assignin('base','localY',localY);

    subplot(2,1,1)                                                         % Checkplot
to see before and after transformation
    scatter(globalX,globalY)                                               % If not
correct check localOrigin and localAxes, if necessary swap x any y column
    title('Before Transformation')
    subplot(2,1,2)
    scatter(localX,localY)
    title('After Transformation')
end
```

B.3 Interpolating and Standardizing Raw Data

```
function fluentInterpolate

    clc
    % Function to generate a grid with specified resolution and interpolate
    % all data points onto the grid because data points from Fluent are
    % rarely exactly alligned.

    localX = evalin('base','localX');                                    % Fetching
data from global workspace
    localY = evalin('base','localY');
    WaterFraction = evalin('base','WaterFraction');
    timesteps = size(WaterFraction,2)
    VelocityMagnitude = evalin('base','VelocityMagnitude');

    GridRes = 0.01;                                                      % Specifying
grid resolution in meters
    GridHeight = 0.3;                                                    % Monitoring
plane height in meters
    GridLength = 10;                                                     % Monitoring
plane length in meteres

    [xq,yq] = meshgrid(0:GridRes:GridHeight-GridRes,0:GridRes:GridLength-GridRes);  %
Generating grid with specified resolution
    WaterFractionInterpolated = zeros(GridLength/GridRes,GridHeight/GridRes,timesteps);
% Preallocating array
    VelocityMagnitudeInterpolated =
zeros(GridLength/GridRes,GridHeight/GridRes,timesteps);

    tic
    h = waitbar(0,'Interpolating timestep ');
    for t = 1:timesteps
        F = scatteredInterpolant(localY,localX,WaterFraction(:,t),'nearest');   %
Interpolation function
        I = scatteredInterpolant(localY,localX,VelocityMagnitude(:,t),'nearest');
        WaterFractionInterpolated(:,:,t) = F(xq,yq);
        VelocityMagnitudeInterpolated(:,:,t) = I(xq,yq);
        remaining = toc*((timesteps-t)/t);
        waitbar(t/timesteps,h,['Interpolating timestep ' num2str(t) ' / '
num2str(timesteps) ' (' num2str(floor(remaining/60)) ':'
sprintf('%02d',round(mod(remaining,60))) 'm remaining)']);
    end
    close(h)

    Velocity = WaterFractionInterpolated.*VelocityMagnitudeInterpolated;
    liquidLevel = zeros(timesteps,GridLength/GridRes);
    avgVelocity1 = zeros(timesteps,GridLength/GridRes);
    avgVelocity2 = zeros(timesteps,GridLength/GridRes);
    h = waitbar(0);
    for t = 1:timesteps

        for i = 1:(GridLength/GridRes)

            liquidLevel(t,i) = sum(WaterFractionInterpolated(i,:,t));
            avgVelocity1(t,i) = max(VelocityMagnitudeInterpolated(i,:,t));
            avgVelocity2(t,i) = max(Velocity(i,:,t));
        end
        waitbar(t/timesteps,h,['Calculating mud level and avg. velocity ' num2str(t) ' /
' num2str(timesteps)]);
    end
    close(h)

    assignin ('base','WaterFractionInterpolated',WaterFractionInterpolated);
    assignin ('base','VelocityMagnitudeInterpolated',VelocityMagnitudeInterpolated);
    assignin ('base','liquidLevel',liquidLevel);
    assignin ('base','avgVelocity1',avgVelocity1);
    assignin ('base','avgVelocity2',avgVelocity2);

end
```

Appendix C Mesh Independence Study

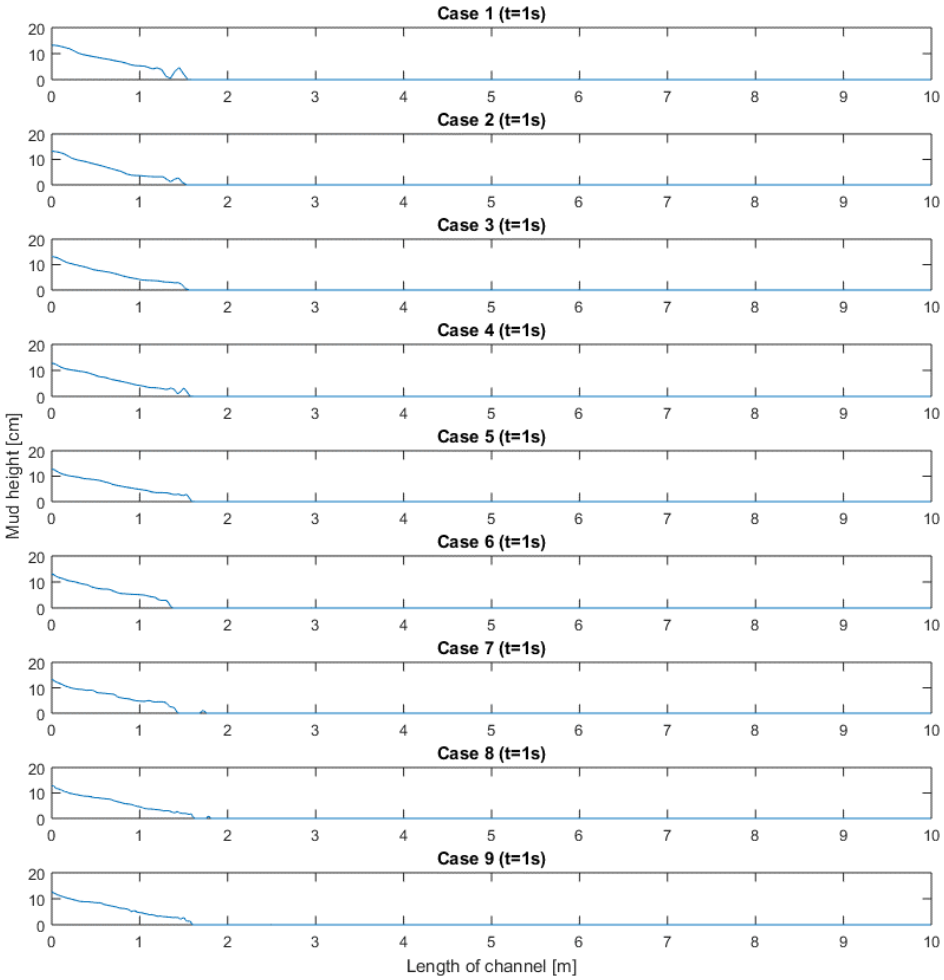

Figure 77: Comparison of cases after simulation runtime 1 second.

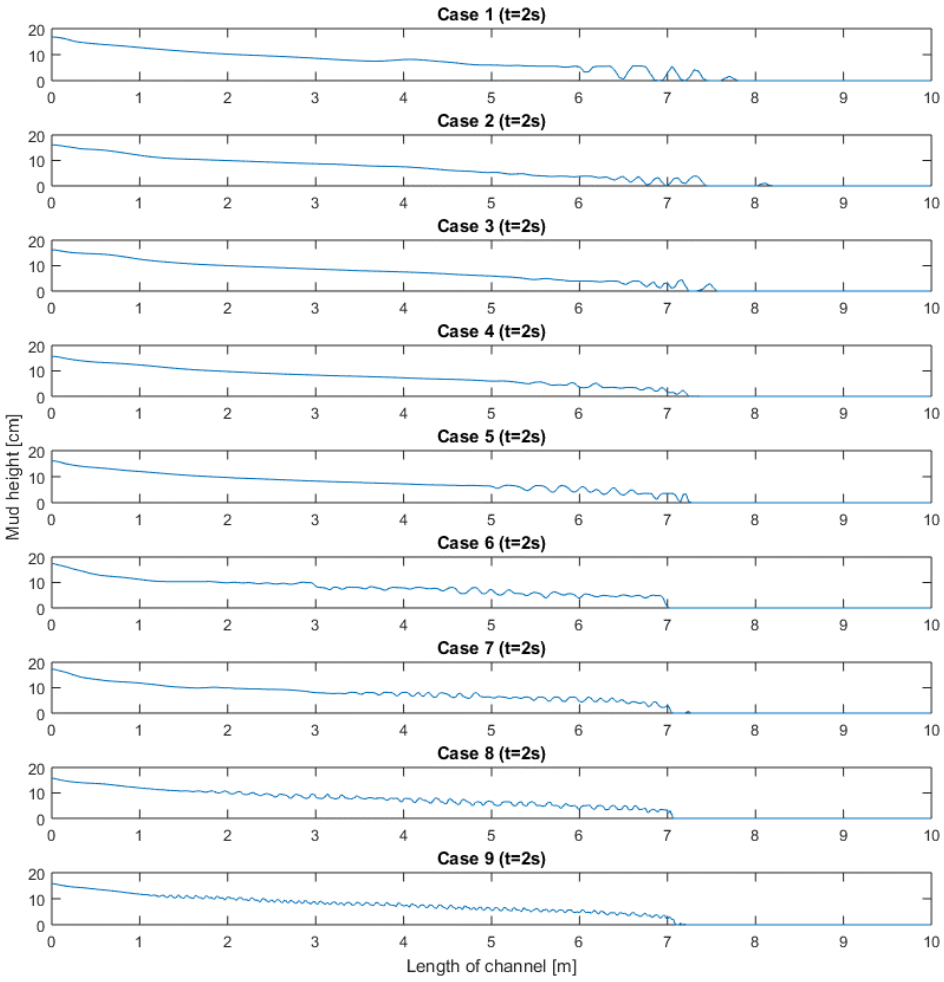

Figure 78: Comparison of cases after simulation runtime 2 second.

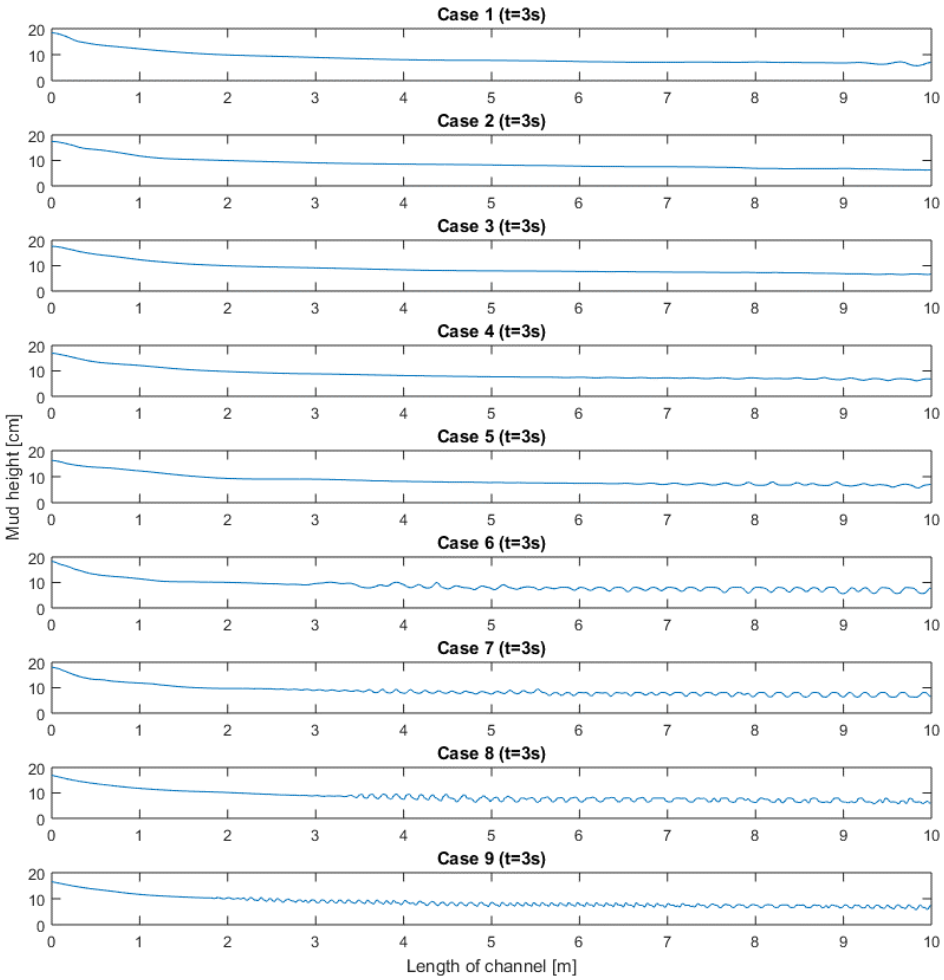

Figure 79: Comparison of cases after simulation runtime 3 second.

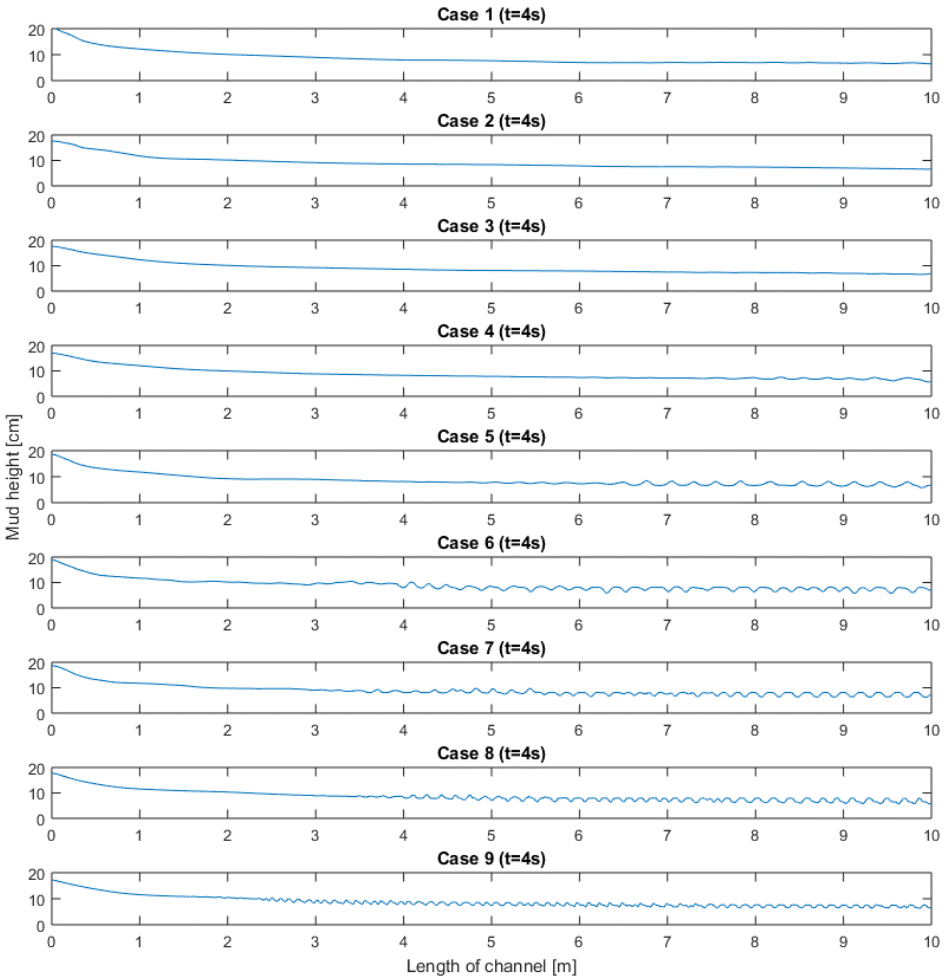

Figure 80: Comparison of cases after simulation runtime 4 seconds.

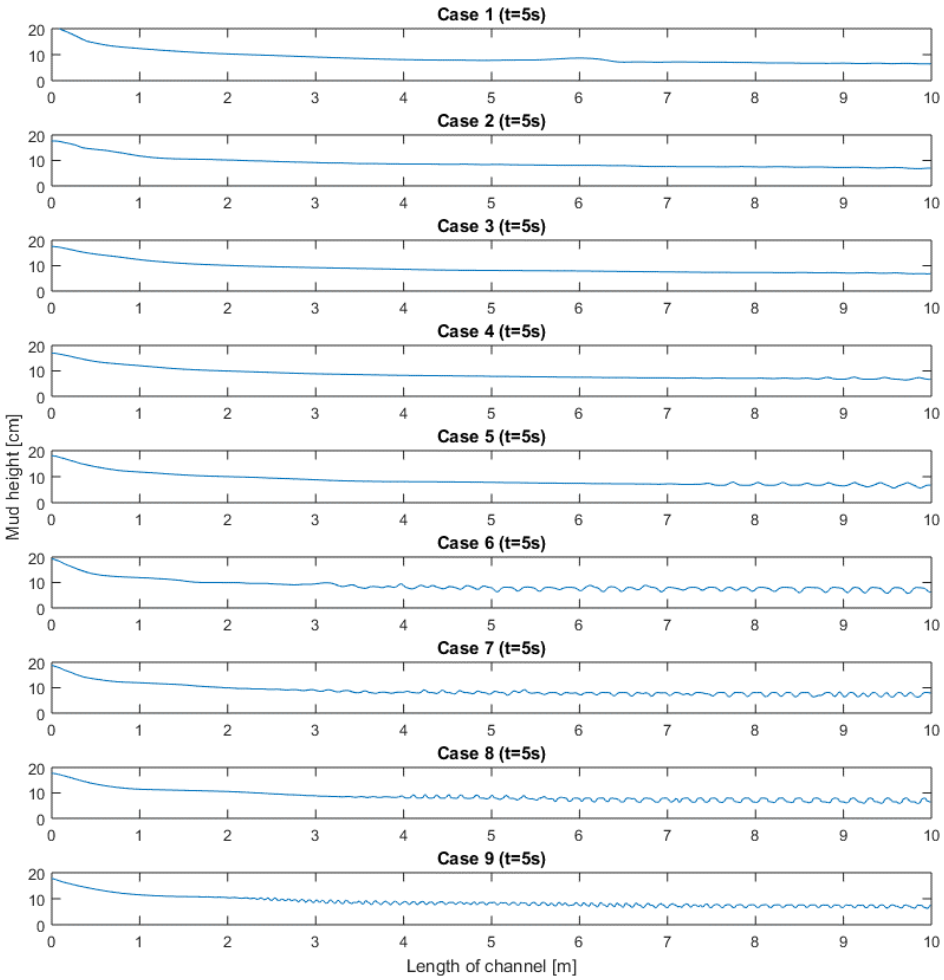

Figure 81: Comparison of cases after simulation runtime 4 seconds.

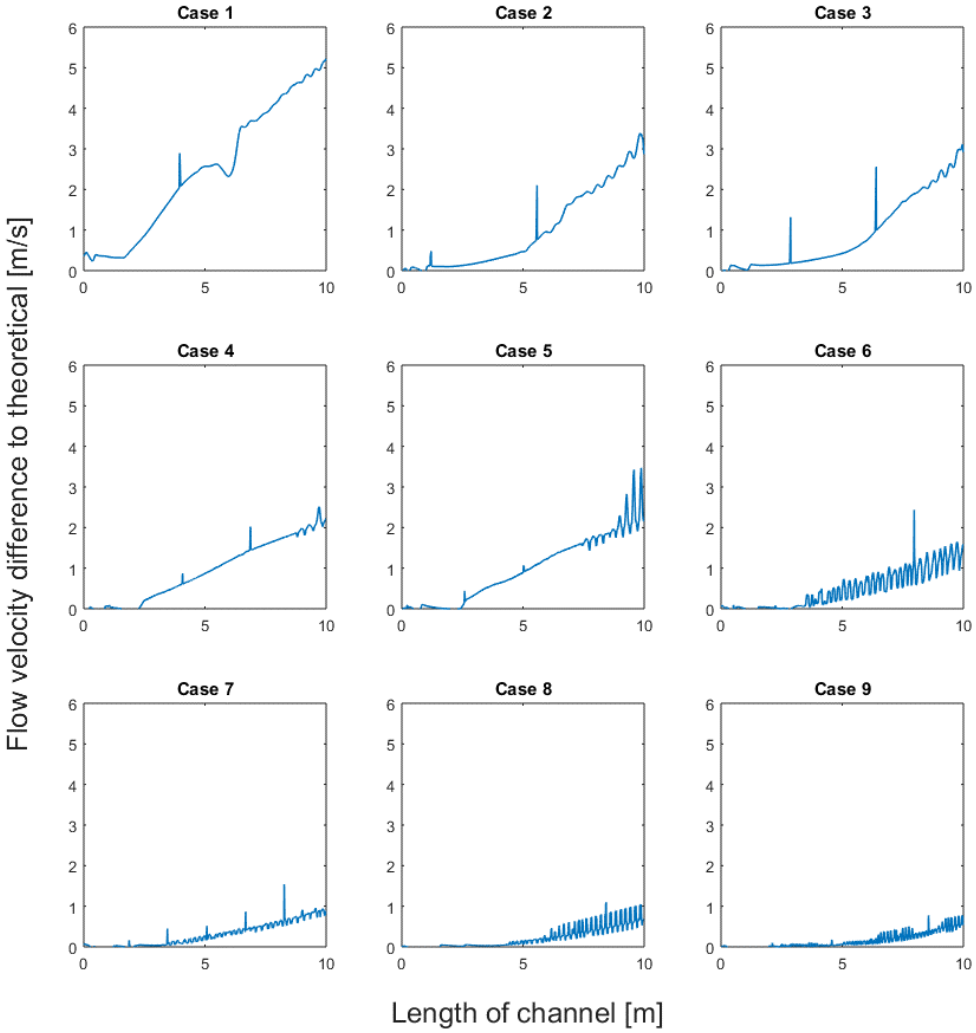

Figure 82: Difference between the theoretical and the simulated velocity profiles based on Figure 48. It can be noted that in case 8 and 9 the difference in the first half of the channel is negligibly small which is important for subsequent simulations as the focus lies predominantly on the upper half of the channel.

Bibliography

4runntertech. 2016. *Paddle and Rolling Float Meter quote and interview* (Mar).

AAPG. 2015. *AAPG Wiki.* 14. Nov. http://wiki.aapg.org/Risk:_expected_value_and_chance_of_success.

2015. *ABB CoriolisMaster Operating Instructions.* 10. Sep. https://library.e.abb.com/public/d65feba9d7ab7fd7c1257cdd0046180e/OI_FCB300_FCH300_EN_F.pdf.

ABB. 2015. „Die neuen Coriolis Masse-Durchflussmesser CoriolisMaster FCB330 und FCB350 – Die bessere Alternative!" *www.ABB.com.* 26. Mar. Zugriff am 28. May 2015. https://library.e.abb.com/public/c34496734187f104c1257e14003148fd/DS_FCB300_FCH300_DE_G.pdf?filename=DS_FCB300_FCH300_DE_G.pdf.

2015. *ABB Electromagnetic Flowmeters Operating Instruction.* 10. Sep. https://library.e.abb.com/public/a16e8e2e9e307a41c12577ca003b4d35/D184B140U02-B-08_2010.pdf.

2014. „Advanced Petroleum Economics Lecture Notes." Leoben: MUL.

Akan, A. Osman. 2006. *Open Channel Hydraulics.* Oxford: Butterworth - Heinemann. Zugriff am 10. May 2016. http://www.globalspec.com/reference/24097/203279/4-3-significance-of-froude-number-in-gradually-varied-flow-calculations.

Baker Hughes. 2015. *Rig Count Overview & Summary Count.* 15. September. http://www.bakerhughes.com/rig-count.

Baker, R C, und J E Deacon. 1983. *Tests on turbine, vortex and electromagnetic flowmeters in 2-phase air-water upward flow.* Coventry, England: BHRA Fluid Engineering.

Beda, G, und C Carugo. 2001. *Use of Mud Microloss Analysis While Drilling to Improve the Formation Evaluation in Fractured Reservoir.* New Orleans, LA: SPE 71737.

2015. *Businessdirectory.* Nov. http://www.businessdictionary.com/definition/expected-monetary-value.html.

Carl Joseph Thaemlitz, Halliburton Energy Services. 2004. Electrically conductive oil-based mud. USA Patent US 6691805 B2.

Chopty, J, und A Sardo. 2011. *Managed Pressure Drilling as a Tool to Reduce Risks and Non-Productive Time: an Update on Field Experience.* Ravenna, Italy: OMC.

Emerson Process Management. 2009. „Reconciling Mass And Energy Balances In An Ethylene Complex." *www.Slideshare.net.* 11. Nov. Zugriff am 28. May 2015. http://www.slideshare.net/JimCahill/reconciling-mass-and-energy-balances-in-an-ethylene-complex.

Enertek, APS. 2012. *RFM-3600 Advanced Rolling Float Meter technical information sheet.* APS Enertek. Zugriff am 30. Mar 2016.

http://4runnertech.com/yahoo_site_admin/assets/docs/RFM-3600.103105606.pdf.

engineeringexcelspreadsheets.com. 2012. *Non Uniform Flow in Open Channels.* 15. Dec. Zugriff am 29. Mar 2016. http://www.engineeringexcelspreadsheets.com/wp-content/uploads/2011/07/uniform-and-nonuniform-flow.jpg.

Expro. 2016. „ActiveSonar QEX1000 Flow Meter Datasheet." July. http://70830b58906668d321d3-fdabdf1ed13d1990275f510cf3764dd3.r27.cf3.rackcdn.com/ssp00001_activesonar_qex1000_meter_data_sheet.pdf.

Expro. 2016. *Interview Flowmeter Sales* (Apr).

2015. *Expro QEX1000 datasheet.* 25. Sep. http://exprogroup.com/media/41999/ssp00001_activesonar_qex1000_meter_data_sheet.pdf.

Fluent Inc. kein Datum. *Ansys Fluent User's Guide.* Zugriff am 21. Mar 2016. https://www.sharcnet.ca/Software/Fluent6/html/ug/node1.htm.

Freebigpictures.com. 2009. *Mountain River.* Sept. Zugriff am 28. Mar 2016. http://freebigpictures.com/wp-content/uploads/2009/09/mountain-river.jpg.

Harlan H. Bengston, PhD, P.E. 2011. *Uniform Open Channel Flow and the Manning Equation.* Zugriff am 28. Mar 2016. http://www.pdhsite.com/courses/Uniform%20Open%20Channel%20Flow%20and%20the%20Manning%20Equation%20Course.pdf.

Inc., Greyline Instruments. kein Datum. *Area-Velocity Flowmeter Installations in Denmark.* Zugriff am 6. Apr 2016. http://www.greyline.com/images/Denmark/QZ02%20Sensor.jpg.

Kuhny, Dave. 2011. *Compensating for the effects of high pressure on the measurement accuracy of Coriolis flowmeters.* Boulder, CO: Micro Motion.

Lally, Lindsay , und Lee Hixon. kein Datum. *Energy–depth relationship in a rectangular channel.* Zugriff am 10. May 2016. https://en.wikipedia.org/wiki/Energy%E2%80%93depth_relationship_in_a_rectangular_channel.

Lesage, M, C G Casso, und K J Zanker. 1990. *A New Approach to Rig Sensors.* Houston, TX: IADC/SPE 19999.

Liu, K T, D R Canfield, und J T Conley. 1988. „Application of a Mass Flowmeter for Allocation Measurement of Crude Oil Production." *SPE Production Engineering* 635.

Livelli, Greg. 2008. *New Magmeter Combines Benefits of AC and DC Technologies.* ABB. 30. Mar. Zugriff am 1. Apr 2016. http://legacy.risiinfo.com/magazines/March/2008/PP/PPMagMarch-New-Magmeter-Combines-Benefits-of-AC-and-DC-Technologies.html.

Loeppke, Glen E., Diane M. Schafer, David A. Glowka, Douglas D. Scott, Marcus D. Wernig, und Elton K. Wright. 1992. *Development and Evaluation of a Meter for Measuring Return Line Fluid Flow Rates During Drilling.* Oak Ridge, TN: Sandia National Laboratories. http://www.osti.gov/scitech/servlets/purl/5036200.

Magoon, Leslie B., und Edward A. Beaumont. 1999. „Petroleum Systems." In *Handbook of Petroleum Geology*.

Malvic, T. 2009. *Stochastical approach in deterministic calculation of geological risk - theory and example.* Zagreb: NAFTA.

Martin, Christopher. 2012. *Vermilion River Photo.* May. Zugriff am 28. Mar 2016. https://chrismartinphotography.files.wordpress.com/2012/05/vermilion-river-c2a9-2012-christopher-martin-9748.jpg.

2015. *Micro Motion Product Data Sheet.* 10. Sep. http://www2.emersonprocess.com/siteadmincenter/PM%20Micro%20Motion%20Documents/ELITE-PDS-PS-00374.pdf.

Micro Motion, Emerson Process Management. 2013. *Micro Motion Coriolis meters accurately detect and quantify wellbore ballooning.* Micro Motion.

Mitchell, Robert F. 2006. *Petroleum Engineering Handbook: Drilling Engineering Volume 2.* Richardson, TX: Society of Petroleum Engineers.

Newendorp, P., und J. Schuyler. 2000. „Decision Analysis for Petroleum Exploration. 2nd Edition." Aurora: Planning Press.

Orban, J J, K J Zanner, und A J Orban. 1987. *New Flowmeters for Kick and Loss Detection During Drilling.* Dallas, TX: SPE 16665.

Orban, J J, und K J Zanker. 1988. *Accurate Flow-Out Measurements for Kick Detection, Actual Response to Controlled Gas Influxes.* Dallas, TX: IADC/SPE 17229.

pason. kein Datum. *Pit Level Totalizer (PVT).* pason. http://www.pasonusa.com/rig-site/pit-volume-totalizer/.

2015. *Petrowiki.* Nov. http://petrowiki.org/Decision_tree_analysis.

Ponce, Prof. Victor Miguel. kein Datum. *THE OPEN-CHANNEL HYDRAULICS CHALLENGE.* Zugriff am 6. Apr 2016. http://ponce.sdsu.edu/cive530_lecture03_hj.jpg.

Process, Micromotion / Emerson. 2015. *Coriolis flowmeter quote* (Dec).

Process, Rosemount / Emerson. 2015. *Rosemount Online shop quote* (Dec).

Rigminder. 2015. *Flow Paddle Sensor.* Rigminder. Mai. Zugriff am 9. Apr 2016. http://rigminder.com/2015/wp-content/uploads/2015/05/New-Flow-Paddle.png.

Robbie, Jeff, und Charles Orbell. 2016. *State of the Art for Drilling Fluid Measurements and the Industrie Needs.* http://upmforum.com/lectures-presentations-forum-documents/presentations/UPM%202016%20Drilling%20Fluid%20Measurements%20Industry%20Needs24thFeb2016rev1.pdf.

Roger, C. Baker. 2000. *Flow Measurement Handbook.* Cambridge University Press.

Rose, P. R. 1987. *Dealing with risk and uncertainty in exploration - how can we improve?* AAPG Bulletin.

2015. *Rosemount 8700 Series Data Sheet.* 15. Sep. http://www2.emersonprocess.com/siteadmincenter/pm%20rosemount%20documents/00813-0100-4727.pdf.

Russel, Chris, und Mark Simons. 2013. „Understanding and Selecting Coriolis Technology for Drilling fluid Monitoring." *Micro Motion White Paper, www.micromotion.com.*

Schafer, D M, G E Loeppke, D A Glowka, D D Scott, und E K Wright. 1992. *An Evaluation of Flowmeters for the Detection of Kicks and Lost Circulation During Drilling.* New Orleans, LA: IADC/SPE 23935.

2015. *Schlumberger FLAG Product Video.* 10. Sep. http://www.slb.com/services/drilling/engineering_modeling/support/flag.aspx.

2015. *Schlumberger FLAG Service Brochure.* 10. Sep. http://www.slb.com/~/media/Files/geoservices/brochures/flag_br.pdf.

Slurry Pipes Ldt. kein Datum. *Pipe Roughness.* Zugriff am 23. Mar 2016. http://www.slurrypipes.com.au/wp-content/uploads/2012/04/Screen-Shot-2012-04-09-at-12.49.02-AM.png.

University of Illinois. kein Datum. *ANSYS Fluent Introduction & Workflow.* Zugriff am 13. Jan 2016. https://uiuc-cse.github.io/me498cm-fa15/lessons/fluent/intro.html.

Upp, E L. 1993. *Fluid Flow Measurement.* Gulf Publishing Co.

VEGA. 2016. *Radar level meter quote* (July).

Vega. kein Datum. *VEGAPULS 62 Radar level meter brochure.* Vega. https://www.vega.com/PdfExportHandler.ashx?itemid=154ea1e8-590b-49fd-bca1-2e4a7631b246&language=en.

Visavale, Ganesh. 2014. *Introduction to Turbulence.* 15. May. Zugriff am 28. Mar 2016. https://www.linkedin.com/pulse/20140515112132-58050580-introduction-to-turbulence.

Woodco. 2014. *Bell nipple flange.* Woodco USA. http://www.woodcousa.com/_derived/bell-nip.htm_txt_bell-assy.gif.

Acronyms

BHP	Bottom Hole Pressure
BOP	Blowout Preventer
CFD	Computational Fluid Dynamics
CPU	Central Processing Unit
DSP	Digital Signal Processor
ECD	Equivalent Circulating Density
HPC	High Performance Computing
MPD	Managed Pressure Drilling
NPT	Non – Productive Time
OBM	Oil Based Mud
PVT	Pit Volume Totalizer

Symbols

q_m	Mass flowrate	[m^3/s]
K_s	Spring constant	[N/m]
τ	Time difference	[s]
ω	Driving frequency	[Hz]
ω_s	Free vibrating frequency of twisting U-tube	[Hz]
K	Shape factor	-
d	Pipe width	[m]
c	Speed of sound in the fluid	[m/s]
Δf	Frequency difference	[Hz]
f_t	Transmission frequency	[Hz]
θ	Relative angle fluid/ultrasonic beam	[°]
v	Maximum flow velocity	[m/s]
L	Travelled length of the fluid	[m]
μ	Dynamic viscosity	[Pa s]
ν	Kinematic viscosity	[m^2/s]
ρ	Fluid density	[kg/m^3]
D	Hydraulic depth	[m]
g	Gravity	[m/s^2]
E	Specific energy	[m]
y	Depth	[m]
Q	Discharge	[m^2/s]
A	Cross – section area of the stream	[m^2]

List of Figures

List of Tables